AN ABSTRACT OF THE THESIS OF

Glenn R. Tinseth for the degree of Doctor of Philosophy in Physical Chemistry presented on September 24, 1996. Title: Modeling Catalytic Hydrodeoxygenation in Ultra-High Vacuum: Furan on Clean and Sulfided Mo(110).

Redacted for Privacy

Abstract approved: _____

Professor Phillip R. Watson

The interactions of a model synthetic liquid fuel reactant (furan) with a model hydrodeoxygenation catalyst (clean and sulfided single crystal molybdenum) were investigated using the following UHV tools: Auger electron spectroscopy (AES), low energy electron diffraction (LEED), and temperature programed reaction spectroscopy (TPRS). In addition to furan, the reactions of hydrogen, carbon monoxide, ethylene, and propene on clean and sulfided Mo(110) were also examined. All adsorbates exposed to the extremely reactive clean or sulfided Mo(110) surface decomposed, yielding gaseous H_2 and surface C. In addition, furan TPRS caused the production of gaseous CO. The presence of background hydrogen caused no major changes in the TPRS of furan or the other adsorbates. Sulfur pre-adsorption caused the chemical shifting of H_2 TPRS peaks. Both sulfur and carbon pre-adsorption resulted in the Van der Waal's radius blocking of adsorption sites for all adsorbates studied.

Modeling Catalytic Hydrodeoxygenation in Ultra-High Vacuum: Furan on Clean and Sulfided Mo(110)

by

Glenn Tinseth

A THESIS

submitted to

Oregon State University

in partial fulfillment of
the requirements for the
degree of

Doctor of Philosophy

Presented September 24, 1996
Commencement June 1997

Doctor of Philosophy thesis of Glenn R. Tinseth presented on September 24, 1996

APPROVED:

Redacted for Privacy

Major Professor, representing Chemistry

Redacted for Privacy

Head of Department of Chemistry

Redacted for Privacy

Dean of Graduate School

I understand that my thesis will become part of the permanent collection of Oregon State University libraries. My signature below authorizes release of my thesis to any reader upon request.

Redacted for Privacy

Glenn R. Tinseth, Author

ACKNOWLEDGMENT

This would never have happened without the love and support of my family, especially my wife: Romi Hitchcock. Together with my good friend Louise Comden, Romi kept my feet to the fire until I finally "saw the light" (of my socks burning?!) and finished this degree.

I also must thank my old lab mates, Scott Mokler and John Mishenko, who taught me everything I needed to know to work in the lab, including the procedure for making the perfect cup of coffee. Phil Watson, my major professor guided and goaded me along the way and made sure I kept my eyes focused on the goal.

Thanks to Steve Kevan for providing the Mo(110) crystal slice and to the Department of Energy for their generous financial support of this research.

TABLE OF CONTENTS

TABLE OF CONTENTS, CONTINUED

LIST OF FIGURES

LIST OF FIGURES, CONTINUED

LIST OF FIGURES, CONTINUED

LIST OF FIGURES, CONTINUED

LIST OF FIGURES, CONTINUED

LIST OF FIGURES, CONTINUED

LIST OF FIGURES, CONTINUED

LIST OF TABLES

To my daughters, Skyler and Zoë.

MODELING CATALYTIC HYDRODEOXYGENATION IN ULTRA-HIGH VACUUM: FURAN ON CLEAN AND SULFIDED MO(110)

CHAPTER 1: OVERVIEW

1.1 INTRODUCTION

Fossil fuels are a static resource; they take much longer to form than to burn. In the last 40 years the consumption of petroleum resources has proceeded at ever increasing rates. As petroleum stocks dwindle, more research is being dedicated to develop and study other fuel sources, with emphasis on those that can be used in today's engines and boilers without expensive modifications. One avenue of this research is directed toward creating synthetic liquid fuels from carbon-rich solids, such as coal, oil shale, and different types of biomass.

The hydrodeoxygenation (HDO) of liquid fuels is a subject that has received little attention, especially compared to the closely-related and much-studied processes of hydrodesulfurization (HDS) and hydrodenitrogenation (HDN). Environmental concerns over SO_2 and NO_x emission and the very low O contents of conventional petroleum-based oils have contributed to this imbalance. Recent interest in synthetic liquids as commercial fuels has caused an increased scrutiny in HDO and its interaction with HDS and HDN. This is due to the fact that these synthetic liquids have a 3–70 times higher O content(0.4–3.8% O) than petroleum crude[1]. Oils derived from wood products have O contents of up to 34%[2].

Liquid fuels with a high O content tend to be unstable, quickly forming deposits and greatly increasing in viscosity on exposure to air, probably due to the polymerization of phenolic compounds[3,4]. In addition, HDO of these fuels produces H_20 as a by-product; H_20 is a known poison for common hydroprocessing catalysts[5,6]. This can significantly decrease the operational life of a catalyst bed and require more frequent reactivation treatments. For alternative liquid fuels to be economically feasible, O must be removed from the unrefined stock before further processing.

1.2 HYDRODEOXYGENATION

HDO, HDS, and HDN can be accomplished using both catalytic and noncatalytic processes. In most cases a catalytic process is used due to the much higher efficiencies of heteroatom removal. This is especially true for HDO since compounds common in synthetic fuels, like furans and phenols, require a

---

1. E. Furimsky, Catal. Rev.—Sci. Eng., **25**, 421, (1983)

2. J.R. Longanbach and R.Bauer, ACS Symp. Ser., **32**, 476, (1975)

3. J.N. Bowden and D.W. Brinkman, Department of Energy Report DOE/BETC/4162-10, (1980)

4. G.R. Hill, W.H. McClennen, G.S. Metcalf, Wang Hoah-Hsing, and H.L.C. Henzellaar, Proc. Int. Conf. Coal Sci., Duesseldorf, FRG, Paper C-25, 477, (1981)

5. J.M.J.G. Lipsch and G.C.A. Schuit, J. Catal., **15**, 179, (1980)

6. O. Weisser and S. Landa, *Sulfide Catalysts: Their Properties and Applications*, Pergamon Press, New York, (1973)

catalyst and an active reducing agent to be completely deoxygenated[7]. The most common conditions used in catalytic hydroprocessing are listed below[8].

- 6–15 MPa of hydrogen pressure
- Temperature of 600-650 K
- A catalyst composed of a combination of metals (in oxide form) such as CoMo, NiMo, and NiW dispersed on a SiO_2 or Al_2O_3 support.

The active ingredient in the catalyst, Mo or W, is combined with a promoter, usually Co or Ni, and impregnated into the SiO_2 or Al_2O_3 support. Although both Mo and W catalysts are active for HDO, the Mo-containing catalysts have been demonstrated to be superior[9,10]. The reduced (unmodified) form of the catalyst is sometimes used, but it is much more common to pretreat it with sulfur. The presulfided form of the catalyst is reported to be almost six times more active for HDO than the unpretreated form[11]. Because of this, fuel stocks containing high concentrations of S do not decrease the activity of the catalyst toward further HDS, HDN, or HDO.

O-containing compounds, on the other hand, can retard the activity of the catalyst, especially with respect to the removal of S and N; however, the

---

7. E. Furimsky, Catal. Rev.—Sci. Eng., **25**, 421, (1983)
8. S. Krishnamurthy, S. Panvelker, and Y.T. Shah, AIChe Journal, **27**, 994, (1981)
9. J. B-son Bredenberg, M. Huuska, J. Raty, and M. Karpio, J. Catal., **77**, 242, (1982)
10. C. Lee and D.F. Ollis, J. Catal., **87**, 325, (1984)
11. E. Furimsky, Appl. Catal., **6**, 159, (1983)

retarding mechanism is not well understood. Most researchers believe that it occurs via three processes[12,13]:

- Removal of active hydrogen near the catalyst site
- Competitive adsorption by the removed O on catalyst sites
- Deactivation of catalyst sites by H_2O, an HDO product

Synthetic fuels contain O compounds ranging from alcohols to furanic and phenolic compounds. Alcohols, carboxylic acids, esters, and alkylethers decompose thermally to eliminate O (as CO, CO_2, or H_2O), without a reducing agent or a catalyst. Furans and phenols, on the opposite end of the spectrum, require both for complete HDO. Ketones and amides are in between, usually requiring heat and a reducing agent for decomposition and elimination of O[14].

The mechanism of HDO and the structure and functionality of the catalyst surface with respect to HDO are still not well understood. Although work with the actual catalysts and real feedstocks provides valuable insights into the HDO process, simplified models can provide answers that are impossible to isolate in the complex system.

One way to simplify matters is to use model reactants instead of the raw feedstock. The logical choice for model compounds in an HDO study are those most resistant toward HDO, the furans and phenols; in fact benzofuran and

---

12. E. Furimsky, Catal. Rev.—Sci. Eng., **25**, 421, (1983)

13. S. Krishnamurthy, S. Panvelker, and Y.T. Shah, AIChe Journal, **27**, 994, (1981)

14. E. Furimsky, Catal. Rev.—Sci. Eng., **25**, 429, (1983)

phenol are two of the most common studied HDO subjects[15,16,17]. A schematic diagram of three possible reaction pathways for the HDO of furan is depicted in Figure 1-1 and the product distribution is in Table 1-1.

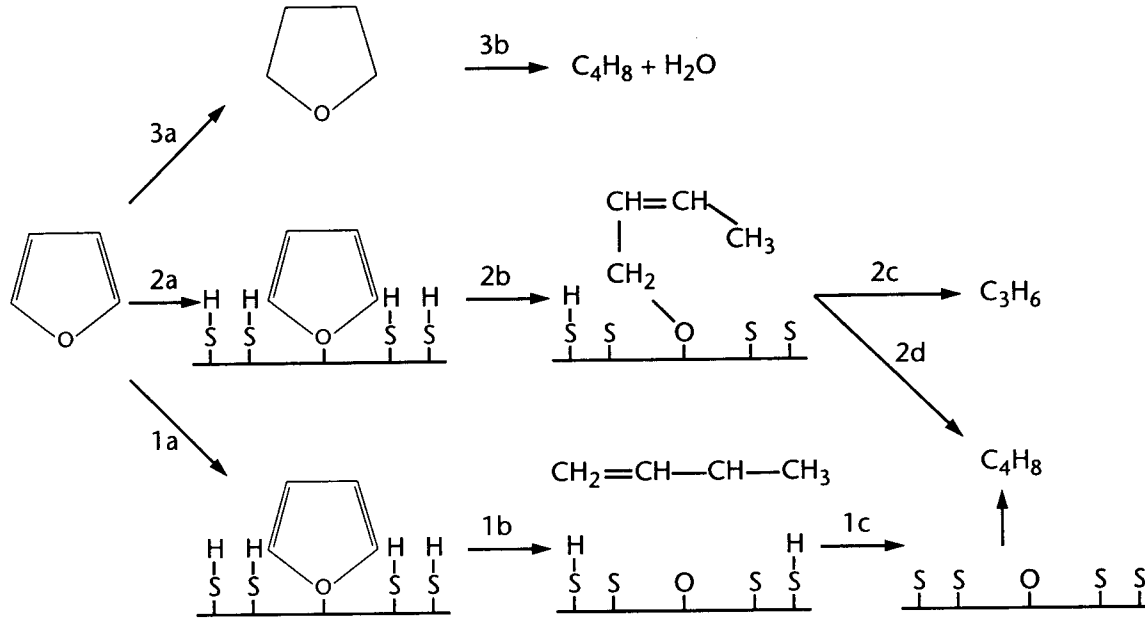

Figure 1-1. Possible reaction pathways for the HDO of furan (C_4H_4O)[18]

15. S. Krishnamurthy, S. Panvelker, and Y.T. Shah, AIChe Journal, **27**, 994, (1981)

16. R.K.M.R. Kallury, W.M. Restivo, T.T. Tidswell,. D.G.B. Boocock, A. Crimi, and J. Douglas, J. Catal., **96**, 535, (1985)

17. C. Lee and D.F. Ollis, J. Catal., **87**, 325, (1985)

18. E. Furimsky, Catal. Rev.—Sci. Eng., **25**, 431, (1983)

Table 1-1. Yields and distribution of products from HDO of furan[19] (400°C, pH_2 = 760 torr, Co-Mo/Al_2O_3 catalyst)

Compound	Reduced Catalyst	Sulfided Catalyst
C_2H_4	0.5	2.3
C_3H_8	Trace	1.2
C_3H_6	1.0	6.5
n-C_4H_{10}	0.5	1.1
l-C_4H_8	2.6	5.0
trans-C_4H_8	0.8	6.8
0.9	0.9	5.3
C_4H_6	Trace	Trace

A second way to simplify the system is to use a model of the catalyst. Instead of sulfided MoO_3 and CoO, on an Al_2O_3 support, a highly polished, well-ordered Mo surface (usually a single crystal), is used. To further simplify matters, and eliminate the inconvenience and complicating effects of surface impurities (i.e. dirt), the whole study is carried out in ultra high vacuum (UHV). Thus the experiment moves from the realm of catalytic chemistry into the domain of surface chemistry/physics.

1.3 Modeling Catalysts in Ultra High Vacuum

One of the basic tools of surface chemistry is the UHV chamber. The ability to work under UHV (~10^{-10} torr) conditions is the reason that surface scientists can

19. ibid, p. 430

carry out such a wide variety of controlled experiments on carefully constructed, well characterized surfaces. The two most important reasons why UHV is necessary for surface studies are:

- UHV allows a freshly cleaned surface to remain relatively free of contaminants for a reasonable working period (about an hour).
- UHV provides the right conditions in which to use surface sensitive electron spectroscopy methods.

For a solid at equilibrium with a gas of molecules of mass m, at a constant pressure P and temperature T, basic kinetic theory provides the following equation which estimates the rate at which molecules impact the surface.

$$\text{rate} = \frac{P}{(2\pi mkT)^{1/2}} \qquad \text{Equation 1-1}$$

For N_2 at 300K and a pressure of 10^{-6} torr, 5×10^{14} molecules hit the surface of a 1.0 cm^2 sample every second. If every molecule of N_2 that hits the surface of the sample sticks (a sticking coefficient of unity), a monolayer of N_2 would cover the surface in 2 seconds (assuming a typical metal surface atom density of 10^{15} atoms/cm^2)[20]. At a pressure of 5×10^{-10} torr, it would take over an hour to achieve the same coverage of N_2. This provides more than enough time to carry out a number of surface analytical probes. At a pressure of 1 torr, on the other hand, the sample surface would be completely covered with N_2 molecules in about 2×10^{-6} sec.

---

20. R.P.H. Gasser, *An Introduction to Chemisorption and Catalysis by Metals*, p. 54, Oxford University Press, New York, (1985)

In addition to the cleanliness advantage, UHV also provides the right environment for a probe that is sensitive to surface structure and composition, namely electrons with energies <2000 eV. Electrons in this energy range have a short mean free path in metals and generally do not penetrate more than 20 atomic layers (5-50 Å). Electrons diffracted or ejected by an incident beam of low energy electrons do not escape from below more than a few atomic layers. An added advantage to electrons is that their wavelength is on the order of 1 Å, the same as the atomic spacing in metals, thus allowing diffraction. To detect low energy emitted electrons, scattering and collisions with gas molecules must be minimized; UHV is ideal.

There are also disadvantages to modeling a complex catalyst in UHV. The conditions under which UHV studies are carried out are very different than what actual catalysts and feedstocks are exposed to. Many assumptions are made and complications eliminated, all to make it possible to carry out controlled experiments that attempt to provide insight into, and examples of, the actual chemistry that occurs under catalytic HDO conditions. This approach has proven successful in the past and will continue to provide answers to fundamental questions that can't be answered using a lab-scale catalytic reactor.

1.4 Research Roadmap

Because of the historic – and continued – interest in catalytic HDS, the catalyst system used for HDO is no stranger to surface chemistry studies. The most common approach is to use a single crystal of Mo as the catalyst model, usually

the (100) or more closely packed (110) surface. For HDS, the model reactant most studied is the five membered ring thiophene, although smaller rings and straight chain hydrocarbons have been examined as well[21,22,23,24]. Both the clean Mo surface, and the S and C modified surfaces have been examined.

This study focuses on the chemisorption and subsequent decomposition of furan on the (110) face of a Mo single crystal, both clean and with sulfur overlayers. An overview of the goals of the research is presented in the list below.

1. Characterize the clean and sulfur-modified surface of Mo(110), using Auger electron spectroscopy (AES) and low energy electron spectroscopy (LEED).
2. Investigate the furan/Mo(110) and furan/S/Mo(110) systems using AES, LEED, and temperature programmed reaction spectroscopy (TPRS). Also look into the effect of preadsorbed and background hydrogen on the furan reaction in an attempt to better model the catalytic conditions (6–15 MPa of hydrogen).
3. Examine the interactions of H_2/D_2, CO, C_2H_4, and C_3H_6 with the clean and sulfur modified Mo(110) surfaces (using the same tools as above) to investigate possible pathways which the furan reaction may follow.

---

21. F. Zaera, E.B. Kollin, and J.L. Gland, Surface Sci., 184, 75, (1987)

22. A.J. Gellman, M.H. Farias, M. Salmeron, and G.A. Somorjai, Surface Sci., 136, 217, (1984)

23. D.G. Kelly, M. Salmeron, and G.A. Somorjai, Surface Sci., 175, 465, (1986)

24. J.T. Roberts and C.M. Friend, Surface Sci., 186, 201, (1987)

The following chapters describe, in more detail, the equipment and experimental techniques used in this research and the methods by which the data were generated and collected. The final chapters discuss the results and present conclusions based on this work and the literature.

CHAPTER 2: EXPERIMENTAL

2.1 INTRODUCTION

As was mentioned in the previous chapter, UHV and electron spectroscopies can be used to model the behavior of catalytic hydroprocessing catalysts. UHV keeps the sample free of background contamination for long enough to do an experiment and provides a relatively obstacle-free environment for surface sensitive electrons. Single crystal surfaces and model reactants simplify the complicated systems that are under investigation, and provide ways to collect fundamental information about reaction pathways and adsorbate interactions.

This chapter discusses the following:

- The UHV apparatus used in this research
- Sample preparation, cleaning, and dosing
- The techniques used in this research: Auger electron spectroscopy (AES), low energy electron diffraction (LEED), and temperature programmed reaction spectroscopy (TPRS)

2.2 ULTRA HIGH VACUUM CHAMBER

The UHV chamber is a multi-port stainless steel vessel, comprised of a stationary bottom and removable top. The lower portion is a standard 12 port unit that contains most of the pumping apparatus, consisting of nine ion pumps powered by a Perkin-Elmer 5 kV power supply, and a titanium sublimation

pump (TSP) which uses the same power supply to evaporate Ti (which "gets" any gas molecules it comes in contact with). It also houses the Granville-Philips ionization gauge which measures a current (generated by ionized gas molecules) that is proportional to the pressure in the chamber. The current is converted into pressure units (torr) by the circuitry in the gauge readout housing.

The top of the chamber was custom-designed for this lab; it has 17 ports, some of which are dedicated to such essentials as the sample manipulator (on a 6 inch port at the center top of the chamber), the view port (a 10 inch side port with a glass and stainless cover), the AES/LEED apparatus, and the TPRS mass spectrometer. Other ports are used for high precision leak valves and the electrolytic sulfur source.

In order to achieve UHV, the chamber is first sealed and "rough" pumped using an oil diffusion pump and two liquid nitrogen (LN_2) cooled sorption pumps. Once a pressure of 10^{-5} torr is reached, the ion pumps and TSP take over the pumping duties. While at atmospheric pressure, the inner walls of the chamber are covered with adsorbed gas molecules. As the chamber is evacuated during pump-down, these molecules begin to desorb, slowing the decrease in pressure. To speed up the desorption and evacuation process, the entire chamber is "baked" in a portable oven. Usually the baking process takes 3–4 days, eventually reaching a temperature of 130° C.

After removing the oven – but while the chamber is still hot – the filaments used by the various instruments and gauges are degassed (operated at a slightly

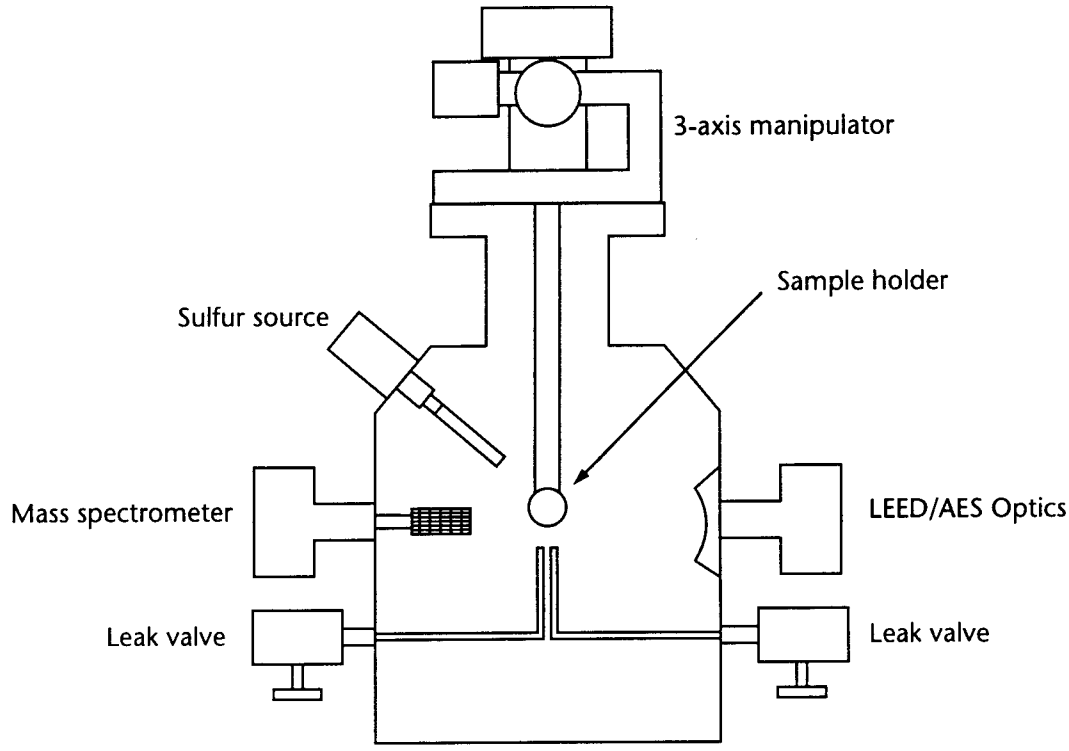

Figure 2-1. Schematic diagram of UHV chamber

higher current/temperature than normal for a few minutes). Because the chamber walls are still hot, any gases desorbing from the filaments are pumped out instead of re-adsorbing onto the walls. Once the chamber cools to room temperature the operating pressure inside is approximately 3 x 10^{-10} torr.

2.2.1 Sample Handling

In order to position the Mo(110) sample in several different locations for the different instruments, it is attached to a Vacuum Generators, UK precision

manipulator. The manipulator is capable of translation along the x (left to right, facing the chamber viewport), y (front to back), and z (up and down) axes and rotation in the xy plane and azimuthally. In addition, once a position is noted, calibrated controls make it easy to return the sample to the position with very little variation. This is important for studies that focus on a small part of the sample surface.

The flange through which the manipulator is attached contains several mini-flanges that are used for electrical, thermocouple, and LN_2 feedthroughs. Since both high voltages and high currents are used in the system; keeping them electrically isolated is essential.

2.2.2 Sample Preparation

The Mo(110) sample is 1.3 cm in diameter and 0.1 cm thick. It was oriented to within $\frac{1}{2}^{\circ}$ of the 110 plane using Laué x-ray back-reflection and wire-saw cut off a single crystal boule. It was polished mechanically, using standard metallographic polishing methods[1], to a roughness of 0.05 μm. Further polishing was carried out in the vacuum chamber by annealing at high temperatures during the sample cleaning process (see the section titled: "Sample Cleaning" on page 17).

1. Metals Handbook, American Society for Metals, Cleveland, OH, pp. 159-162, (1948)

After polishing – but before placing the sample in the UHV chamber – the sample is cleaned in a series of solvents to remove any traces of organic contamination. The cleaning solution program is listed below:

1. Sonicate in laboratory glassware detergent.
2. Rinse with distilled water.
3. Sonicate in acetone.
4. Sonicate in methanol.
5. Sonicate in trichlorethane.
6. Dry with a heat gun.

The sample holder consists of 0.25 mm Ta foil wrapped around the edge of the crystal which is mounted to a Macor machinable ceramic block by two Ta posts (see Figure 2-2 below). Temperature is monitored by a W-5%Re/W-26%Re (Type C) thermocouple sandwiched between the edge of the crystal and the Ta foil. Mounted 0.1 cm behind the crystal is a W filament for electron beam heating. The crystal is thermally connected, using a braided copper strap, to a liquid nitrogen cooled copper block. This arrangement allows resistive heating up to 1000° C at up to 15°/sec, electron beam heating to 2000° C, and cooling to -70° C.

The resistive heating power supply (70A, 7V) is interfaced with a programmable temperature controller, which, using feedback from the thermocouple, makes it possible to carry out linear (with time) temperature ramps. This capability is essential for TPRS, which is discussed in the section titled "Temperature Programmed Reaction Spectroscopy (TPRS)" on page 33.

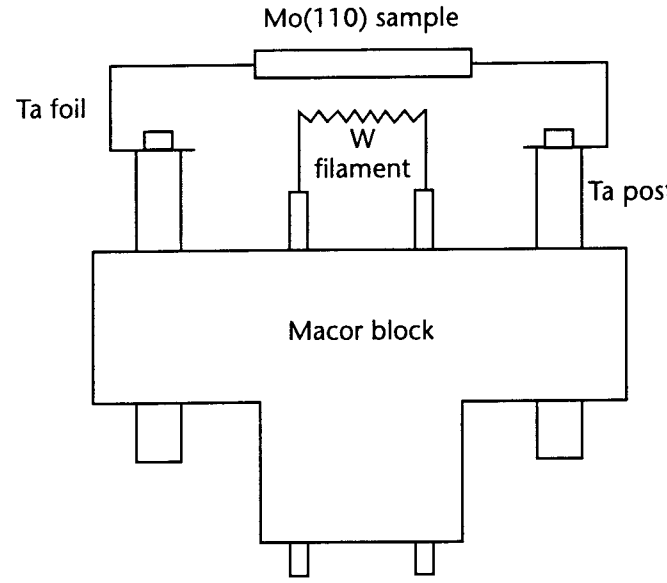

Figure 2-2. Schematic diagram of sample holder (side view)

The electron beam heating system[2] uses two power supplies, one (10A, 16.5V) is used to "light" the electron source filament (taken from a double beam auto headlight), and the other (1.5A, 600V) is used to provide the bias voltage between the filament and the sample. The higher the voltage drop between the filament and the sample, the more energetic the electrons are that impact the back of the sample and the faster the heating rate and the higher the final temperature. During electron beam heating the temperature is monitored using an electrically isolated voltage meter, floating at the bias voltage (~500 volts).

To cool the sample, liquid nitrogen is circulated through a copper block behind the sample holder. The copper block is connected to the back of one of the Ta

2. M.E. Jones, Dept. of Chem., Univ. of CO Boulder, Personal communication, 1990

posts on the sample holder with a braided copper strap. Although this arrangement is not as efficient as a copper block in direct contact with the sample, the temperatures used in the sample cleaning process would melt the copper in a matter of seconds.

2.2.3 Sample Cleaning

After introducing a "clean" sample into the chamber, it is necessary to further clean the surface. Carbon and oxygen are common surface contaminants. The sample is cleaned by oxidizing the C on the surface by heating for five minutes at 700° C in 5 x 10^{-8} torr flowing O_2. The surface oxide is then removed by electron beam heating for 30 secs at 1550° C in vacuum. This cleaning cycle is repeated until the ratio of the C (278 eV) to Mo(221 eV) AES signals is less than 0.01 (see the section titled "Auger Electron Spectroscopy (AES)" on page 19 for a detailed description of AES). Four cleaning cycles usually remove all normal C buildup during the course of experiments. Other contaminants, such as sulfur, are usually removed from the surface with a single 30 second flash to 1550° C.

2.2.4 Sample Dosing

To better model the molybdenum HDO catalyst, the single crystal sample was studied both clean and with carefully calibrated sulfur overlayers. Sulfur is introduced onto the surface of the crystal using a solid state electrochemical cell (Pt | Ag | AgI | Ag_2S | Pt) across which a voltage is applied[3]. This generates a

molecular beam of S, predominantly S_2 at the voltages and temperature used in this work. The sample is positioned directly in front of the outlet of the S cell (approximately 2 mm away) for dosing.

In most cases the sulfur cell was used to deposit multilayers of S on the crystal surface. By annealing the sample (heating for extended times) at various temperatures, a variety of S coverages can be produced. More detail on the interactions of S with the Mo(110) surface is given in the section titled "Clean and Sulfur Modified Mo(110)" on page 49.

The UHV chamber is equipped with two high-precision leak valves that are used to introduce small amounts of gases to the clean or sulfur-modified Mo(110) surface. A stainless steel gas manifold allows two different gases to be stored behind the leak valves at a given time. One leak valve was used for oxygen (for sample cleaning); the other was used for furan, hydrogen, carbon monoxide, ethylene, or propylene, depending on the experiment.

The standard method used to introduce gases to the sample was to establish a constant pressure of the gas in the chamber and record the duration (in seconds) of the exposure. The exposure is usually reported in units of torr·secs, also known as the Langmuir. (See the section titled "Adsorption Isotherms" on page 38 for more information on Langmuir and his coverage unit.) For situations where saturation of the surface is desired, the sample is situated within 0.5 cm of the leak valve outlet during dosing. The resulting chamber pressure, measured by the ionization gauge (30 cm below the leak valve), is lower than

---

3. W. Heegemann, K.H. Meister, E. Bechtold, and K. Hayek, Surf. Sci., **49**, 161, (1975)

the local environment at the sample surface. Saturation, confirmed by AES, is obtained much more quickly using this method, although the exact exposure in Langmuirs can not be calculated reliably due to the pressure differential.

Another factor that is not corrected for is the difference in ionization gauge sensitivities to different gases. For each gas, however, the ionization gauge measurement provides a good relative value for the exposure. A more quantitative measure of the exposure is provided by AES.

All gases used in this work were obtained from Matheson Scientific, were 99.99% pure, and were used without further purification.

2.3 Auger Electron Spectroscopy (AES)

AES is one of the most common tools used in surface chemistry. It is a fairly sensitive probe (<0.01 monolayer) of the surface composition of a substrate that can also provide information about the form and amount of surface contaminants. Together with LEED, it provides the foundation for studies investigating surface structures and reactions.

2.3.1 Theory

Auger electron spectroscopy is named after Pierre Auger, who first described the process in 1925[4]. The Auger process is described below:

4. P. Auger, J. Phys. Radium, **6**, 205, (1925)

1. A core level electron is ejected from a surface atom by an incident electron beam (1–5 keV). See Figure 2-3 below.
2. The atom then does one of two things:
   - Emits an x-ray when a valence shell electron "falls" to fill the core level hole (especially when the binding energy of the core electron is >2 keV)
   - Emits a valence shell electron when a different valence shell electron fills the core hole. The emitted electron is called an Auger electron; its kinetic energy is characteristic of the atom from which it came and not of the exciting radiation.

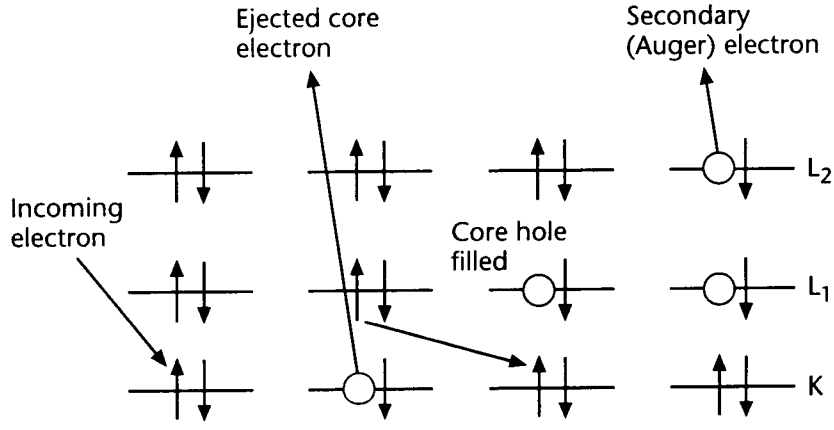

Figure 2-3. Energy level diagram for a KL_1L_2 Auger electron

The energy of the Auger electron in this example is given by

$$E_{kin} = E_K - E_{L_1} - E_{L_2} \qquad \text{Equation 2-1}$$

where E_{kin} is the kinetic energy of the Auger electron, E_K is the binding energy of the ejected core electron, E_{L_1} is the binding energy of the electron that filled the core vacancy, and E_{L_2} is the binding energy of the Auger electron. The letters K (core or 1s electrons), L_1 (2s electrons), and L_2 (2p electrons) are from conventional x-ray spectroscopic nomenclature and are used to describe Auger electrons by their energy level origin.

The quantity (E_K - E_{L_1}) can also be emitted as fluorescence, in a competing mechanism to the Auger process, especially as atomic weight increases. Although AES is usually used for relative coverage information, quantitative data is possible if the Auger-to-fluorescence emission ratio is known.

Auger electrons are surface sensitive mainly due to two reasons. First the incident electron beam can only penetrate a certain distance into the bulk of the sample (<350 Å) before it loses too much energy to be able to ionize a core electron. This energy loss is mostly due to collisions which result in outer shell ionizations, although inner shell ionizations, plasmon losses, and elastic processes that redirect the beam direction contribute also. Second, once an Auger electron is created, it faces the same energy loss mechanisms as the incident beam in its escape. Since its initial energy is lower than the incident beam; an Auger electron can only escape from the top few layers of the sample.

In practical terms, the AES collector measures a current due to electrons striking the collector grid. At the same time that Auger electrons are being emitted, a much larger number of back-scattered secondary electrons (mainly due to ionizations in the valence band of the surface atoms) and elastically scattered

primary electrons are emitted. The grid voltage (the retarding field) is ramped from a low initial voltage to a higher final voltage (close to the exciting electron beam voltage). As the grid voltage increases, fewer and fewer electrons are energetic enough to reach the collector, thus the measured current, when plotted as a function of the retarding field voltage, appears as a smoothly decreasing curve, with some small bumps (see Figure 2-4 below).

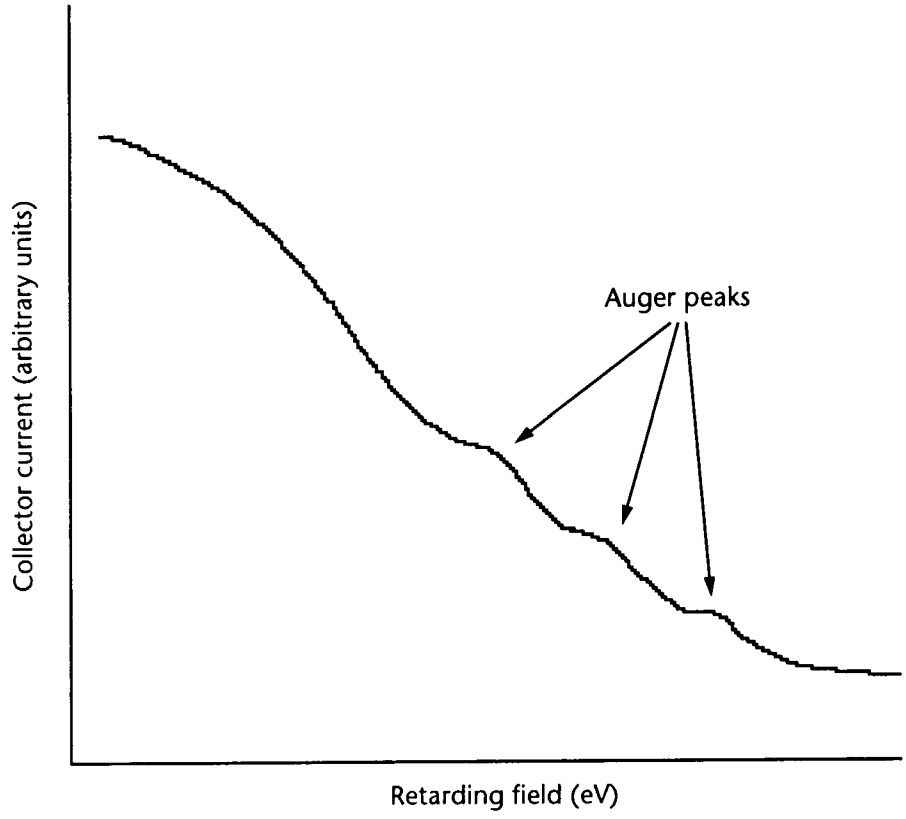

Figure 2-4. Plot of Collector Current vs. Retarding Field for an RFA AES system

To obtain the energy distribution of the electrons striking the collector, it is necessary to differentiate the collector current with respect to the retarding field. Instrumentally, this is done by superimposing a small a.c. voltage on the retarding field and tuning the collector to the same a.c. modulation. A "lock-in"

amplifier is used to selectively enhance the modulated signal, yielding the energy distribution as a function of the retarding field.

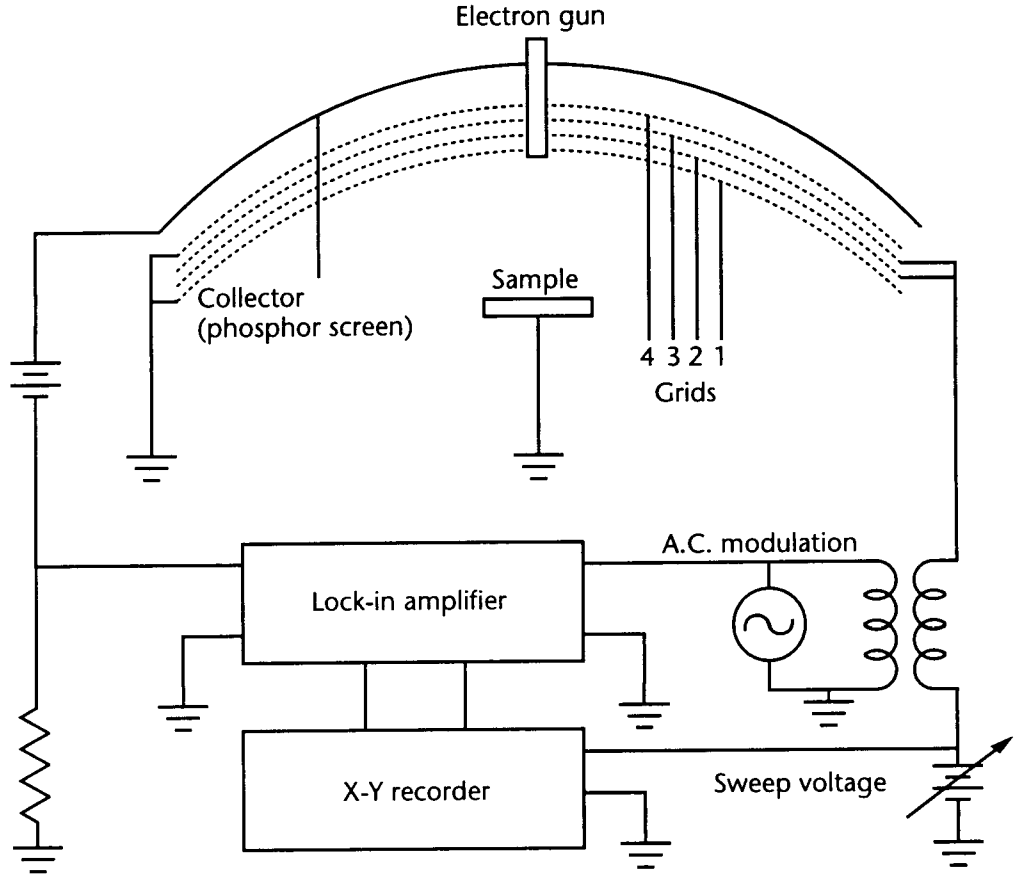

Figure 2-5. Circuit diagram of RFA-AES system

It is necessary to carry out one more differentiation of the current with respect to the retarding field to obtain the characteristically shaped Auger peaks commonly seen in surface chemistry studies. This is accomplished by tuning the collector to the second harmonic (twice the frequency) of the a.c. modulation voltage frequency[5].

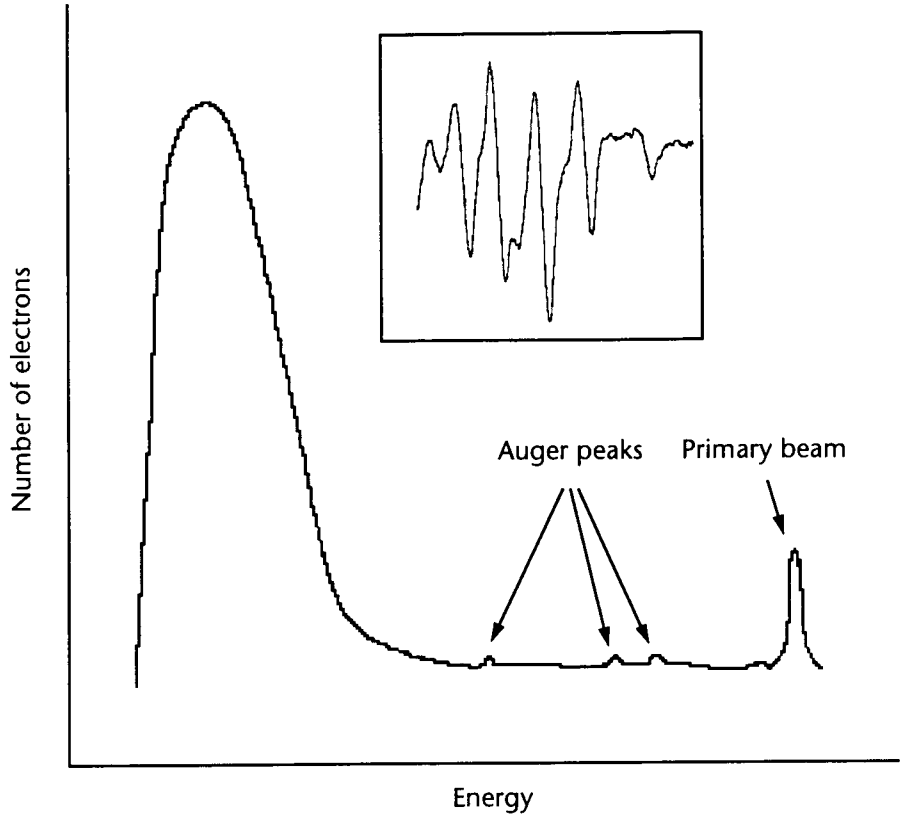

Figure 2-6. Energy distribution of backscattered electrons. Inset is a sample Auger trace which results from the derivative of the energy distribution curve.

The shape and position of peaks obtained in this manner can identify what is on the surface and provide a good relative measure of the surface concentration of the element. The ratio of the peak heights of the adsorbate and the substrate is the most common way to determine the relative surface concentration. In addition to "What?" and "How much?", AES can sometimes answer questions about the way in which an adsorbate bonds to the surface. This is especially

5. R.E Weber and W.T. Peria, J. Appl. Phys., **38**, 4355, (1967)

true for carbon on transition metals; AES peaks have different shapes for amorphous carbon overlayers (graphitic carbon), carbidic chemisorbed carbon, and adsorbed CO[6,7,8].

2.3.2 Experimental

The Auger apparatus used in this study is a retarding field analyzer (RFA) model. One of the principle advantages of an RFA Auger system is that the equipment used to generate the exciting electron beam and to detect the emitted electrons can also be used for LEED work. Switching the potentials on the different grids in the collector is all that is required to convert from one to the other.

A Varian model 891-2145 electron gun control module was used to collect Auger spectra, typically at a beam energy of 1750 eV and a beam current of 20.0 μA. A modulating signal of 2.5 kHz was applied to the retarding field; the lock-in amplifier was tuned to twice the modulation frequency (the second harmonic) to sample the second derivative of the collector current, which was sent to an X-Y recorder. The surface concentrations of C and S, and the Mo substrate, were monitored using the following Auger emissions: Mo(221 eV), S(152 eV), and C(272 eV).

---

6. G. Panzner and W. Diekmann, Surf. Sci., **160**, 253, (1985)
7. R. Ducros, G. Piquard, B. Weber, and A. Cassuto, Surf. Sci., **54**, 513, (1976)
8. K. Ishikawa and Y. Tomida, J. Vac. Sci. Technol. **15**, 1123, (1978)

2.4 Low Energy Electron Diffraction (LEED)

Every single-crystal surface can be viewed as a two dimensional lattice, although not all have the same periodicity as the bulk crystal (i.e. not all are "bulk terminated"). Some surfaces reconstruct or relax, driven by reductions in the surface free energy (ΔG_{surf}). But in most clean metals there is less than a 10% difference between atom spacings on the surface and in the bulk.

X-ray diffraction is a valuable tool for determining bulk properties of three dimensional solids, but x-rays are far too energetic to provide surface information. Low energy electrons (E_{kin} = 20–300 eV) are a much better choice since they meet both of the criteria for surface structure sensitivity listed below:

- Low energy electrons have a de Broglie wavelength ($\lambda \sim 1$Å) in the right range for diffraction from a crystal surface. The de Broglie condition for diffraction requires that the incident wave be of approximately the same frequency as the grid spacing.
- Low energy electrons only penetrate the first few layers of the surface before either elastically back-scattering or losing energy due to ionization events, plasmon losses, or other inelastic collisions.

2.4.1 Theory

LEED takes advantage of the wave properties of electrons to obtain structural information about a surface. A beam of low energy electrons is directed at an ordered surface and is diffracted toward a collector by the periodicity of the

surface. Charged grids in front of the collector reject all electrons that have not been elastically scattered; the 1–2% that are energetic enough pass through the grids and strike a phosphor screen, appearing as spots. The geometry of the spots on the phosphor screen (i.e. the LEED pattern) is reciprocally related to the real space geometry of the surface lattice.

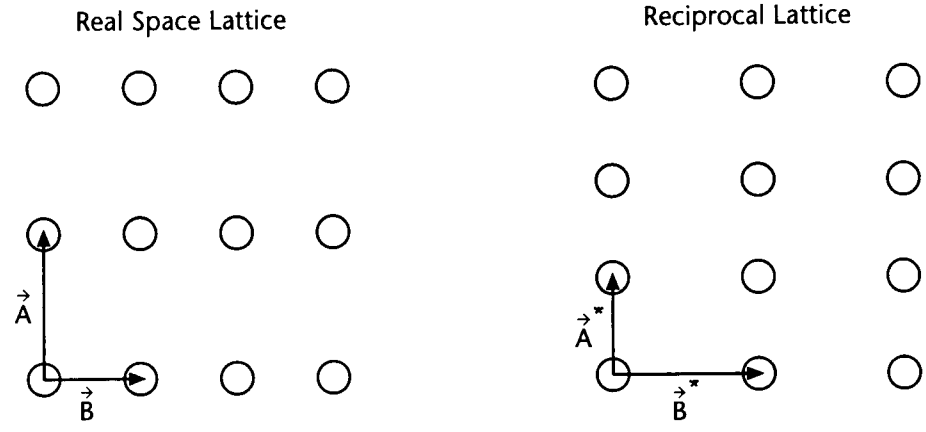

Figure 2-7. Real space and reciprocal lattices and their unit vectors

A rectangular two dimensional lattice with lattice constants $\vec{A}$ and $\vec{B}$, as depicted in Figure 2-7 above, yields a reciprocal lattice with lattice constants $\vec{A}^* = \frac{1}{\vec{A}}$ and $\vec{B}^* = \frac{1}{\vec{B}}$, where $\vec{A} \perp \vec{A}^*$ and $\vec{B} \perp \vec{B}^*$. From any point on the reciprocal lattice, any other point can be specified using an equation of the form

$$g_{hk} = \lambda\left(h\vec{A}^* + h\vec{B}^*\right) \qquad \text{Equation 2-2}$$

where g_{hk} is known as the reciprocal lattice vector.

For a LEED spot to appear, constructive interference must occur. The Laué condition (Equation 2-3) requires that the spacing between diffracted waves be an integral number of wavelengths for constructive interference to occur.

$$A(\sin\theta_f - \sin\theta_i) = n\lambda \qquad \text{Equation 2-3}$$

A is the separation between scatterers, θ_i is the angle between the incident wave and the surface normal, θ_f is the angle between the diffracted wave and the surface normal, and λ is the wavelength of the incident wave. In vector form this can be written

$$\vec{A} \bullet \Delta\vec{S} = n\lambda \qquad \text{Equation 2-4}$$

where

$$\Delta\vec{S} = (\vec{S}_f - \vec{S}_i) \qquad \text{Equation 2-5}$$

and $\vec{S}_f$ and $\vec{S}_i$ are vectors describing the diffracted and incident waves. From these equations, it is evident that there is a reciprocal relationship between the lattice unit vector $\vec{A}$ and the LEED spots, which are determined by $\Delta\vec{S}$.

The Laué conditions in two dimensions are:

$$\vec{A} \bullet \Delta\vec{S} = h\lambda \qquad \text{Equation 2-6}$$

and

$$\vec{B} \bullet \Delta\vec{S} = k\lambda \qquad \text{Equation 2-7}$$

where h and k are integers. Upon rearrangement in terms of the reciprocal vectors these equations yield:

$$\Delta\vec{S} = \lambda\left(h\vec{A}^{*} + h\vec{B}^{*}\right) = g_{hk} \qquad \text{Equation 2-8}$$

This reveals the fact that there is a direct and simple relationship between the LEED pattern and the reciprocal lattice. This relationship allows the real space lattice to be deduced from the observed LEED pattern, although it doesn't reveal the nature of the scattering centers, which, as is described below, may be atomic or molecular.

If an adsorbate forms an ordered overlayer on the substrate, the new surface unit vectors can be described as

$$\left|\vec{A_1}\right| = m\left|\vec{A}\right| \qquad \text{Equation 2-9}$$

and

$$\left|\vec{B_1}\right| = n\left|\vec{B}\right| \qquad \text{Equation 2-10}$$

where m and n are integers. Simply put, the new surface unit vectors are multiples of the clean substrate unit vectors, although they may not be parallel to the substrate. Wood notation, named for Elizabeth Wood, is one way to describe a reconstructed surface or one with an ordered overlayer. The general form of the Wood notation is given below.

$$q(m \times n)R\theta^{\circ} \qquad \text{Equation 2-11}$$

The integers m and n are from Equations 2-9 and 2-10 and q is either p for a primitive unit cell or c for a centered unit cell. If the overlayer vectors are rotated by θ° to the substrate vectors then Rθ° is appended to the notation.

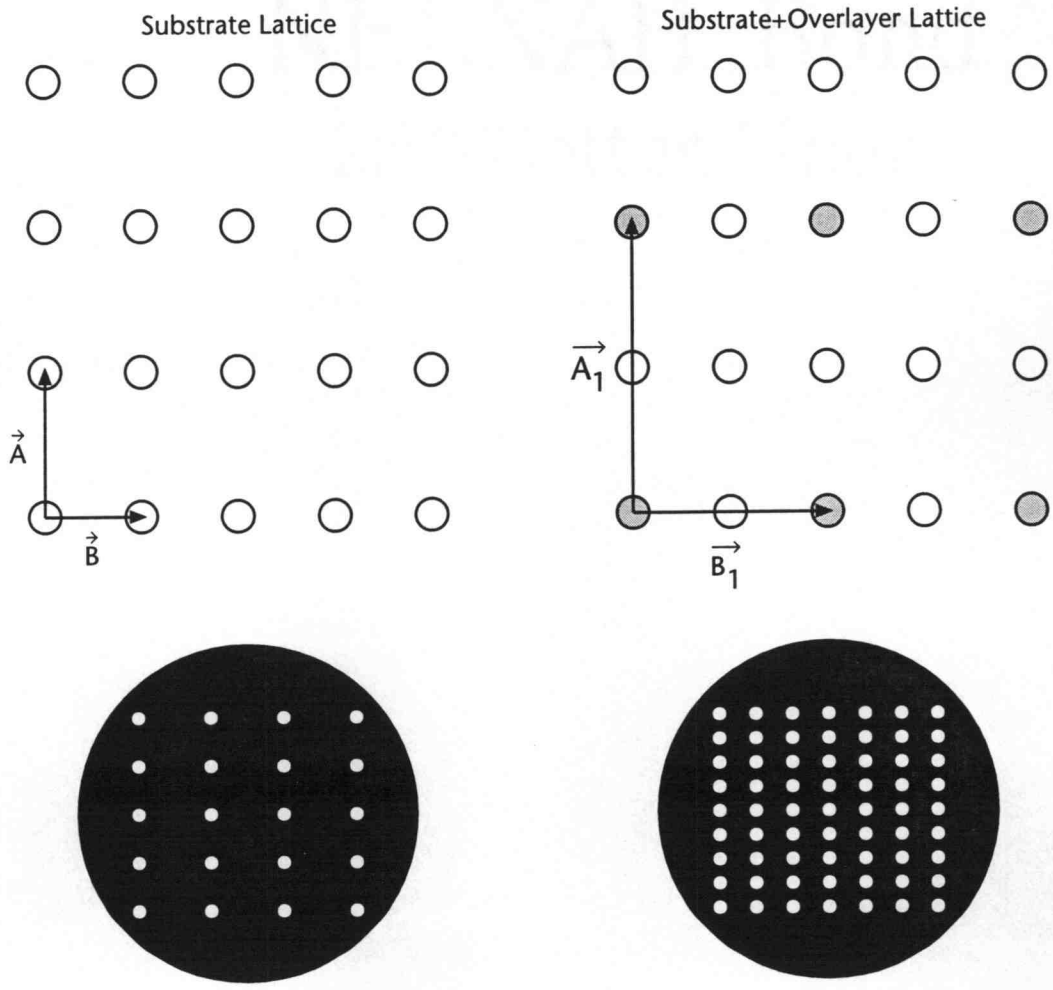

Figure 2-8. Clean substrate lattice and LEED pattern and p(2x2) overlayer lattice and LEED pattern

In Figure 2-8 above, the reciprocal relationship between the LEED pattern and the surface order is evident. The p(2x2) overlayer surface gives rise to a LEED pattern with twice the periodicity as the clean substrate (p(1x1) LEED pattern).

If an additional adatom is placed in the center of each p(2x2) cell, the result is a c(2x2) lattice. The new unit vectors are not parallel to the clean substrate unit vectors, but the resulting LEED pattern is very similar to that of the clean substrate.

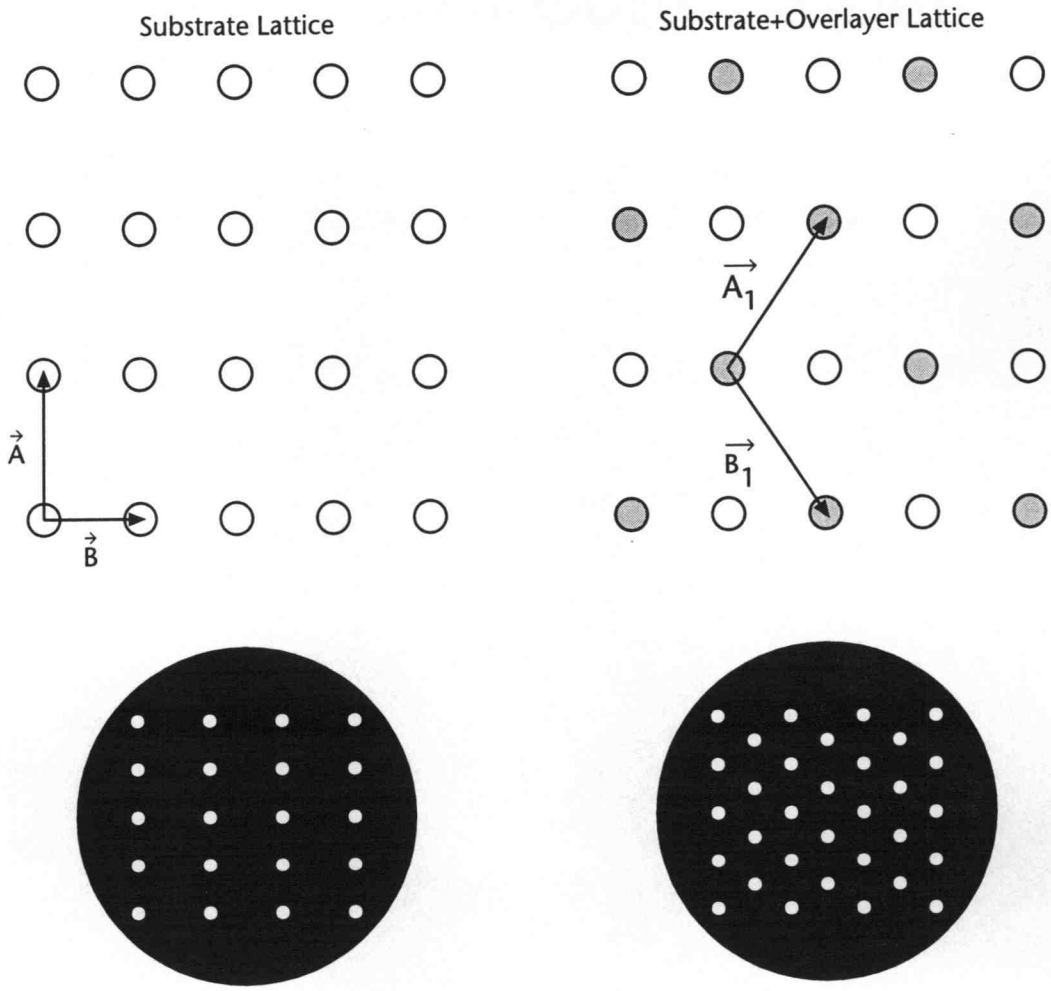

Figure 2-9. Clean substrate lattice and LEED pattern and c(2x2) overlayer lattice and LEED pattern

As is evident in Figure 2-9 above, if an adsorbed layer causes the clean surface's p(1x1) to change to a c(2x2) LEED pattern, there is a good chance that the

surface is covered by 0.5 monolayers of the adsorbate (i.e one adsorbate atom or molecule for every two substrate atoms). AES data and TPRS spectra are often used to bolster the sometimes ambiguous evidence that LEED provides in this type of study. LEED, when used as described above, can only provide the relative size and shape of the surface unit cell. A different type of LEED study, in which the intensity of each diffraction spot is analyzed as a function of the electron beam energy, can provide adsorption site, bond angle, and bond length information. However that type of study was not used in this research and will not be discussed.

2.4.2 Experimental

As was mentioned in the section on AES, the same equipment can be used for both LEED and RFA AES. The four grid LEED optics is controlled by a Varian control module, model 981-1948. The fluorescent screen (collector) on which the LEED spots appear is ~6 kV above ground, while the first and last of the four grids are set to ground in order to eliminate any electric fields that might affect the diffracted electrons. The suppressor grids, (i.e. the center two grids), are held at a negative potential slightly less than the beam energy in order to reject any inelastically scatter electrons. Only elastically scattered electrons (usually from a single elastic collision) with an energy close to the beam energy can make it past the suppressor grids to the collector. Once past the suppressors, electrons are accelerated by the 6 kV bias so that they strike the collector with enough energy to cause a spot to appear.

A low-light video camera is used to monitor the LEED patterns, which are displayed on a video monitor. Use of the video equipment makes it easy to

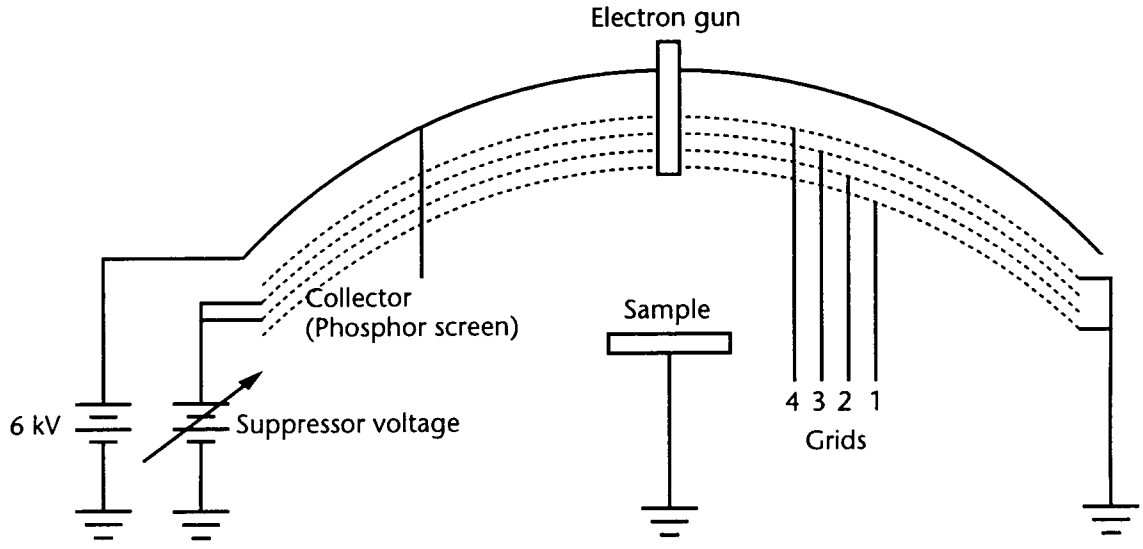

Figure 2-10. Schematic of four grid LEED optics

record dozens of LEED patterns on video tape, without the difficulty and expense associated with still cameras. The video images are digitized using an Oculus-200 frame grabber interfaced with an Intel-based PC.

In this study, LEED (together with AES) was used to confirm the surface structure of the clean and S-modified Mo(110) sample. The C-modified Mo(110) was also examined using LEED.

2.5 Temperature Programmed Reaction Spectroscopy (TPRS)

TPRS, also know as thermal desorption spectroscopy (TDS), temperature programmed desorption, and thermal desorption mass spectroscopy, makes it

possible to probe the surface coverage and the bonding sites in which an adsorbate is bonded. In addition, reactions that occur on or near the surface can be monitored by measuring the composition of evolving gases during heating. It is a common technique in surface science, almost as ubiquitous as LEED and AES.

2.5.1 Theory – Adsorption

When a gas molecule hits a surface it generally does one of three things:

- it bounces off elastically
- it bounces off inelastically
- it adsorbs, either weakly (physisorption) or strongly (chemisorption)

Surface studies aren't usually focused on the molecules that bounce off; it's the ones that stick that are the most interesting.

2.5.1.1 *Physisorption*

When a gas molecule is weakly bound to the surface, it is said to be physisorbed, with binding enthalpies (ΔH_{ph}) of about -40 kJ/mol. Physisorption is a result of the combination of weak, short range attractive (van der Waal's forces) and repulsive forces. The attractive forces, proportional to $-\left(\frac{1}{R}\right)^6$, are usually a combination of London forces (i.e. induced dipole interactions) and dipole forces. The repulsive forces, due to the interactions of the electron clouds of the approaching species, have been empirically determined to be

proportional to $\left(\frac{1}{R}\right)^{12}$ by Lennard-Jones[9], one representation of whose famous equation is reproduced below.

$$E = 4\Delta H_{ph}\left[\left(\frac{\sigma}{R}\right)^{12} - \left(\frac{\sigma}{R}\right)^{6}\right] \qquad \text{Equation 2-12}$$

where ΔH_{ph} is the potential well depth, R is the distance between the gas molecule and the surface, and σ is described in Figure 2-11 below.

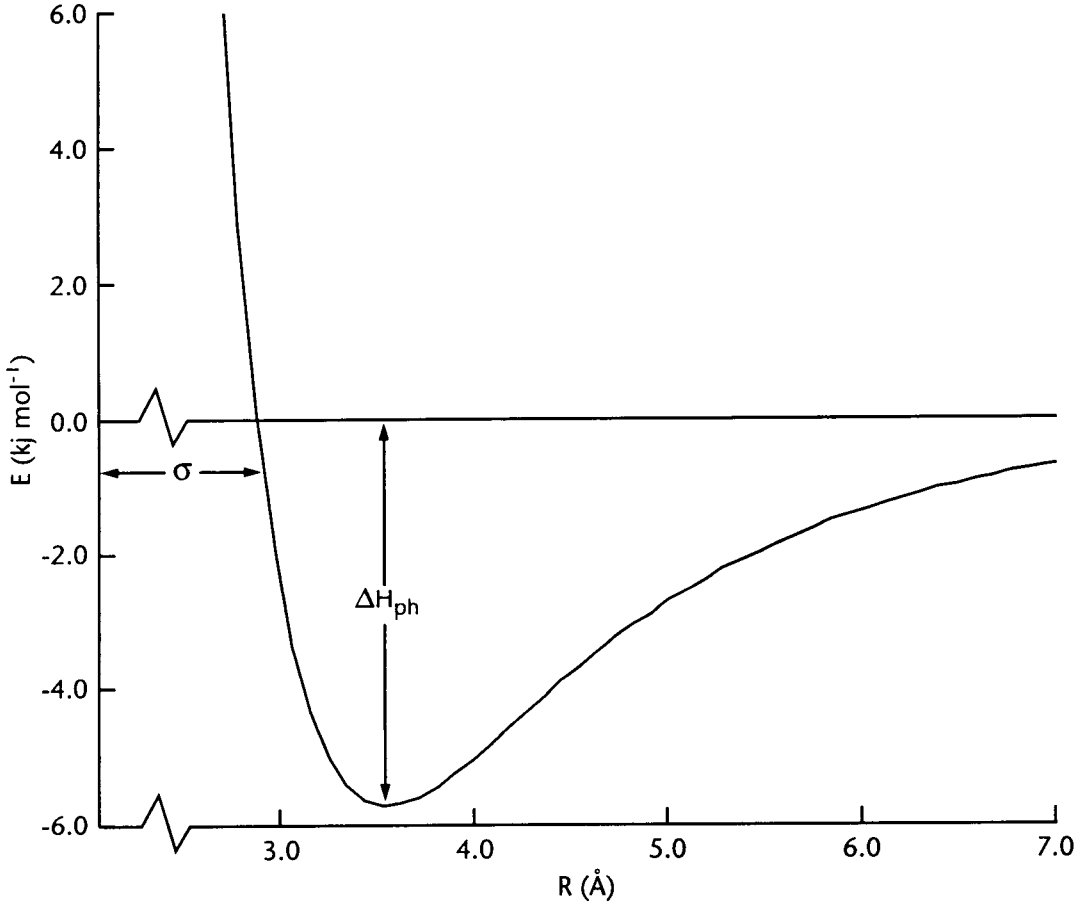

Figure 2-11. Lennard-Jones potential for an adsorbate-substrate system with a

9. J.E. Lennard-Jones, Trans. Farad. Soc., **28**, 333, (1933)

well depth of 5.8 kJ/mol and σ = 2.9

Physisorption is a non-specific process – the identity of the gas and the substrate are not particularly important. Much more important is the temperature; the weak nature of the physisorption process ensures that, in general, it will only occur with any frequency at low temperatures. As the temperature increases, the physisorbed molecule usually does one of the following:

- Migrate across the surface, still weakly bound
- Desorb back into the gas phase
- Transfer to a much more tightly held chemisorbed state

2.5.1.2 *Chemisorption*

In contrast to physisorption, chemisorption is not only much more energetic, it is also quite dependent on the specific gas and substrate involved; even different faces of the same metal crystal can have different interactions with the same gas. In fact, chemisorption is very similar to bond formation, complete with sharing of electrons, with typical binding enthalpies (ΔH_{ch}) of about -400 kJ/mol. The substrate–gas bond can be viewed as a diatomic bond; the Morse potential is a good representation of this:

$$E = D_e(1 - e^{-a(R - R_e)})^2 \qquad \text{Equation 2-13}$$

where D_e is the potential well depth, a is a constant, R is the separation between the gas and the substrate, and R_e is the equilibrium separation.

In most cases, an approaching gas molecule is first captured into a physisorbed state. Then, depending on the overlap between the physisorbed and chemisorbed states, the gas molecule can move "downhill" into the chemisorbed state via a non-activated process, or it may require a "push" (specifically one equal to or greater than the activation energy) to move into the chemisorbed state. The latter process is illustrated in Figure 2-12.

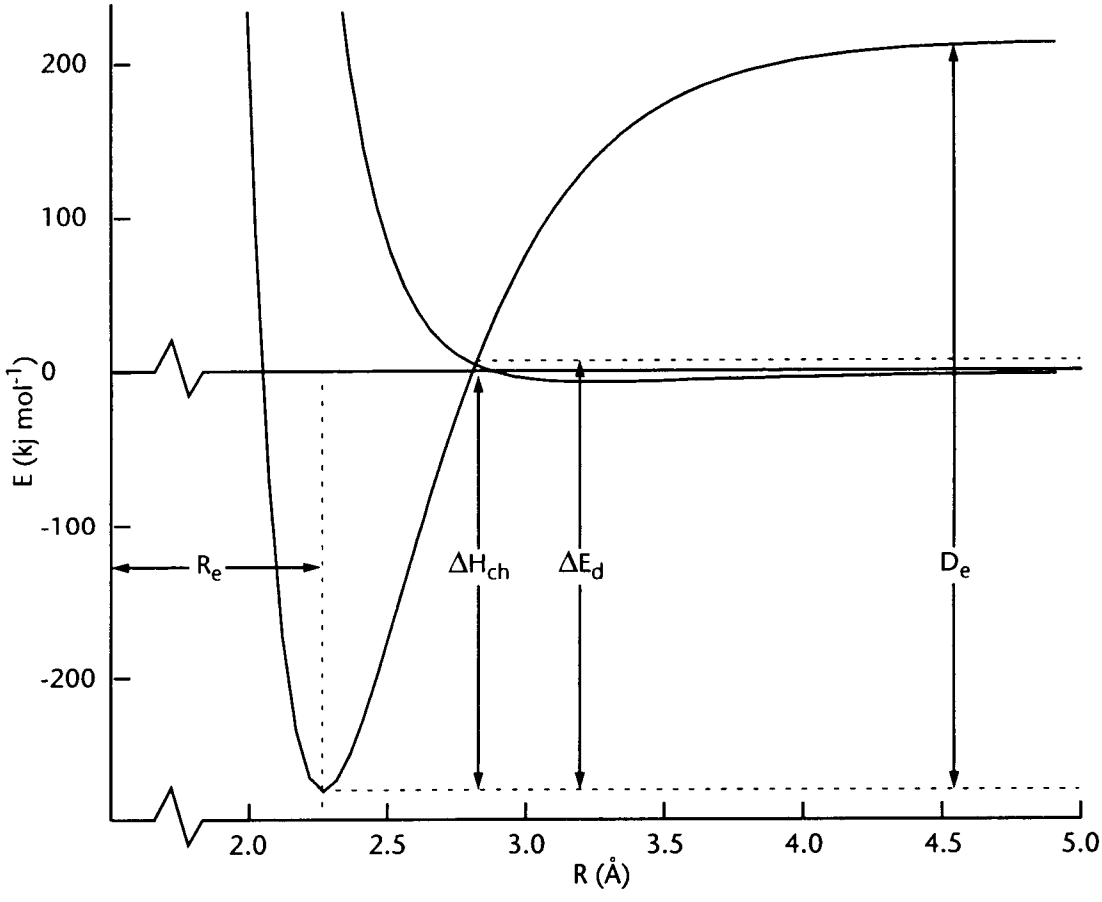

Figure 2-12. Adsorption potential for activated adsorption

The activation energy, E_a, is the difference between ΔH_{ch} (the enthalpy of chemisorption) and ΔE_d (the energy of desorption).

2.5.1.3 *Adsorption Isotherms*

An adsorption isotherm is a way to describe how a substrate adsorbs a gas at a fixed temperature as a function of the gas pressure. The Langmuir isotherm is the most general, and, consequently, the most useful isotherm. Langmuir's model makes the following assumptions:

- The surface is homogeneous.
- The surface has a specific number of bonding sites, like a checkerboard, each of which can host one, and only one, adsorbate molecule. This limits the coverage to a monolayer.
- All bonding sites are degenerate and unaffected by increasing coverage, i.e the heat of adsorption is independent of coverage. The only effect of increasing coverage is the direct blocking of sites.
- Once bound to the surface, an adsorbate molecule neither migrates nor desorbs.

From the kinetic theory of gases' collision rate equation, the following equation for the rate of adsorption can be written:

$$\text{rate of adsorption} = \frac{p}{(2\pi mkT)^{1/2}} f(\theta) s^* \exp\left(\frac{-E_{ad}}{RT}\right) \qquad \text{Equation 2-14}$$

where $\frac{p}{(2\pi mkT)^{1/2}}$ is the rate of collision at the surface at pressure p, $f(\theta)$ is some function of fractional coverage, $\theta = \frac{\text{amount adsorbed}}{\text{amount for a monolayer}}$, $\exp\left(\frac{-E_{ad}}{RT}\right)$ is the Boltzmann factor, giving the fraction of molecules with energy greater than or equal to the adsorption activation energy, E_{ad}, and s^* is the sticking coefficient, i.e. the fraction of molecules with sufficient energy that actually adsorb. Similarly the rate of desorption is given by:

$$\text{rate of desorption} = k_d f'(\theta) \exp\left(\frac{-E_d}{RT}\right) \qquad \text{Equation 2-15}$$

where k_d is the rate constant for desorption, $f'(\theta)$ is a function of the fractional coverage, and $\exp\left(\frac{-E_d}{RT}\right)$ is the fraction of molecules with enough energy to desorb.

Setting the two equal yields

$$p = (2\pi mkT)^{1/2} \frac{k_d f'(\theta)}{s^* f(\theta)} \exp\left(\frac{E_{ad} - E_d}{RT}\right). \qquad \text{Equation 2-16}$$

In the most simple case, molecular adsorption, $f(\theta) = (1 - \theta)$ (the fraction of unoccupied sites) and $f'(\theta) = \theta$ (the fraction of occupied sites). The energy expression $(E_{ad} - E_d)$ is the enthalpy of adsorption; substituting and rearranging gives,

$$\theta = \frac{bp}{1 + bp} \qquad \text{Equation 2-17}$$

where

$$\frac{1}{b} = (2\pi mkT)^{1/2}\frac{k_d}{s^*}\exp\left(\frac{\Delta H_{ad}}{RT}\right). \qquad \text{Equation 2-18}$$

Equation 2-17 is the Langmuir isotherm for molecular (non-dissociative) adsorption, ($A_2(g)$ + surface site $\leftrightarrow$ A_2-surface bond). For dissociative adsorption, ($A_2(g)$ + 2 surface sites $\leftrightarrow$ 2 A-surface bonds), $f(\theta) = (1-\theta)^2$ and $f'(\theta) = \theta^2$ and the isotherm becomes,

$$p = \frac{1}{b}\left(\frac{\theta}{1-\theta}\right)^2 \qquad \text{Equation 2-19}$$

or solving for θ,

$$\theta = \frac{(bp)^{1/2}}{1+(bp)^{1/2}}. \qquad \text{Equation 2-20}$$

Figure 2-13 depicts the Langmuir isotherms for both cases outlined above.

Because dissociative adsorption requires two adjacent sites, the isotherm doesn't approach monolayer coverage as closely as the associative adsorption case, which requires only one site for bonding.

The biggest flaw in the Langmuir model is its assumption that the enthalpy of adsorption (ΔH_{ad}) is independent of increasing coverage. Also the related assumption that there is only one type of site on a surface can cause problems for surfaces with multiple bonding sites. In the multi-site case, the most reactive sites are filled first, when $|\Delta H_{ad}|$ is the largest. As those sites fill and other less

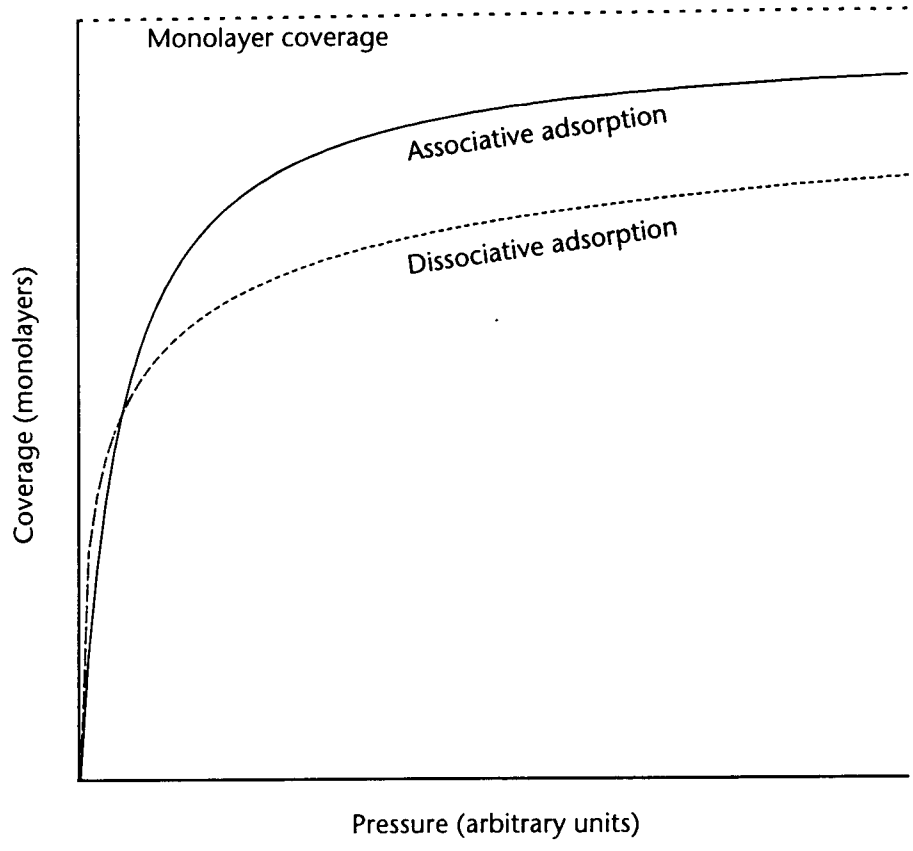

Figure 2-13. Langmuir isotherms for associative and dissociative adsorption

reactive sites begin to fill, $|\Delta H_{ad}|$ decreases. In addition, lateral interactions between adsorbed neighbors can reduce $|\Delta H_{ad}|$. There are isotherms that treat ΔH_{ad} as a function of coverage, but they are only applicable in certain coverage and pressure domains[10].

Despite its shortcomings, Langmuir's model is widely used and provides a baseline from which to make comparisons between widely varying systems.

---

10. R.P.H. Gasser, *An Introduction to Chemisorption and Catalysis by Metals*, p. 15, Oxford University Press, New York, (1985)

One very useful application of the Langmuir isotherm is the unit named after its creator. The Langmuir is defined as 1 torr·sec, and is a very common way to express surface coverage as a function of exposure in UHV studies.

2.5.2 Theory – Desorption

Another formulation for the rate of desorption from a surface is based on the Arrhenius equation

$$-\frac{dn}{dt} = \nu_a n^a \exp\left(\frac{-E_d}{RT}\right) \qquad \text{Equation 2-21}$$

where

- n is the surface concentration in atoms or molecules per cm^{-2}
- a is the kinetic order of the reaction
- ν is the frequency factor
- E_d is the activation energy for desorption.

For a linear heating ramp $T = T_0 + \beta t$ with rate $\beta \frac{K}{s}$, the desorption rate can be reformulated in terms of temperature[11],

$$-\frac{dn}{dT} = \frac{\nu_a}{\beta} n^a \exp\left(\frac{-E_d}{RT}\right). \qquad \text{Equation 2-22}$$

11. P.A. Redhead, Trans. Faraday Soc., 57, 641, (1961)

There are two competing factors that affect the rate of desorption, the exponential T factor which increases with time, and the surface concentration which decreases with time. Initially the exponential factor dominates, causing an upward curving P vs. T plot. As desorption continues, the surface concentration decreases to a point where it causes desorption rate to slow. This is why the P vs. T trace appears as a peak as in the example below.

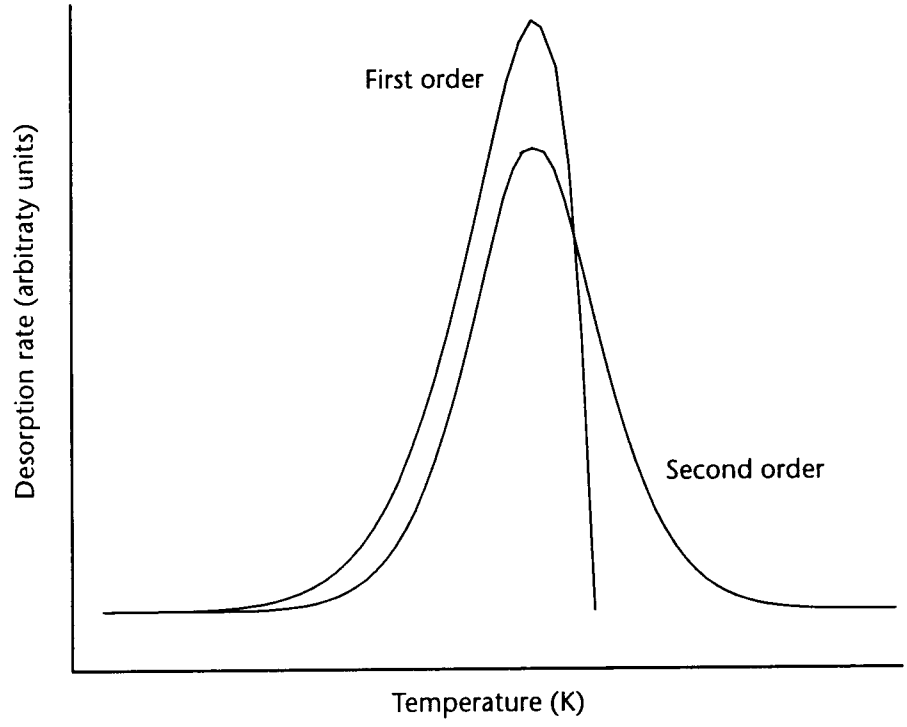

Figure 2-14. P vs. T plot for first and second order desorption kinetics

The shape of the desorption peak is dependent on the kinetic order of the desorption reaction, as is demonstrated in Figure 2-14 above. The first order peak is asymmetric about the maximum rate while the second order peak is

symmetric under ideal conditions (ignoring uneven heating of the sample and other instrumental difficulties).

At the maximum rate of desorption, $\frac{d^2n}{dT^2}$ is zero; differentiating Equation 2-22 with respect to T and rearranging yields,

$$\frac{\nu}{\beta}\exp\left(\frac{-E_d}{RT_p}\right) = \frac{E_d}{RT_p^2} \qquad \text{Equation 2-23}$$

for first order kinetics and

$$\frac{2\nu n_p}{\beta}\exp\left(\frac{-E_d}{RT_p}\right) = \frac{E_d}{RT_p^2} \qquad \text{Equation 2-24}$$

for second order kinetics. In Equation 2-23, there is no term for surface concentration, thus for a first order desorption reaction, the temperature at which the maximum desorption rate occurs, T_p, is independent of coverage. If a series of TPRS runs are carried out with different initial surface concentrations, and T_p does not change the desorption reaction is most likely first order. If ν is known, E_d can be calculated directly from Equation 2-23. Often, ν is assumed to be 10^{13} s^{-1}, since from transition state theory, the pre-exponential factor $\frac{kT}{h}$ is 1.6×10^{-13} at 300K. Another rationalization that supports this assumption is the fact that vibrational frequencies are of the order of 10^{13} s^{-1} and that surface vibrational modes are part of the desorption process. In most cases 10^{13} s^{-1} is used, or if another value is used it is reported along with the result for E_d.

A second way to calculate E_d is to vary the heating rate β over approximately two orders of magnitude (say from $1\frac{K}{s}$ to $100\frac{K}{s}$). If the natural logarithm of Equation 2-23 is taken and the result differentiated with respect to $\ln T_p$, the following relationship is obtained

$$\frac{d(\ln\beta)}{d(\ln T_p)} = 2 + \frac{E_d}{RT_p}. \qquad \text{Equation 2-25}$$

A plot of $\ln\beta$ vs. $\ln T_p$ can be made, which if linear, confirms the first order nature of the desorption. The slope of the curve is E_d. Unfortunately most TPRS equipment is not capable of the rigors of temperature ramps varied over such a wide range, so this method is not used very frequently.

The second order kinetics case is concentration dependent – as the initial surface coverage (n_0) increases, T_p decreases. Since the peak is symmetrical, as was mentioned above, the surface coverage at T_p, n_p, is roughly half of the initial coverage, n_0. If the substitution $n_p = \frac{n_0}{2}$ is made into Equation 2-24, the following rearrangement can be made

$$\ln(n_0 T_p^2) = \frac{E_d}{RT_p} - \ln\left(\frac{\nu R}{\beta E_d}\right) \qquad \text{Equation 2-26}$$

E_d can be obtained from the slope of a plot of $\ln(n_0 T_p^2)$ vs. $\frac{1}{T_p}$. If the plot is not linear, then the assumption of second order kinetics is not valid. Taken together, however, the combination of symmetrical peaks and decreasing T_p is usually a good indicator of second order desorption kinetics.

While both of the situations described above for first and second order desorption reactions occur under ideal conditions, there are complications that can change things from the ideal. The surface may have more than one bonding site, which gives rise to two or more, often overlapping TPRS peaks. Each of the sites has a different binding energy; the higher the binding energy, the more likely that site will preferentially fill before the other sites. The TPRS peaks for this situation typically show one peak at low coverage and multiple (lower T_p) peaks appearing with increased coverage. After the preferred sites are filled, the weaker sites begin to fill. During a TPRS run, the first sites to be vacated are the weaker sites, followed by the stronger sites as the temperature ramp continues.

Another possibility is that multiple peaks can appear even from a surface with only one adsorption site. High resolution energy loss spectroscopy (HREELS) has been used to show that hydrogen on a molybdenum single crystal resides in only one type of site despite the fact that at that hydrogen coverage, three desorption peaks are present during TPRS[12,13].

Another situation that makes the TPRS results more difficult to interpret, occurs when the desorption activation energy is a function of the coverage of the surface. At higher coverages the desorption activation energy is lower, possible due to the additional surface crowding and repulsive forces. This gives rise to a series of TPRS peaks whose T_p decreases with increasing coverage – even for a first order desorption. Luckily the shape of the desorption curves still provide a

---

12. H.R. Han and L.D. Schmidt, J. Phys. Chem, **75**, 221, (1971)

13. F. Zaera, E.B. Kollin, and J.L. Gland, Surf. Sci., **166**, L149, (1986)

clue to the kinetic order, although multi-peak TPRS curves make it even more difficult to interpret.

2.5.3 Experimental

The original work on TPRS was done by Redhead[11]. The basic guidelines for a TPRS study are:

1. The study compound is adsorbed onto the sample surface. This is usually done by admitting the sample gas into the chamber at a constant pressure. By measuring the time that the exposure continues, the amount of compound the sample is exposed to can be estimated (in Langmuirs).
2. The surface is heated; a linear heating rate is the most common.
3. The pumping speed must be much higher that the rate of evolution of gas from the surface.
4. The desorbing products are monitored, traditionally using an ion gauge, but in more modern installations using a mass spectrometer. The mass spectrometer allows more than one compound to be tracked at one time.
5. The results are plotted as pressure vs. temperature.

The TPRS measurements in this study were made using a Dycor quadrapole mass spectrometer. Up to five masses can be followed at one time in pressure vs. time display mode and the data can be viewed on the Dycor display screen and sent to a PC for storage and further analysis. To screen out unwanted interference from other filaments and desorbing gases from the chamber walls, a stainless steel collimator was fabricated and attached to the mass spectral

ionizer. The aperture to the collimator is 5mm in diameter; the sample was typically placed within 1.0 cm of the aperture during a run.

The heating ramp was generated using a 70A, 7V power supply, controlled by an RHK temperature control module. The heating rate was either $10\frac{K}{s}$ or $12\frac{K}{s}$ and most runs ended at either 400°C or 800°C. The settings used for all runs, unless otherwise noted were: electron multiplier +2500V, resolution 5.0, +70V electron energy, 2mA emission current from the filament, and 10-8A sensitivity settings.

In addition to the standard TPRS mode (pressure vs. time), the mass spectrometer could also be used in analog mode and tabular mode. Analog mode displays a pressure vs. m/e plot for 100 masses at a time. It is used primarily for monitoring background gases or for checking the cracking pattern of adsorbate gases. Tabular mode is used mainly for leak checking and displays a table of masses and pressures.

CHAPTER 3: RESULTS

3.1 INTRODUCTION

The main focus of this research was to investigate the reaction of a model synfuel reactant on a model HDO catalyst. The Mo(110) face was chosen as the target substrate and the first section of this chapter is devoted to describing the physical characteristics of the clean and sulfur-covered Mo(110) substrate, including LEED and AES data. Subsequent sections discuss the reactions of furan, carbon monoxide, hydrogen, ethylene, and propene on the model catalyst surface. TPRS results, including peak areas, positions, and shapes, together with AES data, all provide pieces of the furan/S/Mo(110) puzzle. Hopefully the correct positions of those puzzle pieces will be evident as more and more are uncovered throughout this chapter.

3.2 CLEAN AND SULFUR MODIFIED MO(110)

Molybdenum is a refractory transition metal that crystallizes as a body-centered-cubic (bcc) crystal. It is a fairly ductile, high melting point metal (2540°C) that finds wide applicability in steel production and as a catalyst, the latter of course being the focus in this research.

The two faces of the Mo crystal that have received the most attention in UHV catalyst studies are the (100) and the (110) faces. The numbers used to describe the different crystal faces are Miller indices. They refer to the reciprocal of the

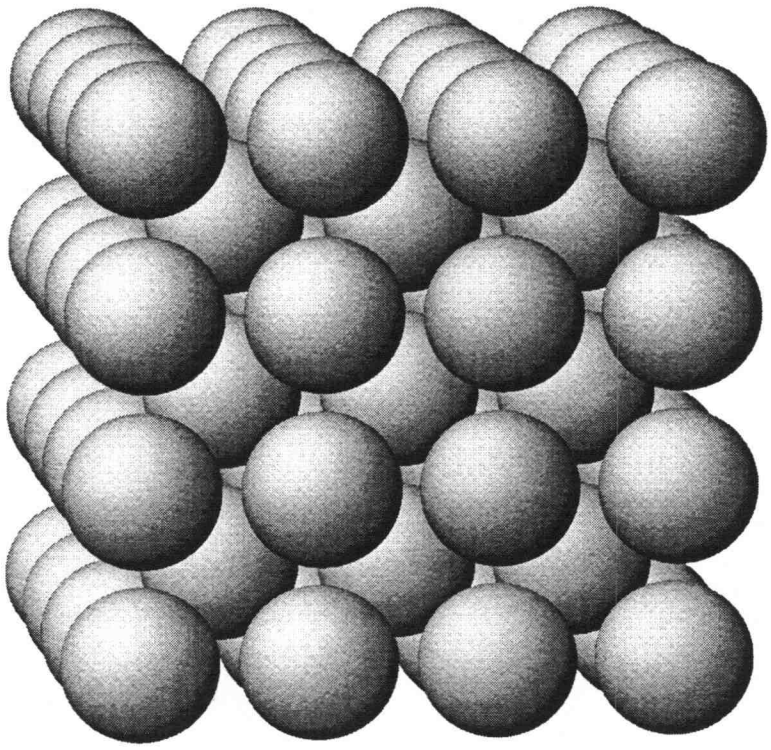

Figure 3-1. 3D representation of a Mo bcc crystal

distance (in lattice constants) along each of the three axes that the plane intersects. For example, the (111) plane crosses each axis one lattice constant from the origin ($\frac{1}{1} = 1, \frac{1}{1} = 1, \frac{1}{1} = 1$). The (110) plane crosses the x and y axes at one lattice constant but never crosses the z axis ($\frac{1}{1} = 1, \frac{1}{1} = 1, \frac{1}{\infty} = 0$). The lattice constant for the Mo single crystal is 3.147Å and the van der Waals diameter of Mo is 2.72Å.

The (110) plane is almost 50% more dense than the (100) plane (1.43×10^{15} vs. 1.01×10^{15} atoms/cm^2), but has a much larger interlayer spacing (2.23Å vs.1.57Å).

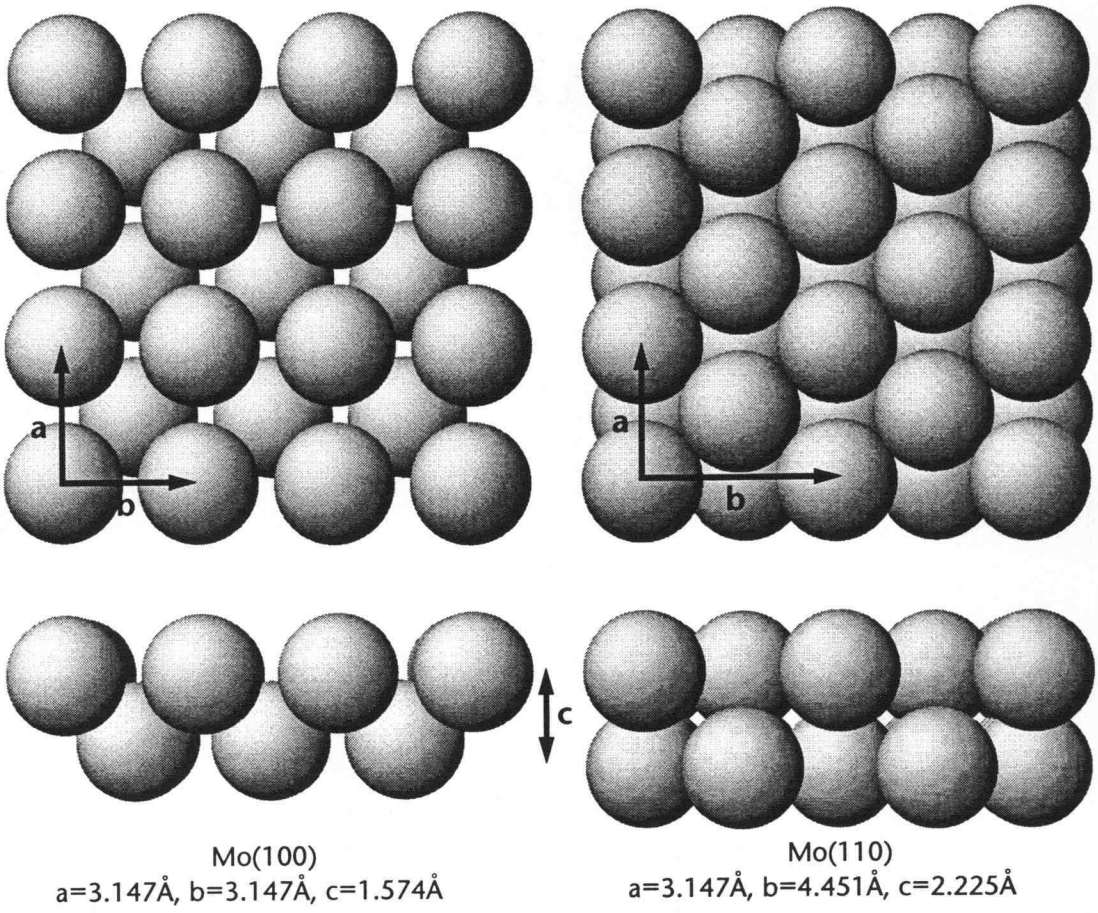

Figure 3-2. 3D top and side views of Mo(100) and Mo(110) planes with first and second atomic layers and lattice constants

The crystal planes (and dimensions) shown in Figure 3-2 are based on the ideal, bulk-terminated surfaces and are not always observed experimentally for all metals. With the advent of scanning tunnelling microscopy, came data that indicated that most, if not all, crystal surfaces are not flat across macroscopic areas. Instead they are composed of terraces of the ideal face, on the order of 10^4 Å^2, with one or more atomic layer steps between[1]. The total number of

1. G. Binnig and H. Rohrer, Surf. Sci., **126**, 236, (1983)

defects (including steps, dislocations, and edges) is estimated to be on the order of 10^{12} cm^{-2}. Comparing this to the atomic surface density of Mo(110) (1.43 x 10^{15} cm^{-2}) yields a defect density of less than 0.07 percent. This is small enough so as to not have a significant effect on the results of any of these experiments.

Another factor that can cause a crystal plane to deviate from the bulk-terminated ideal is the anisotropy of the surface. The exposed surface is missing bonds; to account for this the bonds between the first and second layer increase in energy. This effect increases with the "openness" of the surface and can cause the surface atoms to rearrange (reconstruct) and change the symmetry of the surface. A good indication of surface reconstruction is the presence of a different LEED pattern than the p(1x1) LEED pattern from the ideal, unreconstructed clean crystal surface. Alternatively, the spacing between the first and second layers may decreases, usually 5-20%.

Mo(100) reconstructs at temperatures below 220 K [2] and above that temperature retains the p(1x1) LEED pattern but undergoes a 9.5% contraction between the first and second layers[3]. In this research, no evidence of fractional order beams was found in any of the LEED examinations of the clean Mo(110) surface at any temperature. This agrees with results from other work on the Mo(110) surface[4], although there is evidence that the top layer spacing is contracted by 1.7% of

---

2. J.A. Prybyla, P.J. Estrup, S.C. Ying, Y.J. Chabal, and S.B. Christman, Phys. Rev. Letters, **58**, 1877, (1987)

3. L.J. Clarke, Surf. Sci., **91**, 131, (1980)

4. T.J. Haas and A.G. Jackson, J. Chem. Phys., **44**, 2921, (1966)

the bulk spacing at room temperature[5]. Thus it is reasonable to conclude that this sample is well-ordered and that Mo(110) does not reconstruct at the temperatures and conditions used.

3.2.1 Clean Mo(110)

When the new Mo(110) sample was first installed in the UHV chamber, it was covered with a hard-to-remove C surface layer. It took over 50 cleaning/ annealing cycles before a good clean-surface LEED pattern appeared and the C AES signal was minimized. A cleaning cycle is defined as follows:

1. Heat resistively to 650°C in 1 x 10^{-8} torr flowing O_2 for 5 minutes.
2. Raise (flash) the temperature to 1550°C in approximately 30 seconds using the electron beam heating system.

The p(1x1) LEED pattern for the clean Mo(110) surface is shown below in Figure 3-3.

This LEED pattern was only visible from the clean surface; within several minutes after a cleaning cycle the sharp p(1x1) pattern began to fade, evidence that a disordered surface layer was beginning to form, most likely due to residual H_2 and CO in the UHV chamber. The lower the temperature of the sample and the higher the background pressure (ideally at or below 5 x 10^{-10} torr), the more quickly the contamination accumulated. Once the LEED pattern had faded, usually all it took was a flash to 1550°C to remove the overlayer and

---

5. L. Morales de la Garza and L.J. Clarke, J. Phys. Chem., **C14**, 5391, (1981)

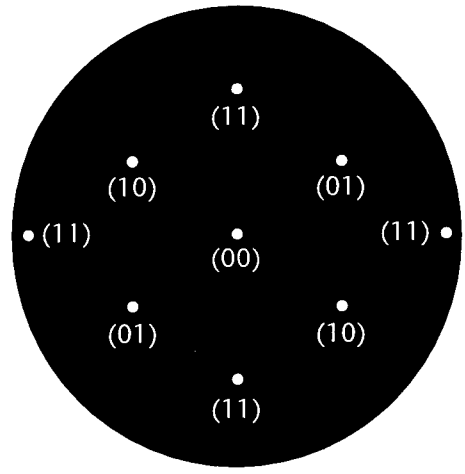

Figure 3-3. Schematic diagram of the p(1x1) LEED pattern for clean Mo(110) with beams labeled

recreate the clean surface. Generally, once the C/Mo AES peak-height ratio fell below 0.05, the surface was considered clean.

The AES spectrum for clean Mo(110) has several transitions; the largest, occurring at 186 eV, was used to monitor the cleanliness of the surface, as a ratio with the principle transition of the contaminating species. As an overlayer grows on the Mo substrate the AES peak for the contaminant species grows and the Mo AES peaks attenuate.

The two most common contaminates on Mo(110) in UHV are C and O, due to a small but constant background presence of CO. The AES spectra for clean Mo(110) and CO/S/Mo(110) are reproduced below.

Carbon chemisorbs very strongly to most transition metals; theoretical calculations suggest that adsorption energies are of the order of 150 kcal/mol[6].

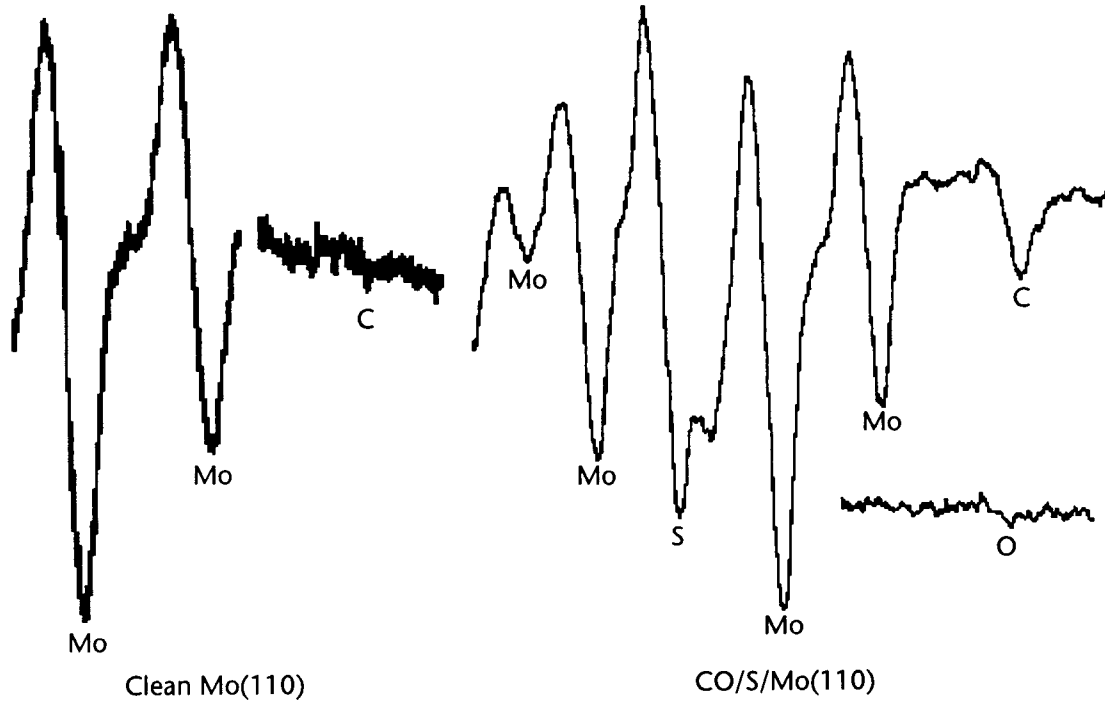

Figure 3-4. AES spectra for clean Mo(110) and CO/S/Mo(110)

AES is sensitive to C adlayers and can provide information on the nature of the carbon overlayer from the shape of the C signal[7,8]. The AES spectra for CO, hydrocarbon (i.e. molecular), and carbidic carbon overlayers on Mo(110) are shown below.

---

6. K.W. Frese, Surf. Sci., **182**, 85, (1987)

7. T.W. Haas and J.T. Grant, Appl. Phys. Lett., **16**, 172, (1970)

8. M.A. Chesters, B.J. Hopkins, A.R. Jones, and R. Nathan, Surf. Sci., **45**, 740, (1974)

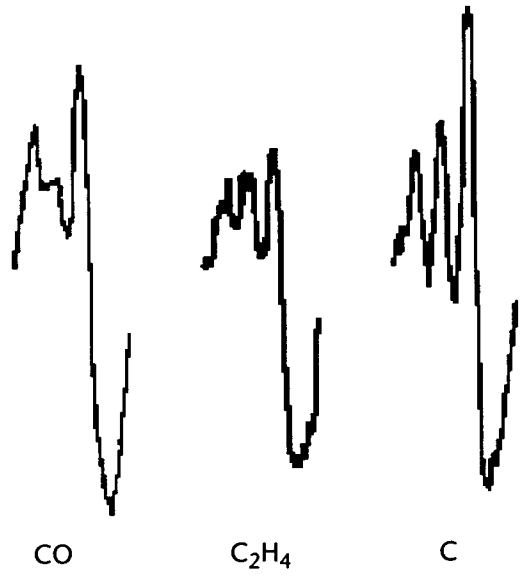

Figure 3-5. AES spectra for different forms of C on Mo(110)

3.2.2 Sulfur-Modified Mo(110)

Sulfur adsorbs strongly (ΔH_{ad} is in the range of 30 kcal/mol at high coverages[9] to 113 kcal/mol at low coverages[10]) on transition metals in accordance with the reaction below:[11]

$$M_X S \leftrightarrow M_X + S_{(g)} \qquad \text{Equation 3-1}$$

In fact, the heat of adsorption for S on transition metal surfaces parallels ΔH_f for the transition metal sulfides. The fact that sulfur is strongly bound to these

9. J. Oudar, Catal. Rev. Sci. Eng., **22**, 171, (1980)

10. H. Wise and J. McCarty, Surf. Sci., **133**, 311, (1983)

11. J. Oudar, Catal. Rev. Sci. Eng., **22**, 171, (1980)

metals supports the observation that in most cases, sulfur acts as a poison to catalytic activity, when present in high enough concentrations.

For Mo(110), a close-packed bcc metal surface, the surface saturation density is reported[12] to be 1.3 x 10^{15} atoms/cm^2, which is approximately 90% of a monolayer (a monolayer is defined as 1 S atom per Mo atom).

Sulfur forms many ordered overlayers on transition metal surfaces; depending on the crystal type and specific plane, both commensurate[13] (the overlayer lattice is in registry with the substrate) and incommensurate[14] structures have been observed using LEED. Dynamical LEED (DLEED) has been used to show that on most transition metal crystal surfaces, S adsorbs in the highest symmetry site at lower coverages, and that the M-S bonding distance on open faces (e.g. fcc and bcc-(100)) is equal to the sum of the covalent radii of the metal and sulfur. On more closely packed surfaces like Mo(110) the M-S bond was found to be 10% less than the covalent radii sum[15,16]. At higher coverages, there is some evidence that lower symmetry sites, such as bridge sites, may be used for bonding[17]. Tensor LEED calculations show that for the p(2x2) S/Mo(110) surface ($\theta_S \leq 0.25$), Mo–S bonds range from about 5% greater to 6% less than the

---

12. L. Peralta, Y. Berthier, and J. Oudar, Surf. Sci., **55**, 199, (1976)

13. H. Ohtani, C.T. Kao, M.A. Van Hove, and G.A. Somorjai, Prog. Surf. Sci., **23**, 155, (1986)

14. W. Heegemann, K.H. Meister, E. Bechtold, and K. Hayek, Surf. Sci., **49**, 161, (1975)

15. C. Kittel, *Introduction to Solid State Physics*, John Wiley and Sons, New York, **100**, (1976)

16. K.A.R. Mitchell, Surf. Sci., **149**, 93, (1985)

sum of the hard-sphere atomic radii of 2.65Å, due to adsorbate-induced substrate "rumpling."[18]

A further concern when studying metal-sulfur interactions is whether the S segregates at the surface or concentrates in the bulk. Sulfur's surface tension, around 60 dyne/cm, is much lower than the 1500-3000 dyne/cm typical for transition metals, and the strength of a M-S bond is generally lower than a M-M bond[19]. Both suggest that sulfur will not dissolve into the bulk to any extent, remaining on the surface instead.

For the Mo-S system, ordered overlayers have been observed and investigated on the (100)[20,21], (110)[22,23,24,25], and (111)[26] planes. Table 3-1 below summarizes the literature results regarding ordered sulfur overlayers on Mo(110).

---

17. T.W. Capehart, C.W. Seabury, G.W. Graham, and T.N. Rhodin, Surf. Sci., **120**, L441, (1982)

18. J. Toofan, G.R. Tinseth, and P.R. Watson, J. Vac. Sci. Technol. A, **12**, 2246, (1994)

19. *CRC Handbook of Chemistry and Physics*, 58th ed., R.C. Weast, Ed, CRC Press, Cleveland, (1975)

20. F. Zaera, E.B. Kollin, and J.L. Gland, Surf. Sci., **166**, L149, (1986)

21. M.H. Farias, A.J. Gellman, G.A. Somorjai, R.R. Chianelli, and K.S. Liang, Surf. Sci., **140**, 181, (1984)

22. L. Peralta, Y. Berthier, and J. Oudar, Surf. Sci., **55**, 199, (1976)

23. A. Sánchez, J.J. de Miguel, E. Martinez, and R. Miranda, Surf. Sci., **171**, 157, (1986)

24. W. Witt and E. Bauer, Ber. Bunsenges. Phys. Chem., **90**, 248, (1986)

Table 3-1. Literature sulfur coverage ranges and corresponding LEED structures on Mo(110)

Coverage Range (θ_S)	LEED Pattern	Reference
0.00	p(1x1)	a,b,c
0.00 – 0.25	p(2x2)	a,b,c
0.25 – 0.50	c(2x2)	a,b
0.40 – 0.50	$\begin{bmatrix} 2 & 2 \\ 1 & \bar{1} \end{bmatrix}$ p(7x1)	a,b c
>0.50	p(4x1), p(1x5), p(1x3), p(1x10) (1x1)p, (1x3)c, (1x5)c, (1x3)p, (1x7)c, (1x4)p, (1x5)p, (1x11)c	c a

a. L. Peralta, Y. Berthier, and J. Oudar, Surf. Sci., **55**, 199, (1976)
b. A. Sánchez, J.J. de Miguel, E. Martinez, and R. Miranda, Surf. Sci., **171**, 157, (1986)
c. W. Witt and E. Bauer, Ber. Bunsenges. Phys. Chem., **90**, 248, (1986)

Witt and Bauer disagree with Sánchez et al. and Peralta et al. regarding the structures that form in the 0.4–0.6 monolayer region. The latter two groups saw a c(2x2) LEED pattern that transitioned into a $\begin{bmatrix} 2 & 2 \\ 1 & \bar{1} \end{bmatrix}$ pattern below 500K. Witt and Bauer saw a p(7x1) at the lower end of the coverage range and a p(4x1) at the upper end. In this study, no conclusive evidence was found to support either opinion. All four LEED patterns were observed in the specified coverage range (the c(2x2) and $\begin{bmatrix} 2 & 2 \\ 1 & \bar{1} \end{bmatrix}$ patterns were the most intense), and two temperature dependent phase transitions were apparent: one from the c(2x2)

25. J.J. de Miguel, A. Sánchez, E. Martinez, and R. Miranda, Vacuum, **37**, 455, (1987)

26. J.M Wilson, Surf. Sci., 59, 315, (1976)

structure to the structure and the second from the c(2x2) to the p(7x1) structure, both as the temperature dropped below about 500K. The fact that a strong clean surface p(1x1) LEED pattern was seen no matter where on the surface the electron beam was focussed, indicates that there was good long-range order. However the simultaneous presence of different sulfur domains on the surface implies that the S/Mo(110) system is not nearly as well-behaved as the clean surface, at least for θ_S~0.5 monolayers. Generally, at $\theta_S \leq 0.25$, the only LEED pattern observed was the p(2x2), which persisted even to very low sulfur coverages, indicating that islands of well-ordered sulfur atoms remained despite increasing numbers of vacant sites.

At higher temperatures, the p(2x2) (>650K) and c(2x2) (>800K) patterns disappeared, indicating a transition from the ordered phases to a disordered 2D-lattice-gas-like phase[27].

At coverages higher than 0.5 monolayers, the Mo(110) surface is passivated toward chemisorption of other species, based on work on the Mo(100) surface[28,29,30] and TPRS results on the Mo(110) reported later in this chapter. Hence this study focussed on those surfaces with $\theta_S < 0.5$ monolayers. The

---

27. A. Sánchez, J.J. de Miguel, E. Martinez, and R. Miranda, Surf. Sci., **171**, 157, (1986)

28. M.H. Farias, A.J. Gellman, G.A. Somorjai, R.R. Chianelli, and K.S. Liang, Surf. Sci., **140**, 181, (1984)

29. F. Zaera, E.B. Kollin, and J.L. Gland, Surf. Sci., **166**, L149, (1986)

30. N.R. Avery and N. Sheppard, Proc. Roy. Soc. (London), **A405**, 1, (1986)

figures below show proposed structures and LEED patterns for the p(2x2), c(2x2), and $\begin{bmatrix} 2 & 2 \\ 1 & \bar{1} \end{bmatrix}$ sulfur overlayers[22].

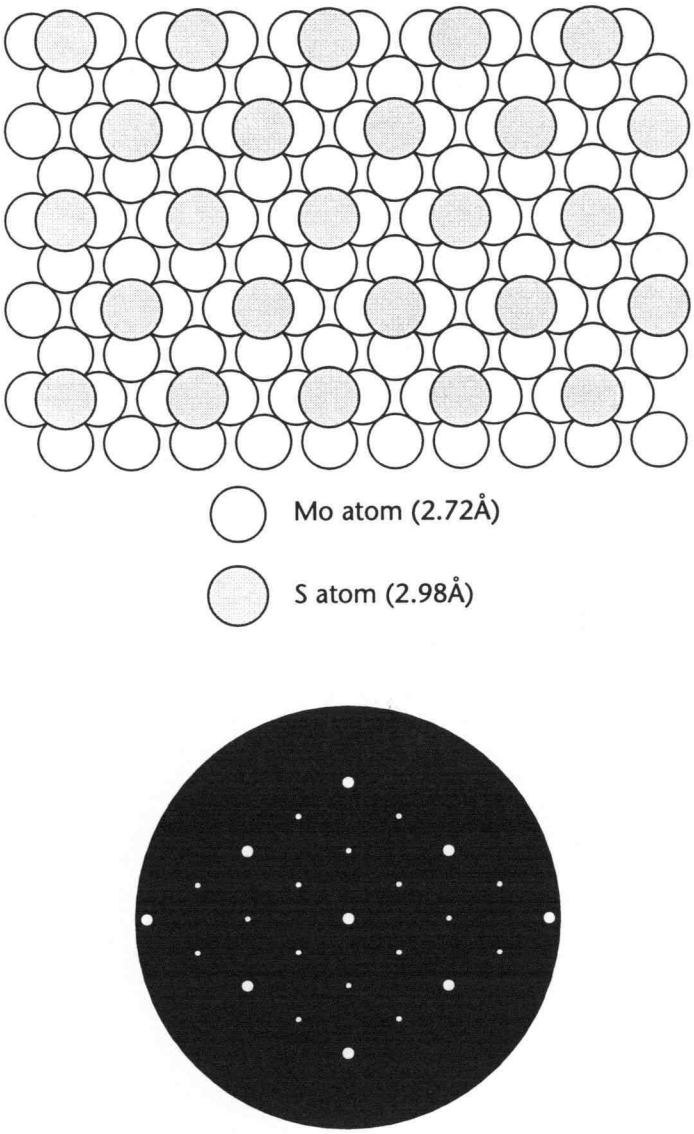

Figure 3-6. S/Mo(110) p(2x2) LEED pattern and proposed surface structure

The sulfur atoms are proposed to occupy high-symmetry adsoption sites in accord with the general trend for atomic species on transition metal surfaces.

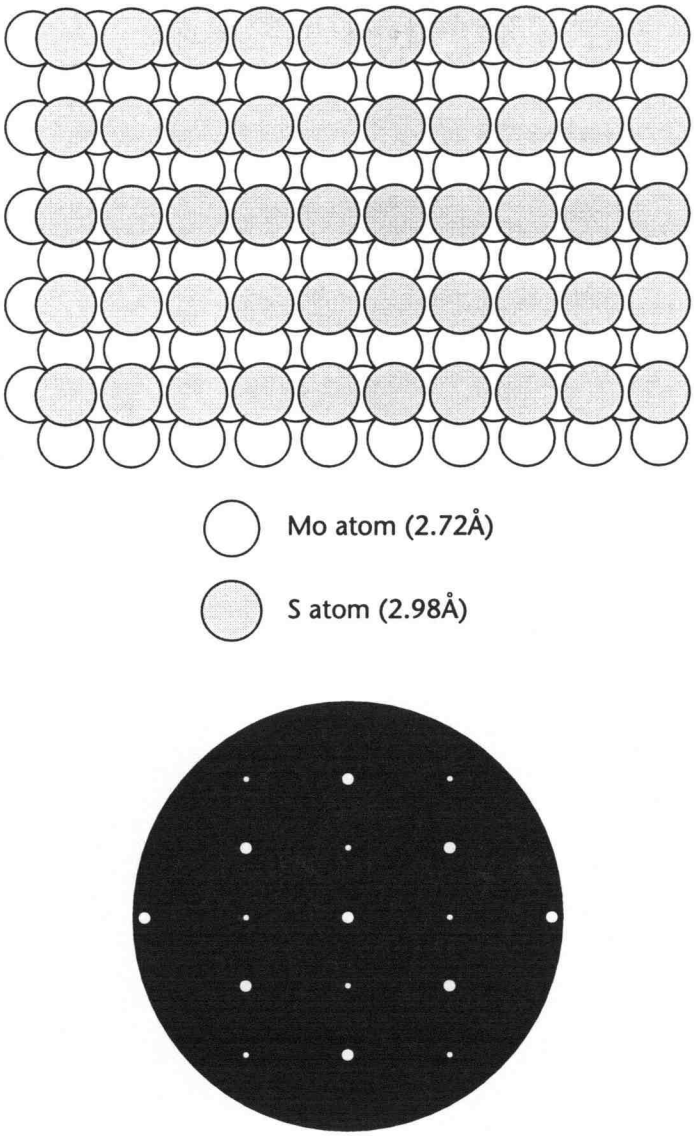

Figure 3-7. S/Mo(110) c(2x2) LEED pattern and proposed surface structure

For the p(2x2) and c(2x2) structures these are four-fold hollow sites. In contrast, in the $\begin{bmatrix} 2 & 2 \\ 1 & \bar{1} \end{bmatrix}$ structure the offset rows of sulfur atoms are proposed to occupy three-fold hollows.

Sulfur adlayers were applied to the Mo(110) surface using an electrochemical sulfur cell described in the section titled: "Sample Dosing" on page 17. In

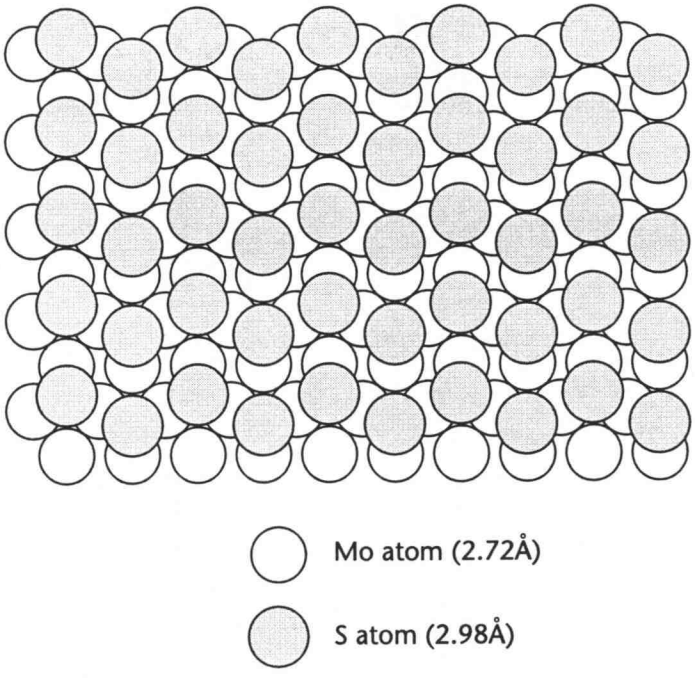

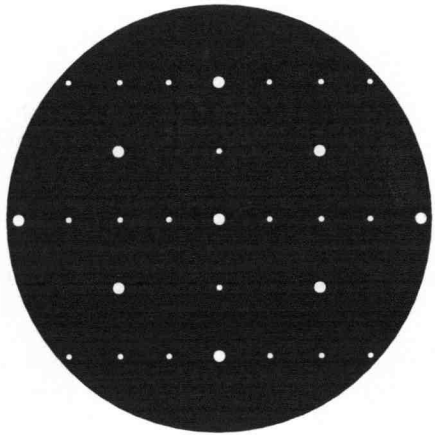

Figure 3-8. S/Mo(110) $\begin{bmatrix} 2 & 2 \\ 1 & \bar{1} \end{bmatrix}$ LEED pattern and proposed surface structure

general, the sulfur cell was heated to approximately 80°C and operated at 25 μA for long enough to deposit an excess of S on the Mo(110) surface. Then the surface was annealed to remove a portion of the deposited sulfur and order the remainder – the higher the anneal temperature, the lower the final sulfur

coverage. To calibrate the anneal temperature scheme with actual surface coverage, the surface was monitored with both LEED and AES during the annealing process; Figure 3-9 is the result.

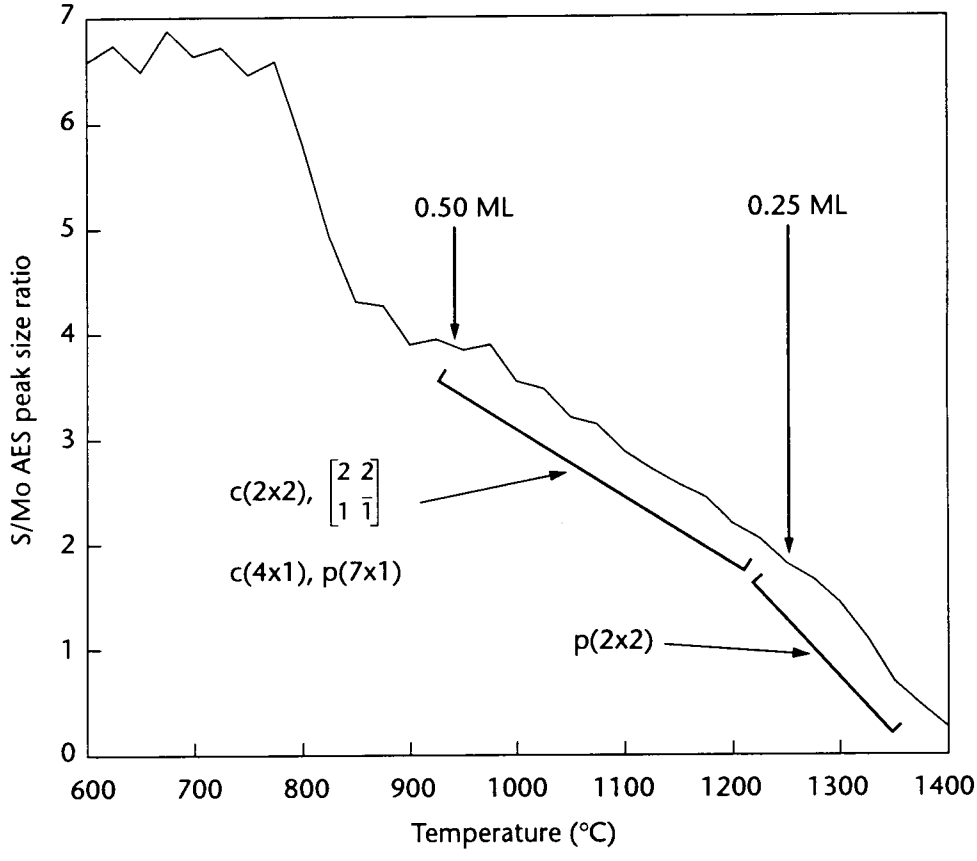

Figure 3-9. S/Mo AES peak size ratios, LEED patterns, and sulfur coverages as a function of annealing temperature

Once the sulfur coverage had been calibrated, and the ability to reproducibly create a given S/Mo(110) surface had been demonstrated, the investigation into the chemisorption and reaction of furan on these surfaces began.

3.3 Model HDO Reactants and Products on Clean And Sulfur-Modified Mo(110)

The chemisorption and reactions of model compounds on metal single crystal surfaces in UHV is a reliable and often-used method to investigate possible bonding energies and geometries which may exist under conditions encountered in industrial catalysis. In this study the chemisorption and reaction of model reactants (furan and hydrogen) and possible products (carbon monoxide, ethylene, propylene) on clean and sulfur covered Mo(110) was investigated using TPRS and AES. In this section, experimental results are presented and compared with those mentioned in the literature, if available.

3.3.1 Furan on Clean and Sulfur-Modified Mo(110)

Furan is a colorless liquid with a sweet odor and the physical properties listed in Table 3-2.

Table 3-2. Physical properties of furan

Property	Value
Boiling point (°C)	31.33
Freezing point (°C)	-85.6
Specific gravity (n_4^{20})	0.9378
Heat of formation, 300 K (kcal/mol)	-8.3

Furan, first isolated in 1870[31], is found in a wide variety of natural products including the oils of fir, pine, and beech[32]; the oil of roasted coffee[33];

carbonized sugar[34]; and of course, synthetic fuels made from coal[35] and other plant-fiber-derived sources like peat[36]. Furan's structure is best described by the following resonance hybrid diagram.

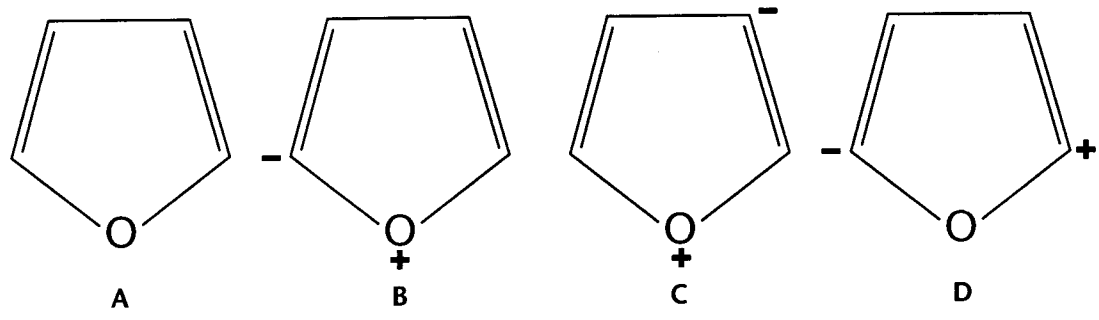

Figure 3-10. Resonance structures for furan

It is difficult to assess the relative importance of the structures above, although B is probably the most important (outside of A) since it involves a smaller separation of charge than either C or D. This rationalization is supported by experimental evidence from furan substitution reactions. An incoming group is almost exclusively oriented toward one of the alpha positions, indicating a higher charge density there than at the beta positions. Structure D is likely less

---

31. B.E. Limpricht, Ber., **3**, 90, (1870)

32. A. Jaquemain, Bull. Assoc. Chim., **54**, 529, (1937)

33. B. Johnston and H. Frey, J. Am. Chem. Soc., **60**, 1623, (1938)

34. L. Fierz-David, Chem. and Ind., **44**, 942, (1925)

35. E. Furimsky, J.A. MacPhee, L. Vancea, L.A. Ciavaglia, and B.N. Nandi, Fuel, **62**, 395, (1983)

36. H. Christiansson, Iva, **18**, 89, (1947)

important due to the fact that it requires that one of the alpha carbons have only six electrons in its outer shell. Thus, structures A and B probably contribute most strongly to furan's hybrid resonance character.

Furan decomposes at 670–740°C in a quartz tube with the products being carbon monoxide, saturated and unsaturated hydrocarbons (mostly ethylene, propene, and propyne), and hydrogen[37]. The literature makes no mention of the interaction of furan with Mo(110) in UHV. However, there are partially related studies that provide insight into the C_4H_4O/Mo(110) system:

- Reaction of thiophene on clean and sulfur-covered Mo(110)[38]
- Reaction of ethylene oxide on clean and oxygen-covered Mo(110)[39]
- Pyrolysis studies of furan[40,41]
- Reaction of furan on Pd(111)[42]

Thiophene is a common target in the battle to understand catalytic hydrodesulfurization and has been studied on many metal surfaces[43,44,45],

---

37. C.D. Hurd and A.R. Goldsby, J. Am. Chem. Soc., **54**, 2530, (1932)

38. J.T. Roberts and C.M. Friend, Surf. Sci., **186**, 201, (1987)

39. J.G. Serafin and C.M. Friend, J. Am. Chem. Soc., **111**, 6019, (1989)

40. M.A. Grela, V.T. Amorebieta, and A.J. Colussi, J. Phys. Chem., **89**, 38, (1985)

41. A. Lifshitz, M. Bidani, and S. Bidani, J. Phys. Chem., **90**, 5373, (1986)

42. T.E. Caldwell, I.M. Abdelrehim, and D.P. Land, J. Am. Chem. Soc., **118**, 907, (1996)

43. J. Stohr, J.L. Gland, E.B. Kollin, R.J. Koestner, A.L. Johnson, E.L. Muetterties, and F. Sette, Phys. Rev. Letters, **53**, 2161, (1984)

44. G.R. Schoofs, R.E. Preston, and J.B. Benziger, Langmuir, **1**, 313, (1985)

including both Mo(100)[46] and Mo(110). Results ranging from direct sulfur abstraction to reversible molecular desorption are reported.

On clean Mo(110), thiophene decomposes quantitatively to gaseous hydrogen, surface carbon, and surface sulfur in the temperature range 120–750 K[38]. At high enough coverages for multilayers of thiophene to form, molecular thiophene desorbs at 180 K. No other desorbing species are observed. Depending on the initial thiophene coverage, hydrogen either desorbs in a single peak centered at 440 K (low initial coverage) or in a series of peaks between 300 and 600 K (saturation coverage). TPRS of 2,5-dideuterothiophene shows at high coverages that the α-hydrogens cleave first. At low coverage, no bond breaking selectivity was observed.

On p(2x2) S/Mo(110) (θ_S ~ 0.25 monolayers), desorption of reversibly chemisorbed thiophene occurs, even before multilayer formation. For initial thiophene coverages greater than 0.33 monolayers, molecular thiophene desorbs in a peak centered at 215 K. The hydrogen desorption peaks resemble those found from the clean surface, although peak areas indicate that the amount of hydrogen that desorbs from the sulfided surfaces is only about half of that from the clean surface. No bond-breaking selectivity was observed on the sulfided surface at any thiophene coverage.

---

45. J. Stohr, E.B. Kollin, D.A. Fischer, J.B. Hastings, F. Zaera, and F. Sette, Phys. Rev. Letters, **55**, 1468, (1985)

46. F. Zaera, E.B. Kollin, and J.L. Gland, Surf. Sci., **184**, 75, (1987)

Ethylene oxide on clean Mo(110) initially irreversibly decomposes to gaseous hydrogen, surface carbon, and surface oxygen[39]. As the surface oxygen layer builds, a second reaction path appears, one which produces surface oxygen and gaseous ethylene in a desorption peak centered at 200K. If the Mo(110) surface is pretreated with oxygen (θ_O ~ 0.25 monolayers), ethylene production is favored over decomposition. Molecular desorption occurs at 150 K if multilayers of ethylene oxide are present.

Very low pressure pyrolysis studies of furan indicate that between 1100 and 1250 K, furan decomposes according to the following reaction[40]:

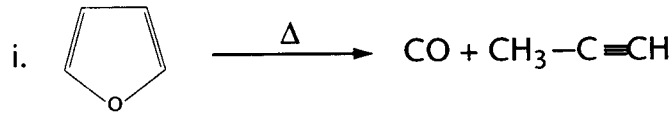

Figure 3-11. Reaction pathway for the very-low-pressure pyrolysis of furan

A similar pyrolysis experiment confirmed reaction (i), but found evidence for another as well (temperature range=1050–1270 K)[41]:

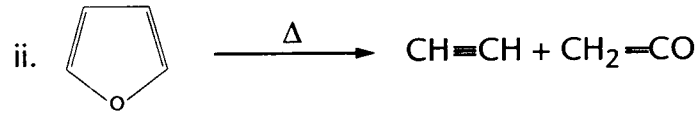

Figure 3-12. Alternative reaction pathway for the pyrolysis of furan

The work involving furan/Pd(111) examined the temperature programmed reaction of furan on the clean Pd(111) surface using laser-induced thermal

desorption (LITD) and showed that furan decomposed to C_3H_3 fragments, H_2, and CO.

3.3.1.1 *Furan/Mo(110)*

According to the literature, the clean Mo(110) surface is highly reactive with most hydrocarbons irreversibly decomposing upon heating. The results presented here tell a similar story for the reaction of furan on Mo(110), although some key differences exist.

For an undetermined reason, whenever furan was admitted to the chamber the ion gauge did not properly monitor the pressure. At a given leak valve setting, both the mass spectrometer and the pressure gauge on the ion pumps showed that the chamber pressure was steady, holding at a value that was the sum of the partial pressure of furan and the background pressure. The ion gauge pressure reading never stopped increasing until the furan leak valve was closed, although it worked fine during the introduction of other gases.

To solve this problem, the "pumpout" rate constant was determined, and, from that value, the exposure as a function of the maximum furan pressure reached was calculated. This method assumes that the pumping rate of the vacuum chamber is constant and that the gas is introduced into the chamber as a single transient impulse. The rate constant of the pumpdown was determined as follows:

$$\frac{dp}{dt} = -kp \qquad \text{Equation 3-2}$$

which upon integration yields:

$$\ln\left(\frac{p}{p_0}\right) = -kt \qquad \text{Equation 3-3}$$

After one half life $p=1/2p_0$, which leads to the following expression for the rate constant:

$$k = -\frac{\ln(0.5)}{t_{1/2}} \qquad \text{Equation 3-4}$$

The half life of 15 seconds was measured in the vacuum chamber using the mass spectrometer in pressure vs. time mode. This gives $k=4.6 \times 10^{-2}$.

Taking the exponential of both sides of Equation 3-3 yields the following expression for the pressure at time t:

$$p = p_0 e^{-kt} \qquad \text{Equation 3-5}$$

Integrating Equation 3-5 gives the exposure in $\frac{\text{Langmuirs}}{10^6}$ (10^{-6} torr secs) at time t:

$$\text{Exposure} = p_0\left[\frac{(1 - e^{-kt})}{k}\right] \qquad \text{Equation 3-6}$$

which, for t > 120 sec, becomes:

$$\text{Exposure} = 22p_0 \qquad \text{Equation 3-7}$$

The constant 22 is applicable only for furan due to different pumping rates for different gases.

When furan is exposed to the ionizing field of a quadrapole mass spectrometer, the parent molecule breaks into a number of ionized fragments. The type and relative amount of these fragments is the mass spectrum, also called the "cracking pattern," and is listed in Table 3-3.

Table 3-3. Mass spectrum for furan

Ion mass (m/e)	Relative amount
39	100
68	65
38	17
29	16
40	12
42	10
37	7
14	4

The contents of the furan leak valve line were periodically checked by admitting the contents to the UHV chamber and monitoring the mass spectrum.

During TPRS experiments, the m/e=39 signal was used to check for molecular desorption from the sample. This would have presented a problem if a m/e=39 peak appeared as a result of a surface reaction. Luckily the only peak of this mass appeared at low temperature (<0°C) and only at very high furan coverages, which is indicative of associative molecular desorption.

A typical TPRS experiment went as follows:

1. Clean the sample until the C/Mo AES ratio was less than or equal to 0.05.
2. Allow the sample and sample holder to cool after the prolonged heating of the cleaning process. During this cooling period a sulfur layer could be applied using the electrolytic sulfur source.
3. If the sample has been sulfided, anneal it until the sulfur coverage reaches the desired level.
4. Quickly flash the sample to 1200°C using the e^- beam heating apparatus. This removes the hydrogen and carbon monoxide that adsorb on the sample during post-cleaning/post-annealing cooling.
5. Cool the sample to the dosing temperature, usually less than 100°C, and dose the sample.
6. Cool the sample to the TPRS starting temperature and start the temperature ramp and the mass spectrometer pressure vs. time scan.

The first few TPRS runs were used to determine the masses of the fragments leaving the surface. It quickly became clear that besides the small peak due to molecular desorption at m/e=39, only a few other peaks were present, the two most significant being m/e=28 and m/e=2. The latter was easily identified as molecular hydrogen, desorbing associatively. The m/e=28 peak didn't immediately reveal its identity. Figure 3-13 shows the m/e=28 and m/e=2 TPRS peaks for furan adsorbed on clean Mo(110).

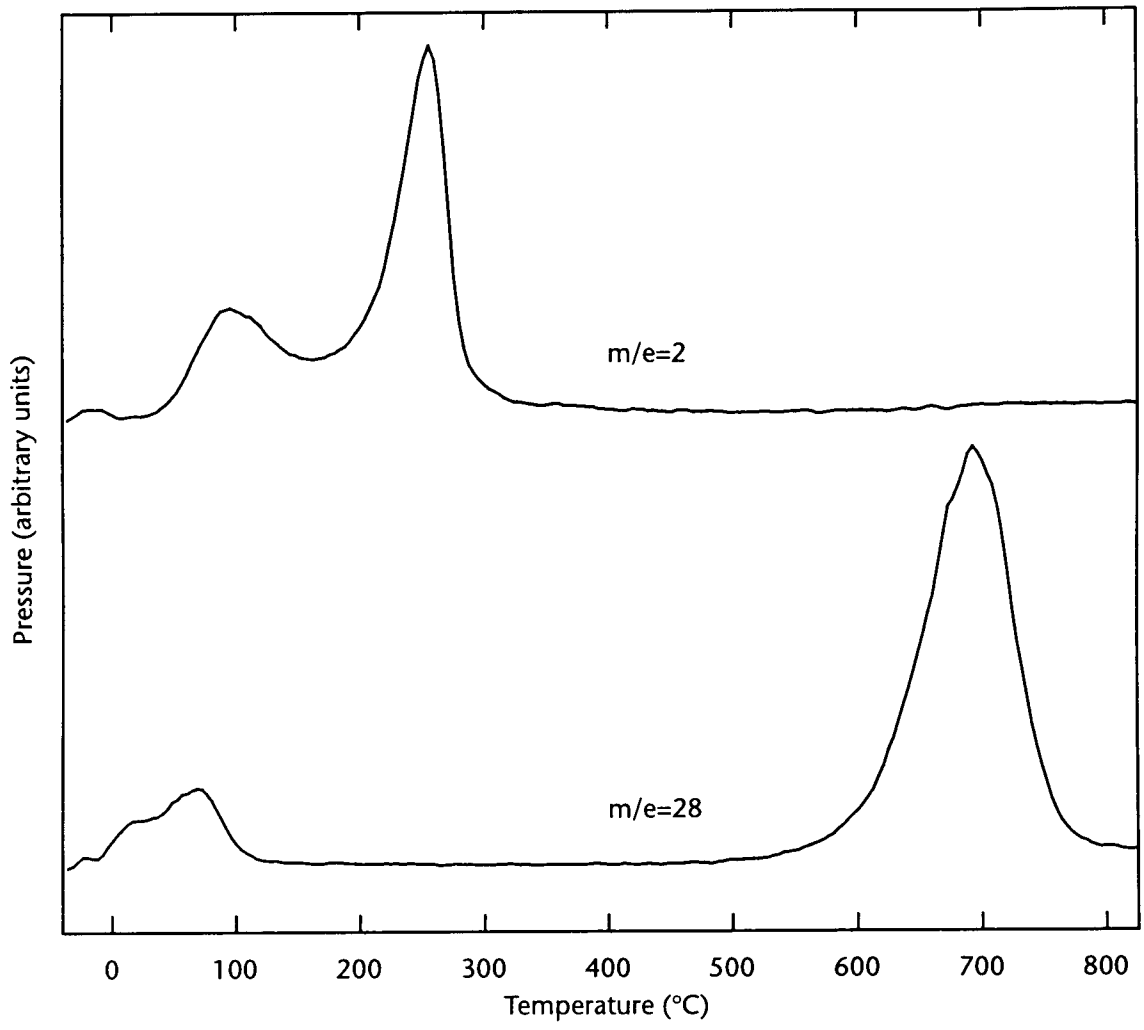

Figure 3-13. TPRS of a saturation dose of furan on clean Mo(110): m/e=28 and m/e=2

The following small hydrocarbons have sizeable m/e=28 peaks in their mass spectra:

- C_4: butane, butene, butadiene
- C_3: propane, propene
- C_2: ethylene (m/e=28 is the parent peak)
- Other: carbon monoxide (m/e=28 is the parent peak)

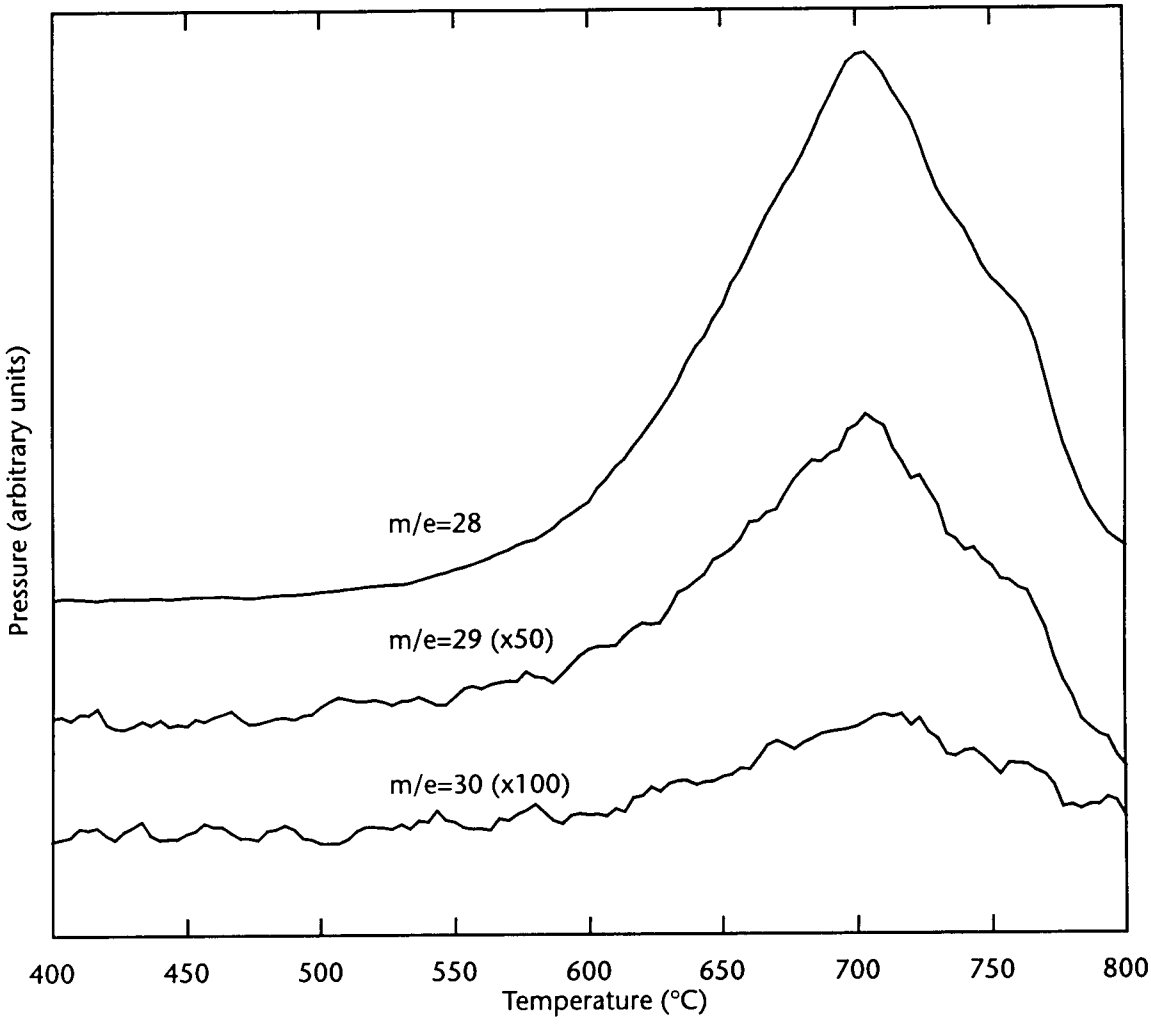

Figure 3-14. TPRS of a saturation dose of furan on clean Mo(110): m/e=28, m/e=29, and m/e=30

Another clue to the m/e=28 peak was the presence of other smaller peaks that mirrored its shape at m/e=29 and m/e=30.

The peak areas of the 28, 29, and 30 peaks are in the proportion of 500:6:1 respectively, which is roughly the relationship that would result if the 28 peak was CO, the 29 peak was $C^{13}O$ (1.16% of CO), and the 30 peak was CO^{18} (0.20% of CO). Although some small hydrocarbons have mass spectra with 28, 29, and 30 peaks, none are close to being in the same proportion as shown

above. Thus, it seems reasonable to assign the peak at m/e=28 to carbon monoxide produced during the TPRS of furan on Mo(110).

The presence of a low temperature peak in the CO spectrum implies that at least some CO is abstracted from the furan molecule without decomposing to C and O, since the low temperature (60°C) α-peak is generally believed to be due to the first order desorption of molecularly adsorbed CO. This is a surprising result especially in light of work with thiophene on the clean Mo(110), where the only gas-phase reaction product was hydrogen. However both furan pyrolysis results and the furan/Pd(111) (described on page 69) indicate that the production of CO is an allowed pathway. In addition, CO is a stable gas-phase product and CS is not, making this process even less surprising especially in hindsight.

The high temperature peak (~690°C) is attributed to the second order associative desorption or recombination reaction of C and O and is well documented when chemisorbed C and O are present on Mo(110)[47].

Figure 3-15 and Figure 3-16 compare the m/e=28 and m/e=2 TPRS peaks for a saturation dose of furan on clean Mo(110) and a blank run. Background hydrogen and carbon monoxide, always present in the vacuum chamber, are responsible for the small peaks at 2 and 28 in the blank TPRS runs.

The shape of the furan m/e=2 peak is very similar to that described in the literature for the TPRS of thiophene on clean Mo(110). For thiophene, the low

---

47. E. Gillet, J.C. Chiarena, and M. Gillet, Surf. Sci., **66**, 596, (1977)

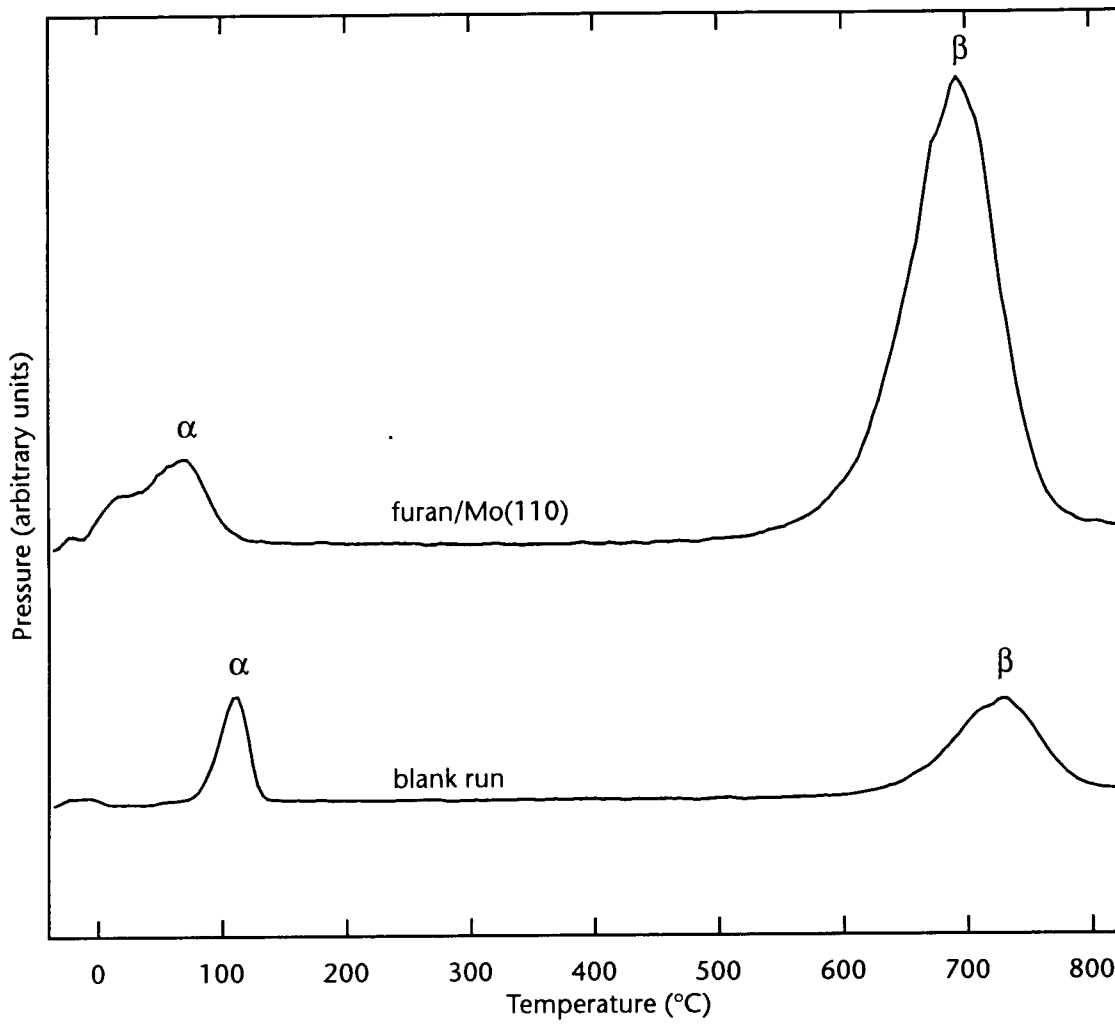

Figure 3-15. Comparison of the m/e=28 peaks from the TPRS of a saturation dose of furan on clean Mo(110) and a blank run

temperature peak is thought to be desorption limited, i.e. β_1 hydrogen becomes available for desorption (as recombinant surface hydrogen atoms) at the time thiophene adsorbs. The high temperature β_2 peak, on the other hand, is attributed to the reaction-limited decomposition of a surface hydrocarbon fragment, resulting from the partial decomposition of thiophene. Interestingly, the two peak TPRS hydrogen spectrum only occurs at high thiophene coverages; at low coverages hydrogen desorbs in a single peak centered at 140°C[48].

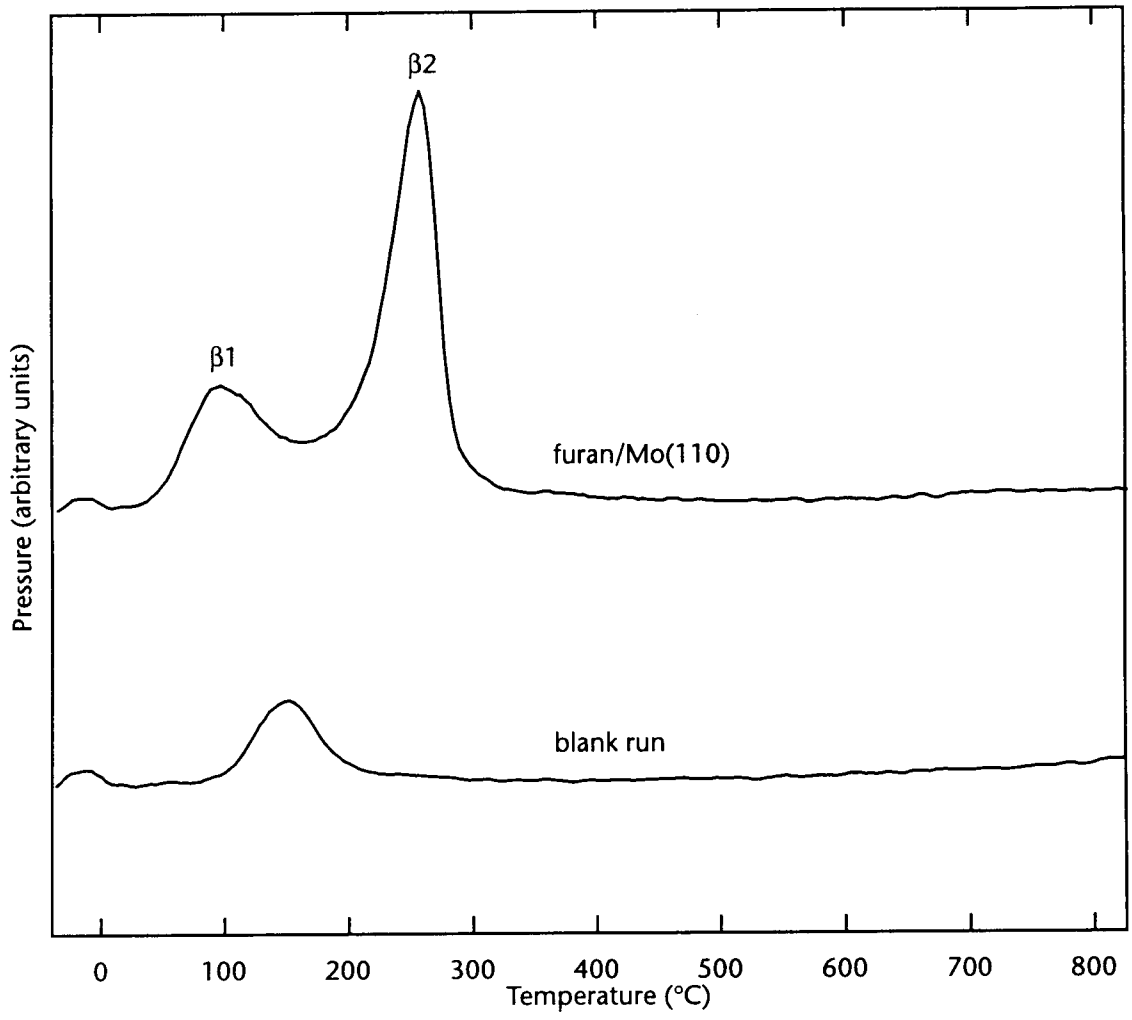

Figure 3-16. Comparison of the m/e=2 peaks from the TPRS of a saturation dose of furan on clean Mo(110) and a blank run

A series of TPRS runs with varying amounts of furan on clean Mo(110) was carried out to monitor the behavior of the 2 and 28 peaks as a function of initial furan coverage. Figure 3-18 shows the results of this series of runs for the low temperature m/e=28 α-peak while Figure 3-18 shows the m/e=2 peak data.

48. J.T. Roberts and C.M. Friend, Surf. Sci., **186**, 201, (1987)

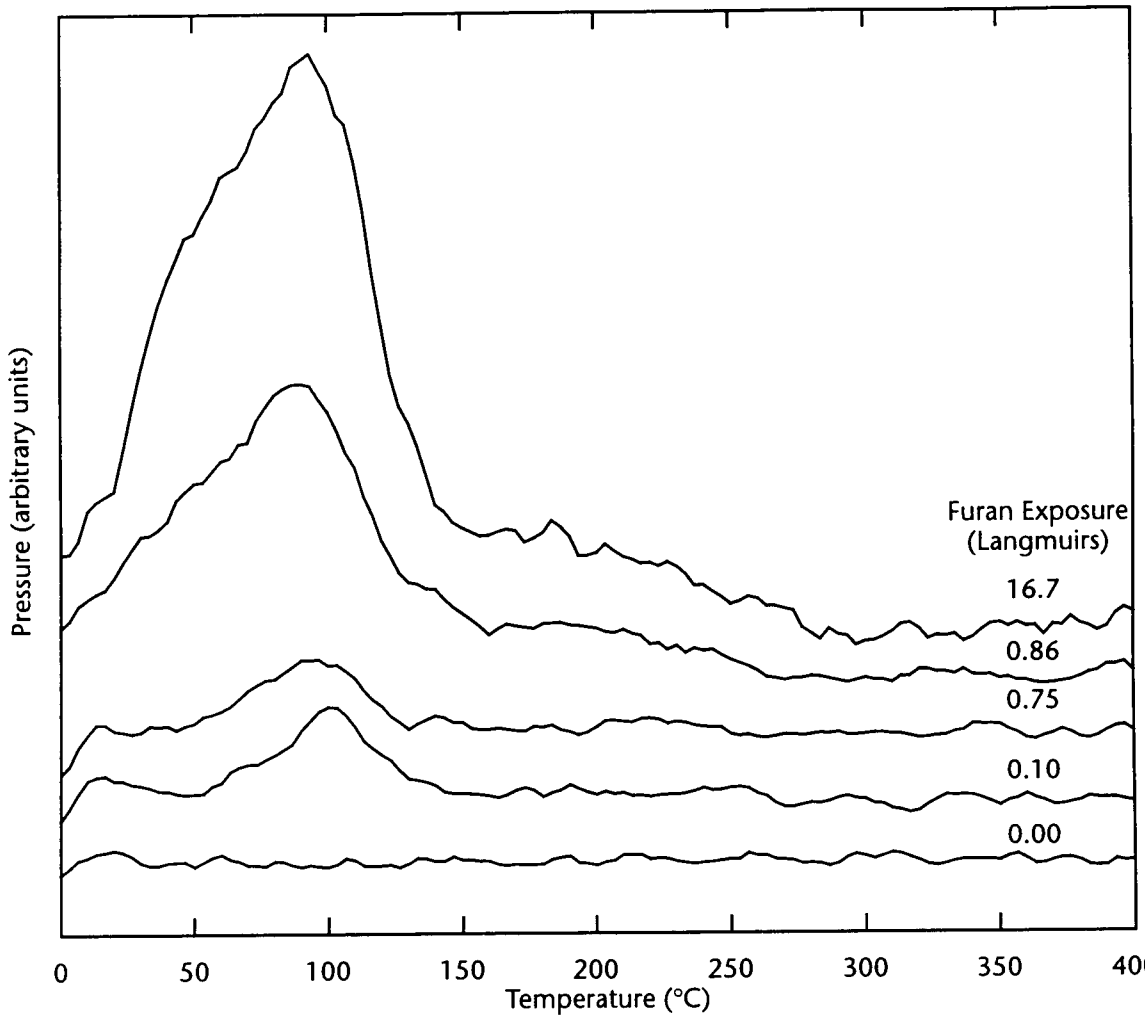

Figure 3-17. TPRS m/e=28 α-peaks as a function of initial furan exposure on clean Mo(110)

These results also parallel the thiophene/Mo(110) results mentioned above[49]. At low furan coverages, a single peak centered on 160°C is detected while at higher coverages, two or possibly three peaks are present.

49. J.T. Roberts and C.M. Friend, Surf. Sci., **186**, 201, (1987)

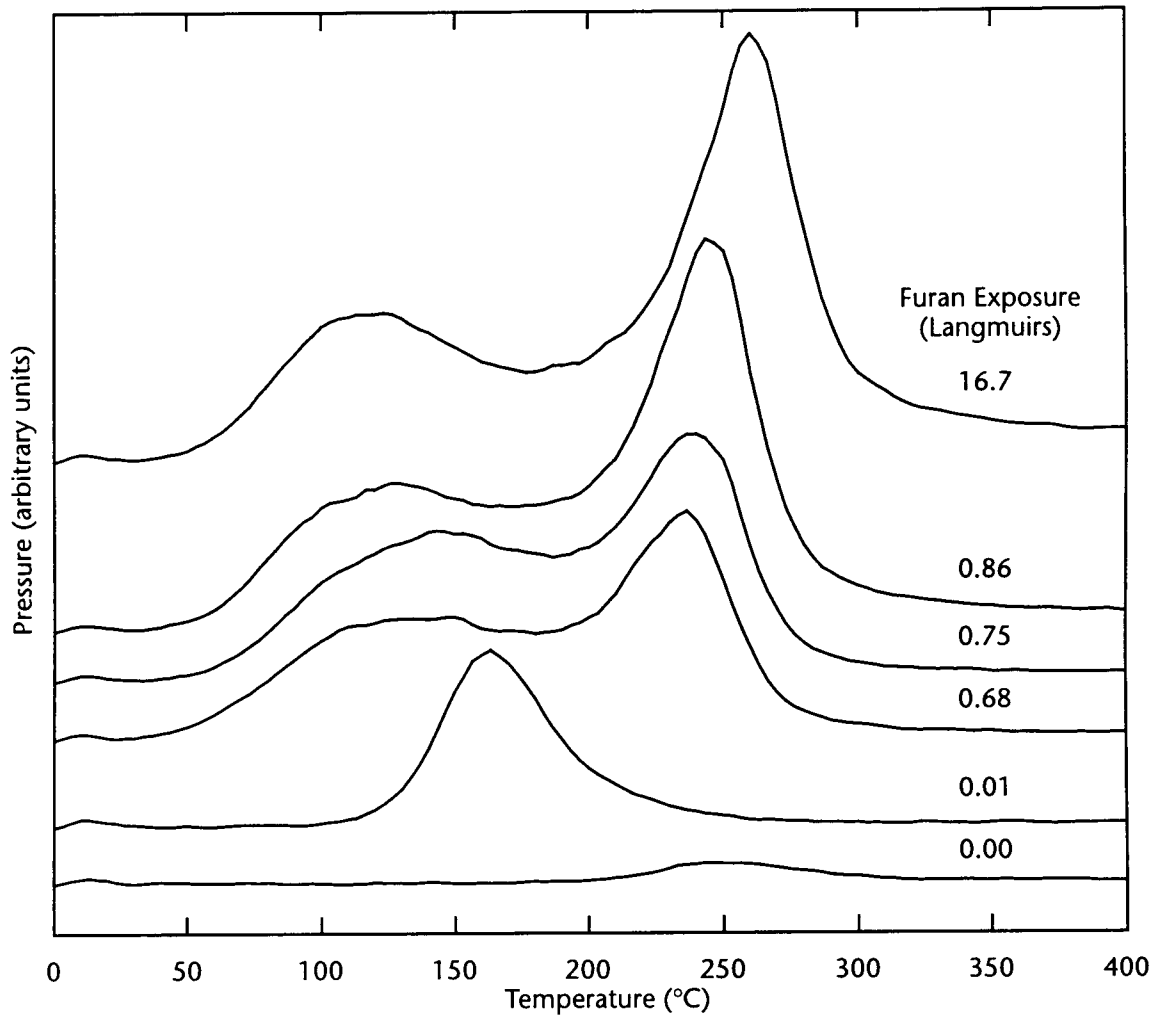

Figure 3-18. TPRS m/e=2 peak as a function of initial furan exposure on clean Mo(110)

If the areas under the m/e=2 peaks are plotted as a function of initial furan exposure (Figure 3-19), the resulting curve illustrates the Langmuirian nature of furan uptake on clean Mo(110). Even though the experiment monitored furan exposures up to 44 Langmuirs, the m/e=2 peak areas show that saturation (the point at which the m/e=2 peak area stopped increasing) occurred at less than 2 Langmuirs.

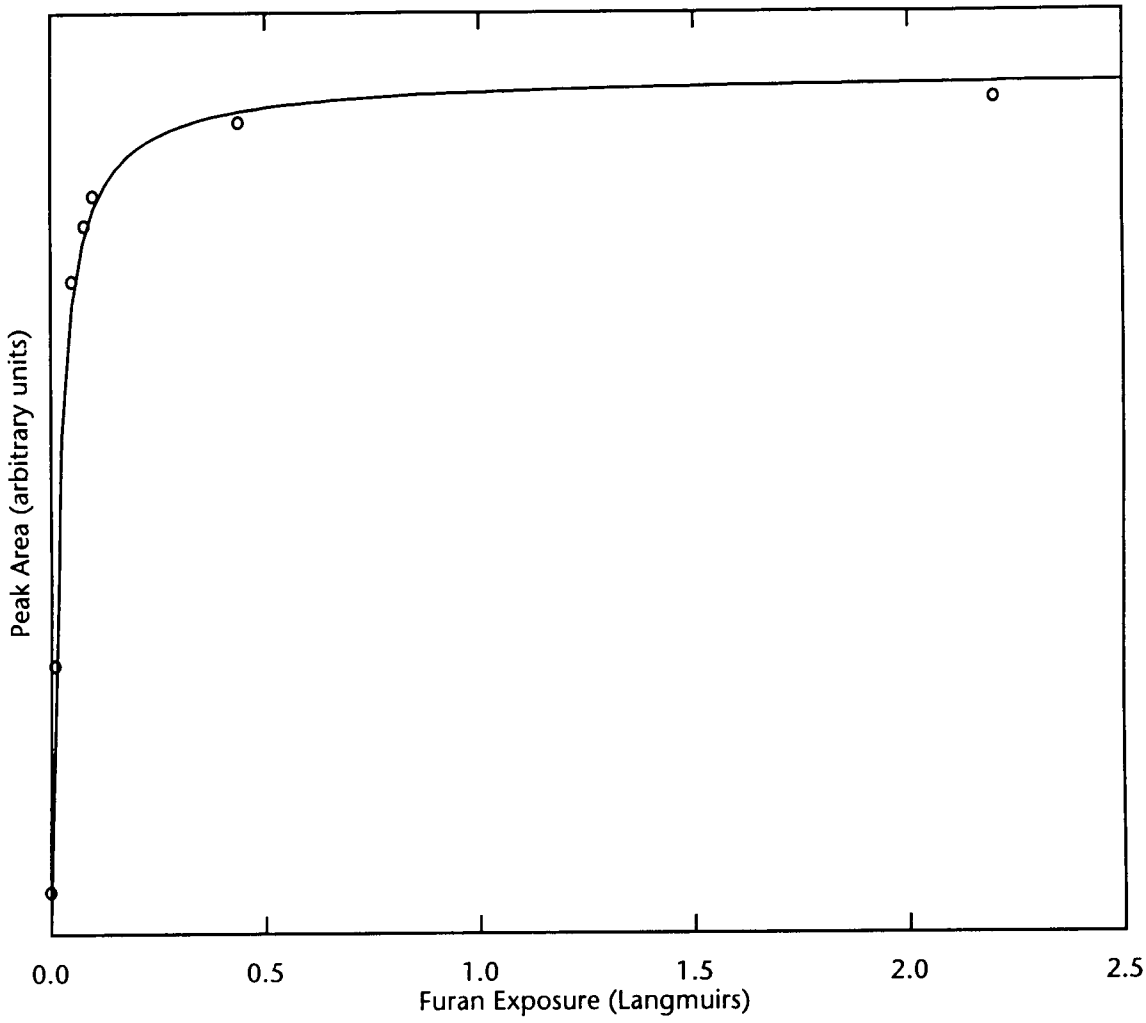

Figure 3-19. Integrated m/e=2 peak areas plotted as a function of initial furan exposure on clean Mo(110), curve fit for second order kinetics

Another way to monitor the uptake of furan on Mo(110) is to measure the C/Mo AES peak height ratio. To eliminate the shielding effect of co-adsorbed hydrogen, the sample was first heating to 400°C (the point at which hydrogen had all desorbed) before measuring the AES peak heights. Figure 3-20 shows the C/Mo AES peak height ratio as a function of initial furan exposure using this method.

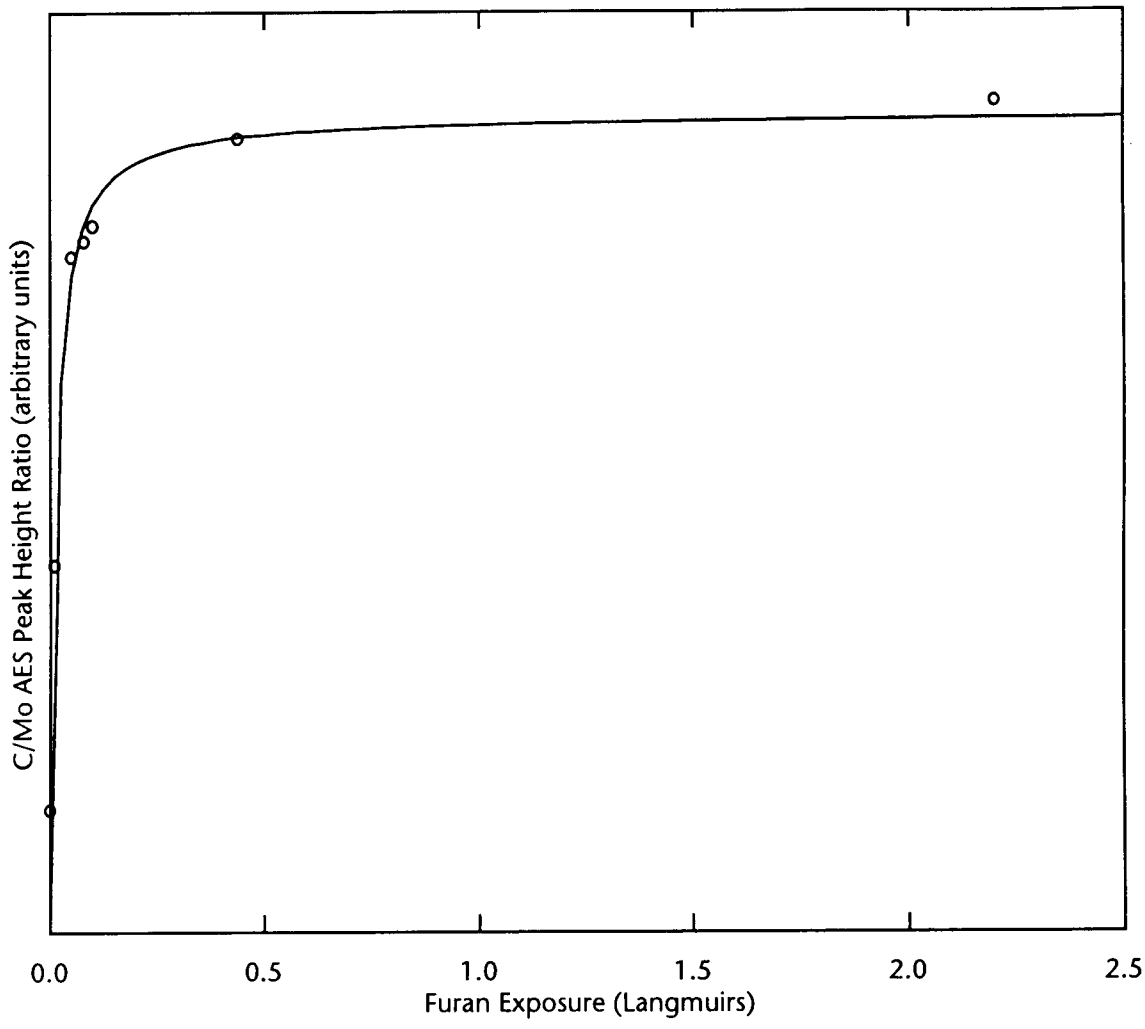

Figure 3-20. C/Mo AES peak height ratio after heating to 400°C, plotted as a function of initial furan exposure on clean Mo(110), curve fit for second order kinetics

The C/Mo AES peak height ratio plot shows the same result as the m/e=2 TPRS peak area plot, namely that furan saturation of the clean Mo(110) surface (counting only furan molecules that decompose, not those that molecularly desorb) occurs at around 2 Langmuirs and that it seems to follow Langmuir's simple model for adsorption (see "Adsorption Isotherms" on page 38 for more information about Langmuir's adsorption model).

Another way to explore a surface reaction is to monitor the surface with AES as a function of temperature. The clean Mo(110) surface was exposed to a saturation dose of furan, after which the surface was annealed for one minute intervals at increasingly higher temperatures. As the amount and nature of the surface furan carbon residue change, the AES C peak heights and shapes, Mo peak heights, and C/Mo peak height ratios change also. Figure 3-21 shows the C and Mo AES peak height results.

The C peak height increases from 50°C to 300°C which correlates with the hydrogen TPRS results, which show that most hydrogen desorption occurs below 300°C. At its lowest level, the Mo signal is attenuated by a factor of 0.33 from its clean-surface value. Because the temperatures at which the AES spectra were obtained were not constant due to the increasing anneal temperatures, the C/Mo peak height ratios shown in Figure 3-22 provide a better measure of relative C coverage than the C or Mo peaks by themselves, i.e. dividing the C signal by the Mo signal "normalizes" the result to account for between-run inconsistencies.

Again there is a steady increase in the carbon coverage from 50°C to 300°C, as measured by the C/Mo AES peak height ratios. However the plateau observed in the C peak heights between 300°C and 700°C is compressed, ending here at 400°C. From this plot, it appears that soon after the hydrogen TPRS signal falls to background levels (around 400°C), carbon begins to leave the surface or dissolve into the bulk, both of which would reduce the C/Mo AES peak height ratio. Part of the leaving C is in the form of CO which desorbs in a second-order

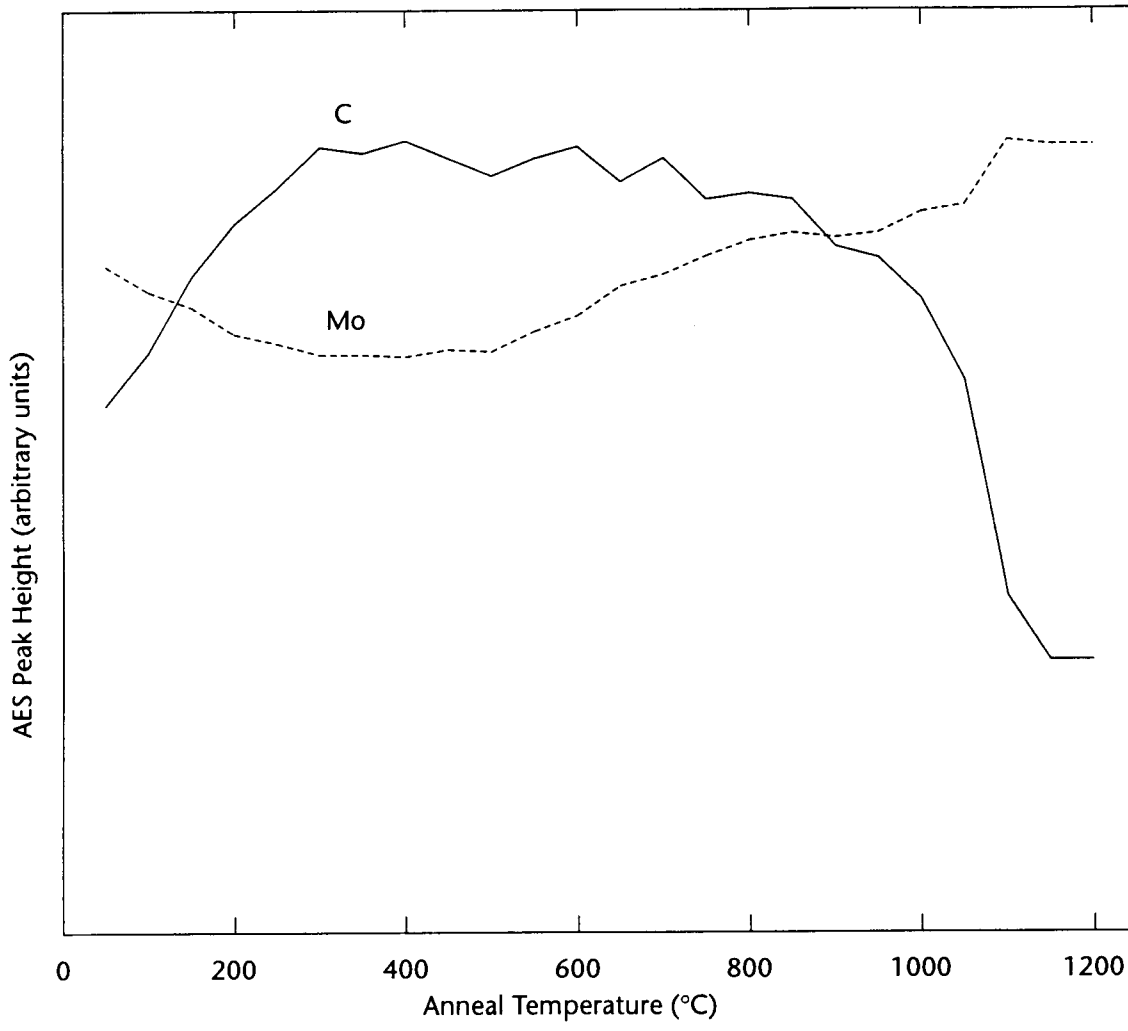

Figure 3-21. C and Mo AES peak heights as a function of anneal temperature for a saturation dose of furan on clean Mo(110)

associative process at about 700 °C; this could account for some of the decrease in the C/Mo peak ratio between 500°C and 900°C. Other research on the reaction of ethylene on the Mo(110) surface, reports the thermal indiffusion of carbon at temperatures above 1100°C[50]. This corresponds roughly to the 950°C to 1150°C region of the plot above in which the C/Mo ratio decreases rapidly.

50. M.B Young and A.J. Slavin, Surf. Sci., **245**, 56, (1991)

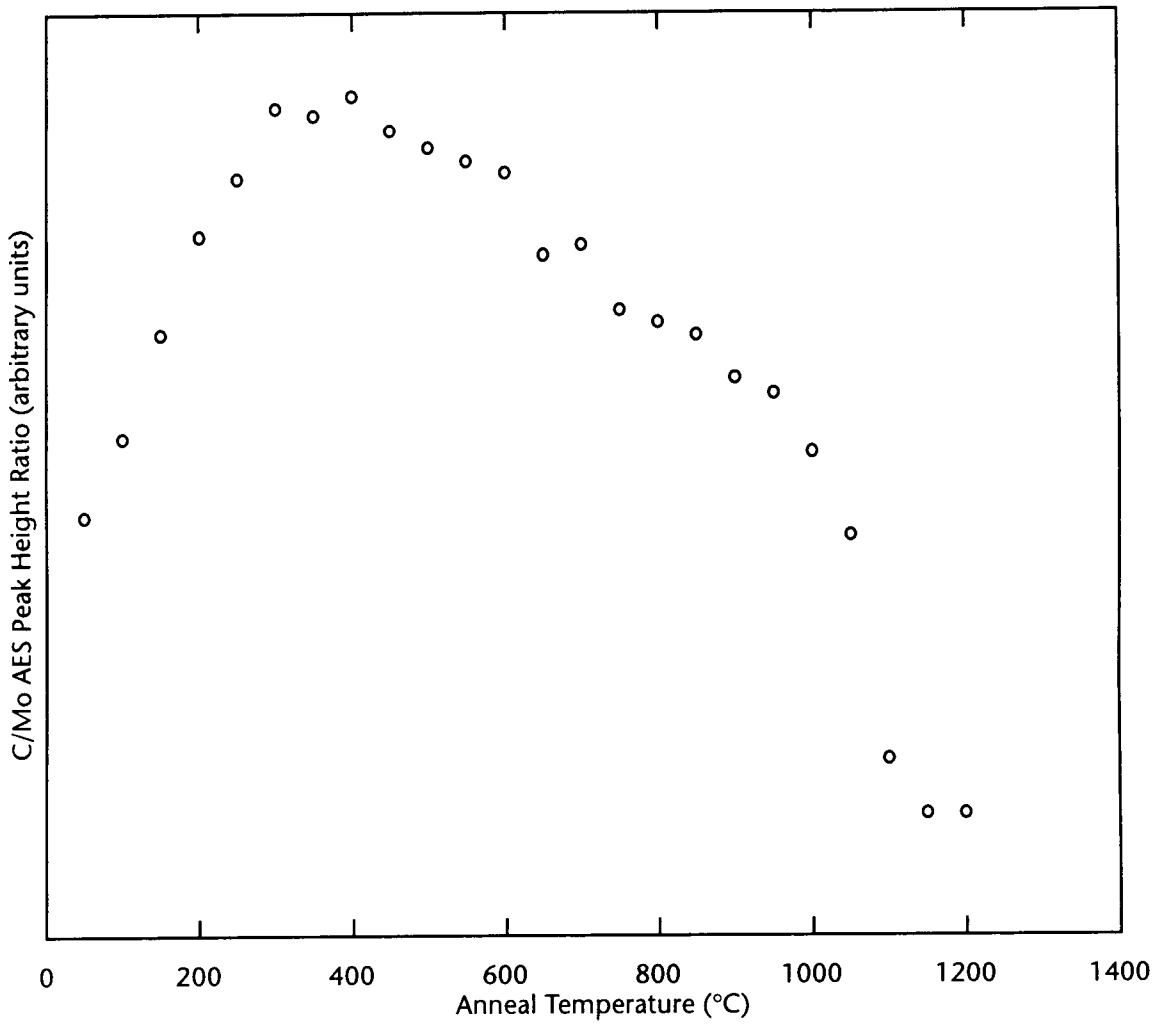

Figure 3-22. C/Mo AES peak height ratio as a function of anneal temperature for a saturation dose of furan on clean Mo(110)

During annealing, the C AES peak not only changes size, it also goes through a peak shape transition.

The C peak shape generally has at least three peaks, at 253 eV, 261 eV, and 272 eV (measured at the bottom of the peak – not the midpoint), although the 272

eV peak is sometimes split due to an interatomic transition[51]. In this experiment, a clear difference is evident between the low temperature C signals (50–200°C)

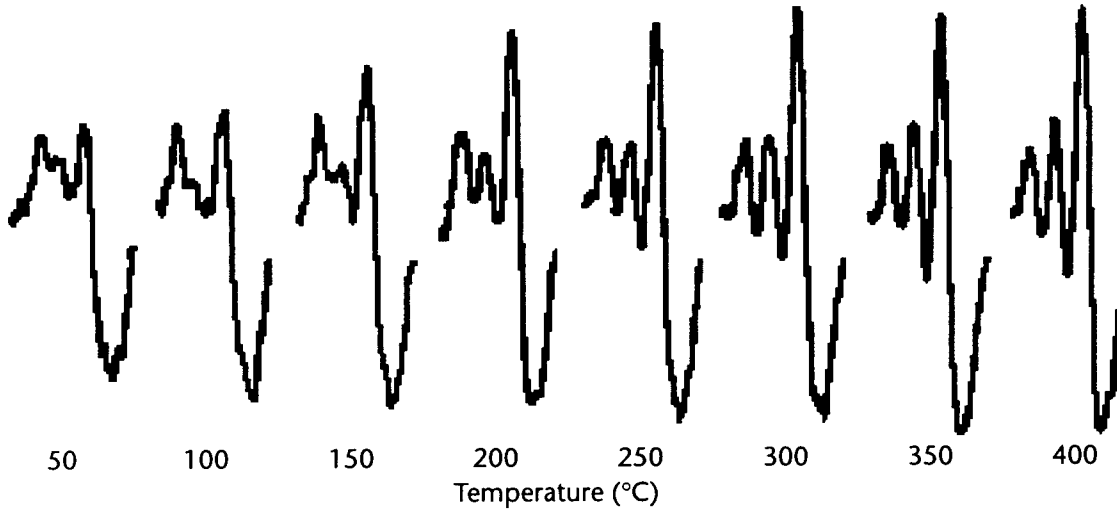

Figure 3-23. C AES peak shape as a function of anneal temperature for a saturation dose of furan on clean Mo(110)

and the higher temperature signals. The transition from low to high temperature shape is complete by 400°C, the same temperature at which the C/Mo peak height ratio stops increasing and the hydrogen TPRS is complete. The C peak shape above 400°C is characteristic of a surface carbide, and the low temperature shape indicates the presence of amorphous carbon, perhaps in the form of hydrocarbon fragments.

From the above evidence a tentative reaction scheme for a saturation dose of furan on clean Mo(110) can be formulated.

---

51. G. Panzner and W. Diekmann, Surf. Sci., **160**, 153, (1985)

1. At low temperatures (≤50°C), furan adsorbs on the clean Mo surface, probably via a carbon atom after the abstraction of one or more hydrogen atoms.
2. The resulting chemisorbed hydrogen desorbs associatively in a peak centered at about 125°C.
3. Some furan adsorbs molecularly, desorbing in a peak centered at about 80°C (the exact location of the peak is dependent on the initial furan coverage).
4. CO is abstracted in a ring-breaking process, a portion of which desorbs molecularly via a first-order process in a peak centered at about 70°C. The remaining abstracted CO decomposes to form chemisorbed C and O.
5. The resulting hydrocarbon fragments dehydrogenate releasing hydrogen in a reaction-limited process that produces a peak centered at about 250°C.
6. The carbon skeletons decompose, leaving only carbon and oxygen atoms chemisorbed on the Mo(110) surface.
7. Chemisorbed C and O atoms desorb associatively as CO in a peak centered at about 700°C.
8. The remaining chemisorbed C, probably in carbidic form, dissolves into the bulk at temperatures above 950°C.

3.3.1.2 *Furan/S/Mo(110)*

Pre-adsorption of sulfur on the Mo(110) surface deactivated the surface to reaction with furan – the more sulfur on the surface the less furan that adsorbs

and subsequently reacts. This parallels results from other research on the sulfided Mo(110) surface[52] and the sulfided Mo(100) surface[53].

Figure 3-24 shows the TPRS m/e=2 signals plotted as a function of sulfur coverage. One thing that is immediately apparent compared to the same plot on the clean surface is the relative stability of the location of the β2 peak (the high temperature peak). In Figure 3-18, the β2 peak moves toward lower temperatures as the furan coverage decreases. In addition, a sulfur coverage of approximately 0.5 monolayers seems to almost completely passivate the surface toward hydrogen production.

Using the same two measures of furan coverage as were used in the section above, the TPRS m/e=2 peak area and the C/Mo AES peak height ratio (after heating to 400°C), the furan "adsorption capacity" was measured as a function of sulfur coverage. Figure 3-25 shows the TPRS m/e=2 peak areas as a function of sulfur coverage.

Increasing sulfur coverages appear to linearly decrease the hydrogen producing capability of the Mo(110) surface during the TPRS of furan.The curve fit crosses the *x*-axis at 0.56±0.6 monolayers, suggesting that θ_S~0.56 is the sulfur coverage at which the surface is completely passivated toward furan dehydrogenation. The peak area at θ_S=0.25 is approximately half of the peak area at θ_S=0.0.

---

52. J.T. Roberts and C.M. Friend, Surf. Sci., **186**, 201, (1987)

53. D.G. Kelly, Doctoral Dissertation, U.C. Berkeley, 171 (1990)

Figure 3-26 tells a similar story for the production of CO. Again, a sulfur coverage of approximately 0.5 monolayers seems to shut down the production of CO during the TPRS of furan on Mo(110). The TPRS m/e=28 peak areas agree with the TPRS m/e=2 peak area result: increasing the sulfur coverage linearly

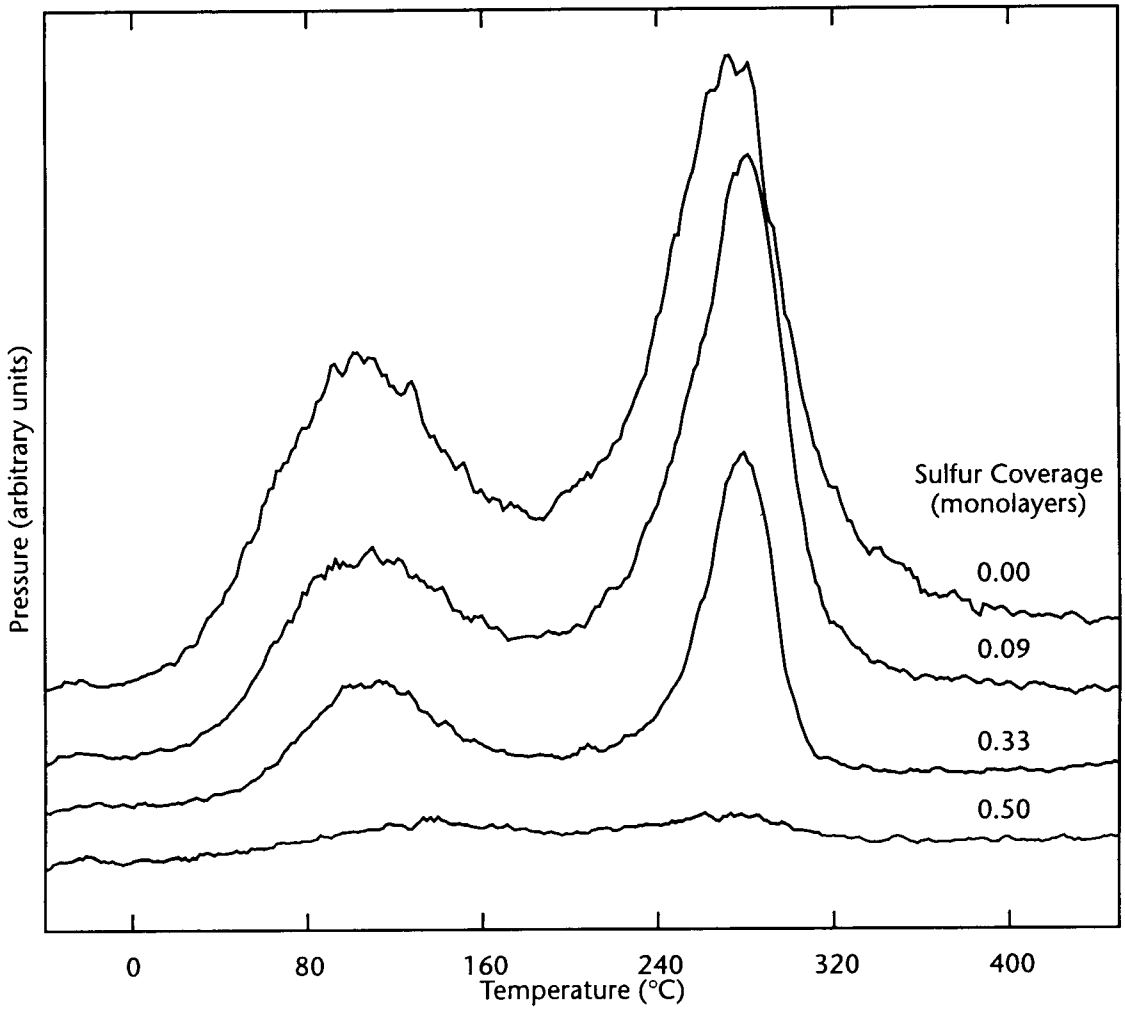

Figure 3-24. TPRS m/e=2 peaks plotted as a function of sulfur coverage for saturation doses of furan on sulfided Mo(110)

decreases the ability of the Mo(110) surface to produce CO during the TPRS of furan. The low temperature peak on the m/e=28 TPRS curve for the sulfur

coverage of 0.5 monolayers is not completely gone; what remains in probably the result of weakly bound CO from background contamination.

A third check of the apparent sulfur passivation of the (normally highly reactive) Mo(110) surface comes from C/Mo AES peak height ratios, measuring the

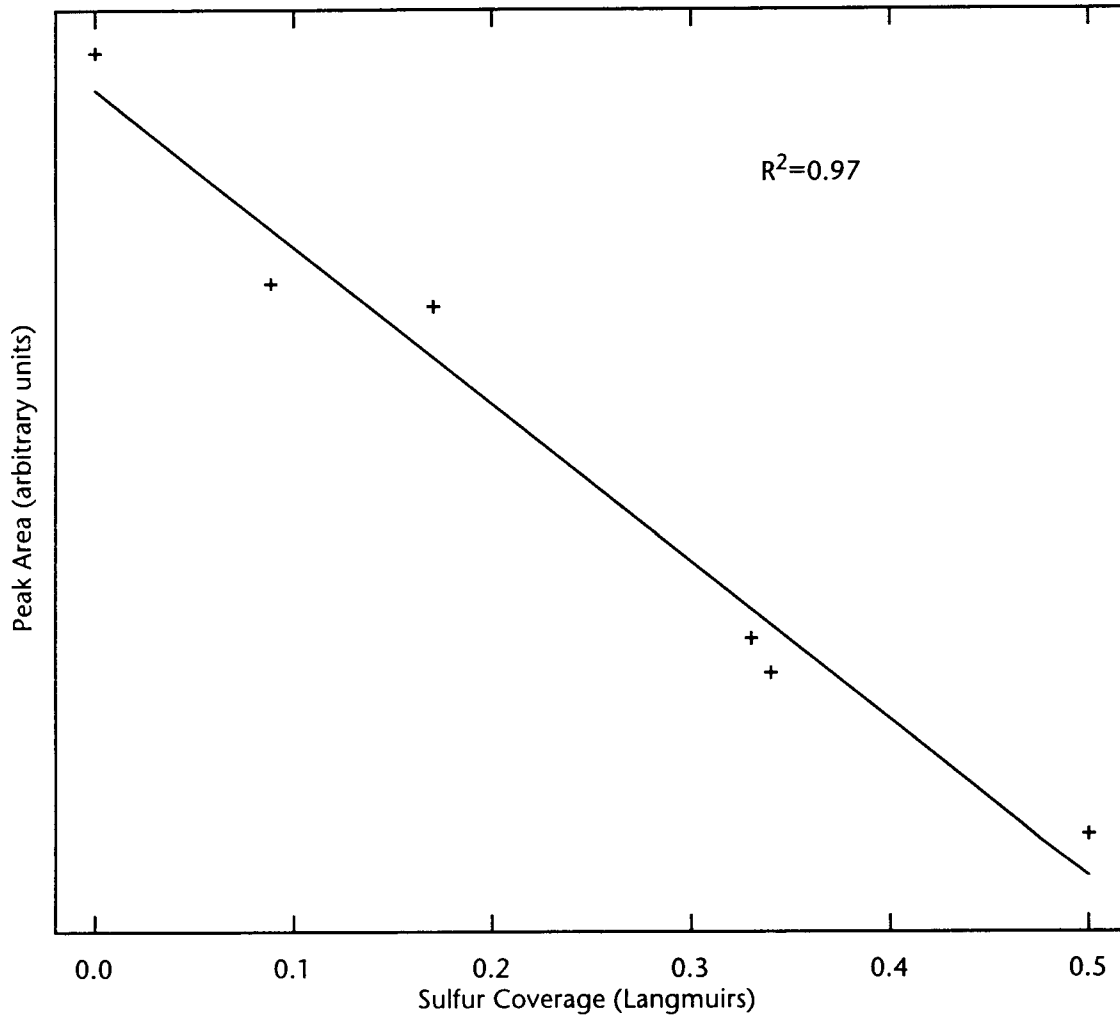

Figure 3-25. Integrated m/e=2 peak areas plotted as a function of sulfur coverage for saturation doses of furan on sulfided Mo(110)

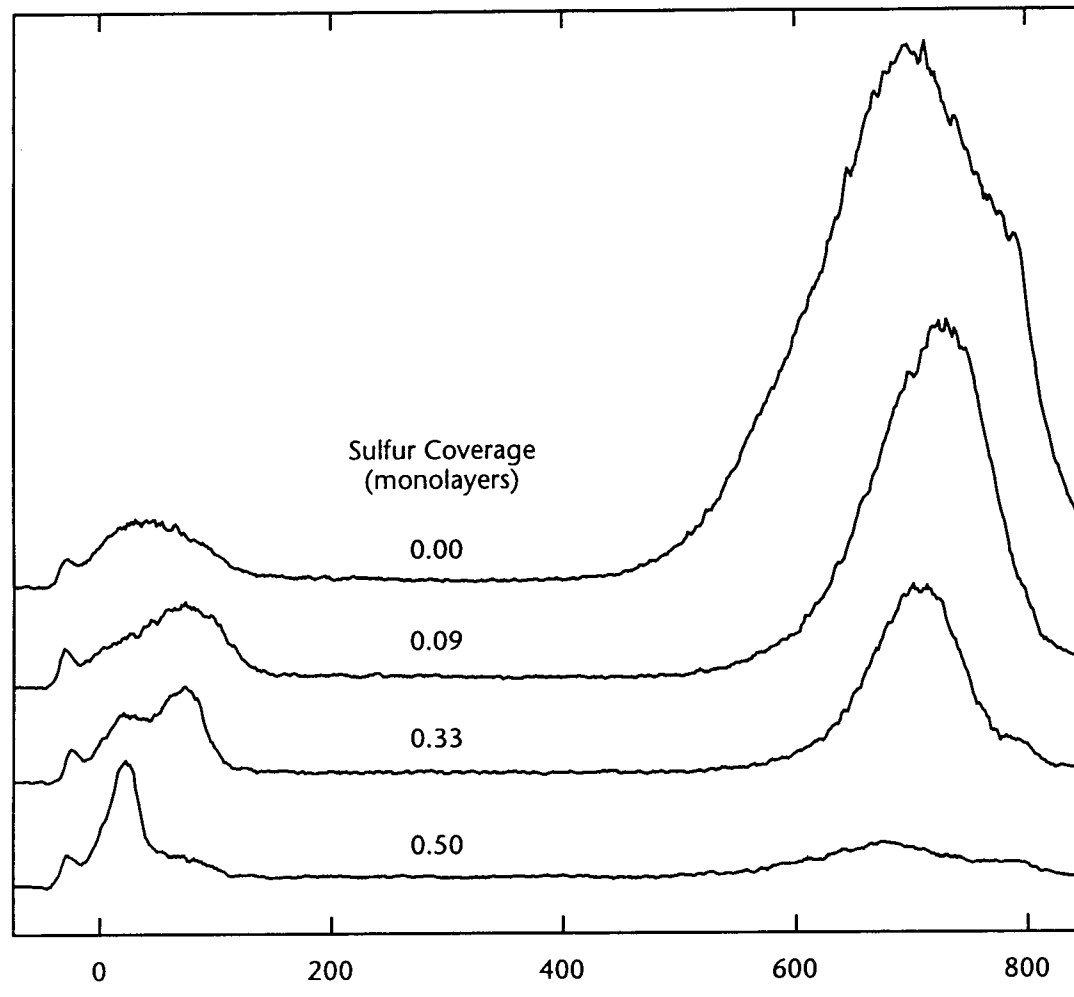

Figure 3-26. TPRS m/e=28 peak as a function of sulfur coverage for saturation doses of furan on Mo(110)

carbon residue on the sulfided Mo surface after adsorbing a saturation dose of furan and heating to 400°C to remove hydrogen.

In agreement with the m/e=2 peak areas, the C/Mo AES peak height ratios decrease linearly as sulfur coverage increases. At θ_S=0, the C/Mo ratio is almost three times bigger than the C/Mo ratio at θ_S=0.25. The curve crosses the *x*-axis at θ_S=0.39, indicating that at or above that sulfur coverage, production of surface carbon is minimized.

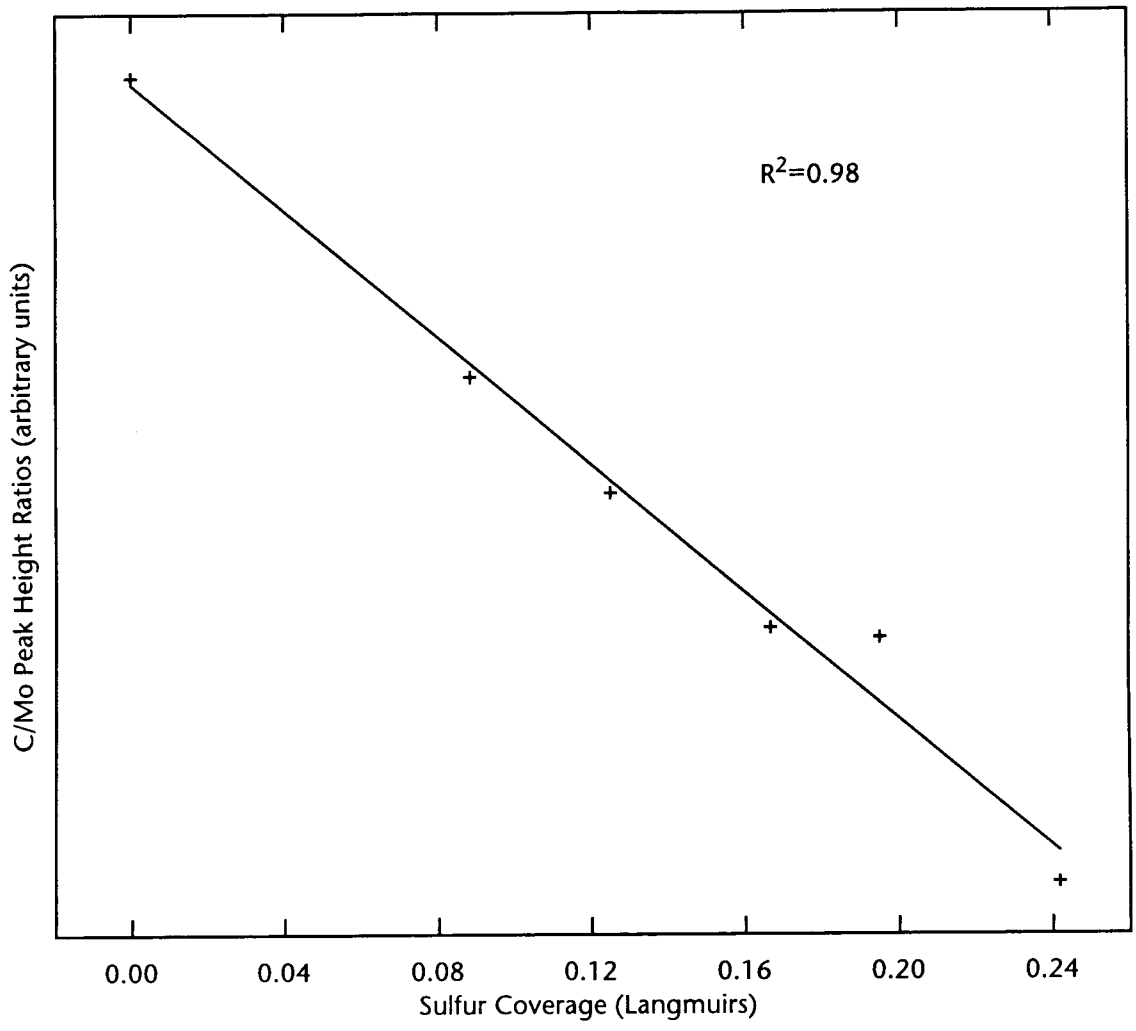

Figure 3-27. C/Mo AES peak height ratios after heating to 400°C, plotted as a function of sulfur coverage for saturation doses of furan on Mo(110)

3.3.1.3 *Furan/D_2/S/Mo(110) and D_2/furan/S/Mo(110)*

Hydrogen is always present during the catalytic hydrodeoxygenation of synfuels, usually at very high pressures (> 10 atm). Obviously this is not possible in a UHV study; although there are UHV chambers that contain a mini-chamber in which high-pressure experiments can be carried out. The mini-chamber can be pumped out after a high pressure experiment and opened to

expose the sample to standard UHV tools for surface analysis. In the absence of such a system, the normal procedure for exploring the affect of hydrogen on a surface reaction involves one or more of three methods:

- Carry out the experiment in a background pressure of hydrogen.
- Predose the surface with hydrogen before dosing with the test compound.
- Co-dose the surface with hydrogen and the test compound simultaneously.

Some combination of the methods above may prove useful if none yield results by themselves.

In this study, all possible permutations of the methods outlined above were used to probe whether furan reacting on sulfided Mo(110) could be induced to produce anything other than gaseous H_2 and CO, and surface carbon. Deuterium was used instead of hydrogen so that no confusion would arise over the source of additional fragments (the furan was not deuterated).

The same results were observed with or without the presence of deuterium: no additional masses were ever observed during TPRS, although the relative size of the m/e=30 peak changed if the experiment was carried out with a background pressure of H_2. Figure 3-28 shows a comparison of the m/e=28, 29, and 30 peaks for runs carried out with no deuterium and with 5×10^{-7} torr of hydrogen for saturation doses of furan on Mo(110). Note that the m/e=30 peak for the deuterium run is roughly ten times larger than that for the no deuterium run. This result was only observed if the TPRS was carried out in flowing deuterium; predosed or co-dosed deuterium had no effect.

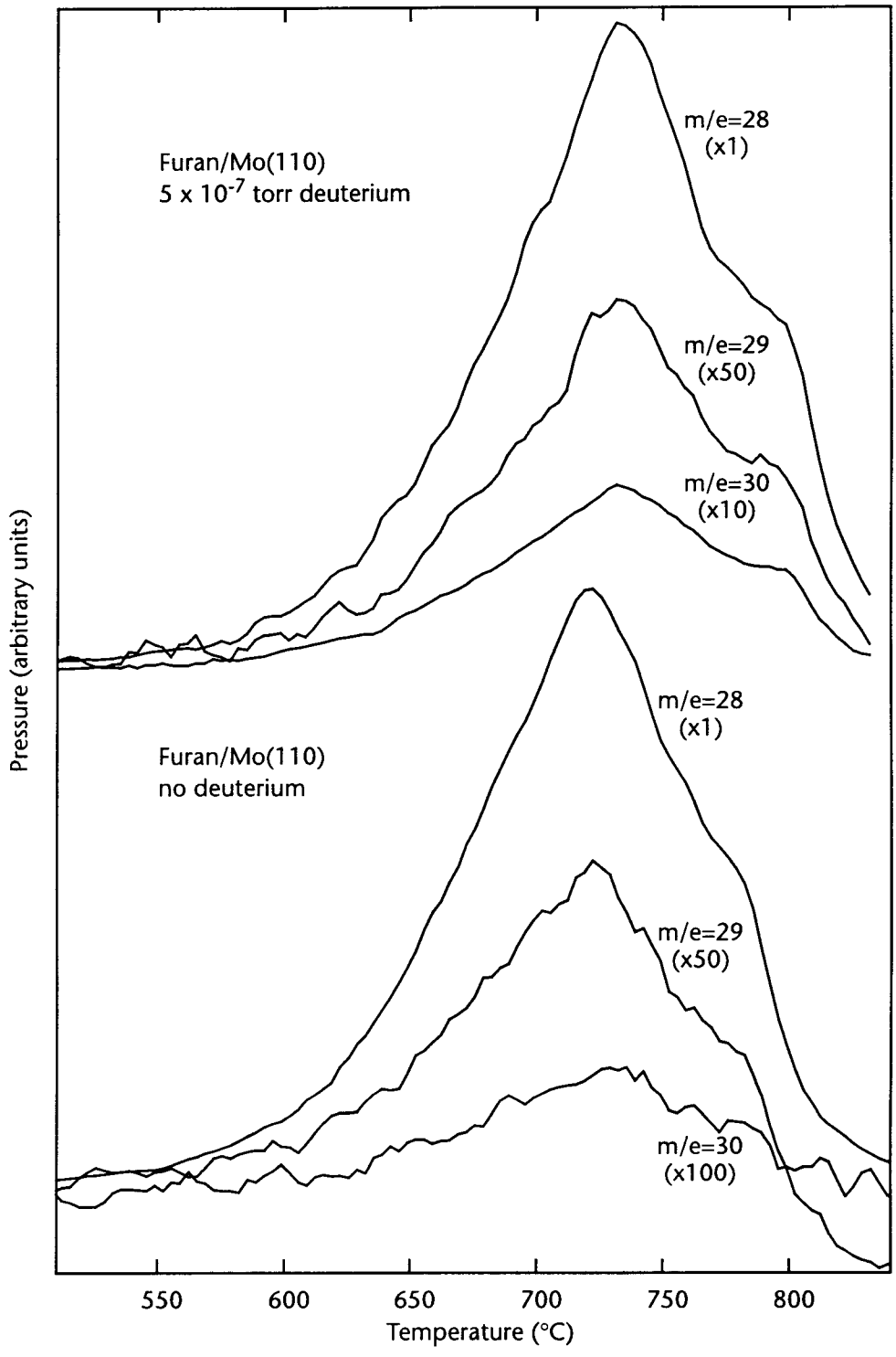

Figure 3-28. TPRS m/e=28, 29, and 30 peaks for runs carried out with no deuterium and with 5 x 10^{-7} torr of deuterium for saturation doses of furan on Mo(110)

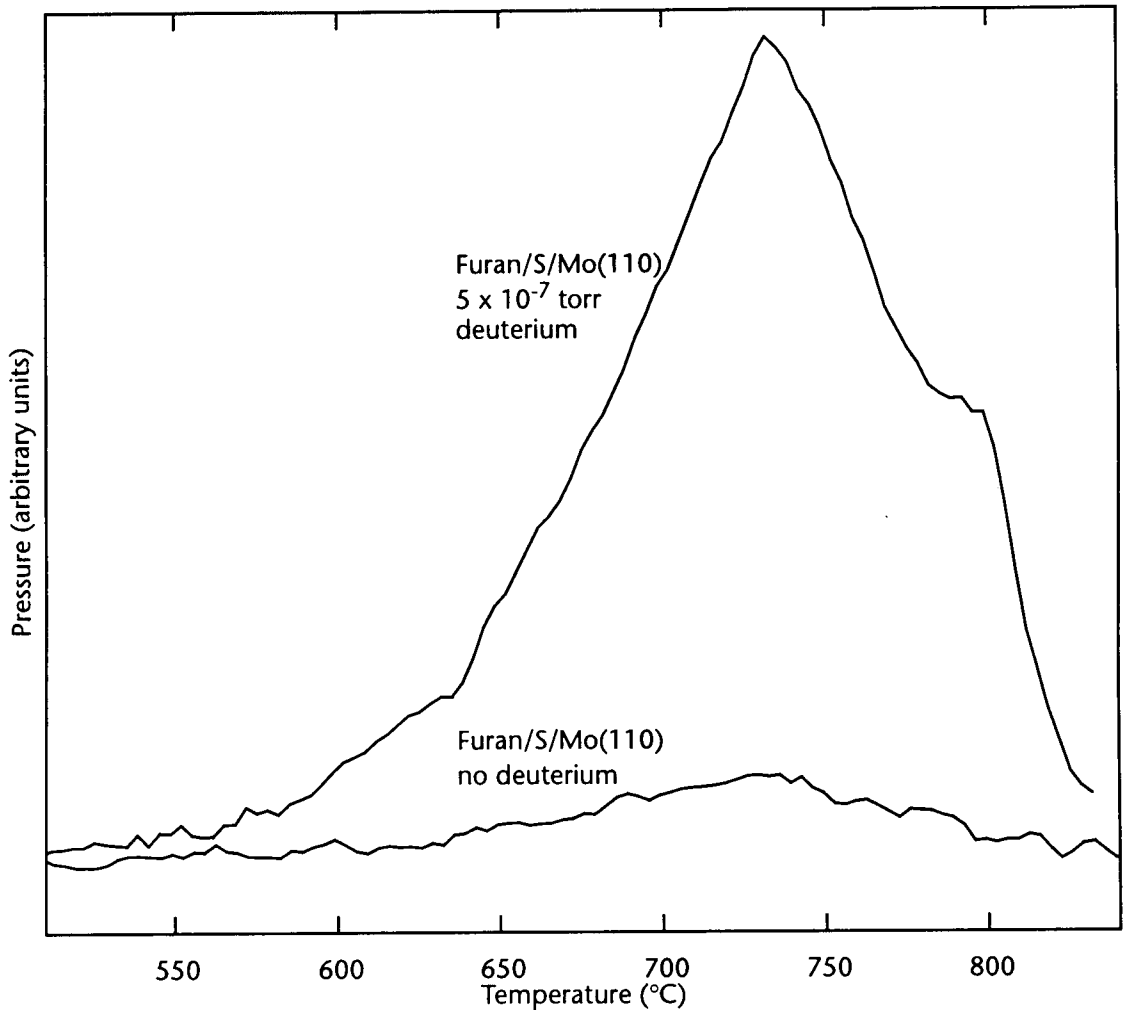

Figure 3-29. TPRS m/e=30 peaks for runs carried out with no deuterium and with 5 x 10^{-7} torr of deuterium for saturation doses of furan on Mo(110)

Figure 3-29 shows a comparison of the two m/e=30 peaks.

The m/e=30 peak closely tracks the m/e=28 peak, but is much too large (8-10 times too large) to be due solely to CO^{18} as it is when the reaction is carried out in the absence of deuterium. Two possible sources are:

- a deuterated hydrocarbon, possibly formed via a Fischer-Tropsch reaction
- a deuterated formyl species – D_2CO or DCO

A deuterated hydrocarbon such as C_2D_4 would have a large peak associated with it at m/e=32 and a smaller peak at m/e=26; this was not case in this experiment. Likewise, D_2CO's mass spectrum has a sizeable peak at m/e=32. This leaves the most likely choice – DCO.

Here are three possible mechanisms by which DCO could form in this situation:

- Gas-phase reaction

$$2CO_{(g)} + D_{2(g)} \rightarrow 2DCO_{(g)}$$

- Langmuir-Hinshelwood reaction

$$CO_{(S)} + D_{(S)} \rightarrow DCO_{(S)} \rightarrow DCO_{(g)}$$

- Eley-Rideal reaction

$$2CO_{(S)} + D_{2(g)} \rightarrow 2DCO_{(S)} \rightarrow 2DCO_{(g)}$$

A gas phase reaction is unlikely due to the long mean free path (~2m) at the deuterium pressures used in this experiment. The sample is held about 1 cm away from the mass spectrometer collimator during a TPRS experiment.

Since no change in the m/e=30 peak was observed in the deuterium predosing and co-dosing experiments, the Langmuir-Hinshelwood reaction seems unlikely. In addition deuterium, like hydrogen, has completely desorbed by 450°C, while the TPRS 30 peak shows up starting at 550°C.

This leaves the Eley-Rideal reaction, although evidence for such reactions is not in good supply[54].

---

54. G. Ertl, Ber. Bunsenges. Phys. Chem., **86**, 425, (1982)

3.3.2 Hydrogen on Clean, Sulfur, And Carbon-Modified Mo(110)

Hydrogen is ubiquitous in catalytic studies, as a reactant as in HDO, and as a product as in dehydrogenation reactions. Thus it is no surprise to find that hydrogen on transition metal surfaces has been studied extensively[55]. For low coverages of H_2, adsorption is dissociative on metals to the left of Group IB; TPRS and adsorption isotherm studies show the expected second-order desorption behavior[56]. With increasing H_2 coverage, additional desorption peaks appear at lower temperatures, some of which don't follow second-order desorption kinetics[57]. In most cases, these new peaks are not the result of the filling of a different site; instead they are caused by adsorbate-adsorbate interactions[58,59].

Pre-adsorbed sulfur and carbon both inhibit H_2 chemisorption, mainly by blocking adsorption sites[60,61], although some instances of a decrease in desorption energy are noted[62] usually accompanied by TPRS peak broadening.

---

55. C.M. Mate, B.E. Bent, and G.A. Somorjai in: *Hydrogen in Catalysis — Theoretical and Practical Aspects*, Z. Paul Ed., Marcell Dekker, Inc., New York, (1990)

56. K. Christmann, O. Schober, G. Ertl, and M. Neumann, J. Chem. Phys., **60**, 4528, (1974)

57. J.T. Yates and J.D. Carette, Phys. Rev. Letters, **39**, 209, (1977)

58. K. Christmann, O. Schober, G. Ertl, and M. Neumann, J. Chem. Phys., **60**, 4528, (1974)

59. K. Christmann, O. Schober, G. Ertl, and T. Pignet, Surf. Sci., **54**, 365, (1976)

60. M. Kiskinova and D.W. Goodman, Surf. Sci., 108, **64**, (1981)

61. J. Benziger and R.J. Madix, Surf. Sci., **94**, 119, (1980)

Both "graphitic" and "carbidic" carbon overlayers have a similar effect on H_2 adsorption and desorption.

Results presented in the next three sections are not aimed at reproducing any of the studies that examine H_2 adsorption in detail. Rather they are intended to provide a baseline from which to compare the more complicated data obtained from furan adsorption on Mo(110).

3.3.2.1 *D_2/Mo(110)*

At least one study has been done on the H_2/Mo(110) system using TPRS[63]. H_2 was observed to desorb from two sequentially populated states labeled β_1 and β_2. The TPRS peak shapes and coverage-dependent maxima are consistent with second order kinetics, i.e. dissociative adsorption. (See the section titled: "Theory – Adsorption" on page 34 for a discussion of adsorption kinetics.) Desorption activation energies were found to be 28 and 34 $\frac{kcal}{mol}$ for the two states, assuming a pre-exponential factor of 0.01 $\frac{cm^2}{molecule \cdot s}$.

In this study, D_2 adsorbed on clean Mo(110) at or below 50°C, desorbs in one, two, or three peaks depending on coverage. At low coverages (>0.05 Langmuirs), only one symmetric peak is present (β_3), but as D2 coverage increases a second peak (β_2) grows out of the side of the original peak. Both the β_2 and β_3 peak maxima change position to lower temperatures as coverage

---

62. M. Kiskinova and D.W. Goodman, Surf. Sci., 108, **64**, (1981)

63. M. Mahnig and L.D. Schmidt, Z. Phys. Chem. Neue Folge, **80**, 71, (1972)

increases, indicating that desorption energies decrease for both states as coverage increases.

At coverages approaching saturation, a sharp low temperature peak (β_1) appears at ~150°C. The β_1 peak does not change position as coverage increases further, indicating first order kinetics. Although the β_1 peak is not mentioned in the literature, similar behavior was noted for Mo(100)[64].

3.3.2.2 *D_2/S/Mo(110)*

Pre-adsorbed sulfur blocks the adsorption of deuterium and changes the appearance of TPRS peaks. Figure 3-31 shows the m/e=4 peaks for saturation doses of deuterium on clean and sulfided Mo(110).

As the sulfur coverage increases a new desorption peak appears (β_4). For S coverages greater than 0.3, the only peaks that appear are β_1 and β_4. In addition to desorption spectra changes, sulfur also physically blocks adsorption sites. One way to measure the site-blocking effect of sulfur is to plot saturation TPRS D_2 peak areas as a function of S coverage.

The x-intercept of 0.51 implies that at or above approximately 0.5 monolayers of S, the Mo(110) surface is passivated toward D_2 adsorption. The linearity of the peak area vs. sulfur coverage curve shows that site blocking monotonically increases with increased sulfur. The x-intercept 0.51 monolayers agrees well with the value obtained from the furan/S/Mo(110) experiments

---

64. D.G. Kelly, Doctoral Dissertation, U.C. Berkeley, 163 (1990)

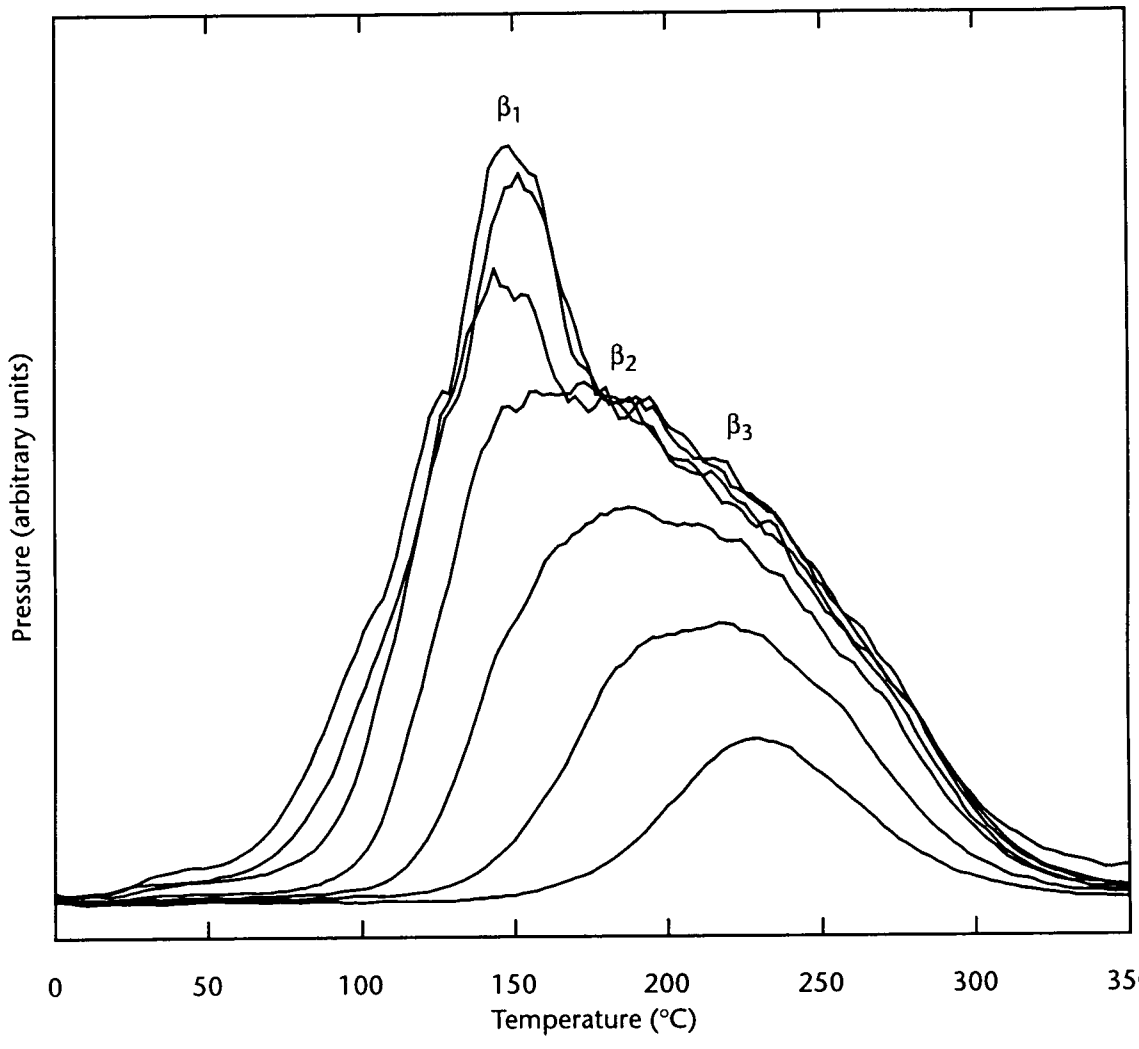

Figure 3-30. TPRS m/e=4 peaks for varying doses (0.02–10 Langmuirs) of deuterium on clean Mo(110)

(0.56 monolayers, see Figure 3-25 on page 90). This value also agrees well with values of between 0.5–0.6 reported by other researchers for both Mo(110) and Mo(100).

A series of experiments was done on four Mo(110) surfaces, three sulfided and one clean. A peak area summary of that data is given in Figure 3-33 below while the TPRS curves are shown in Figure 3-34.

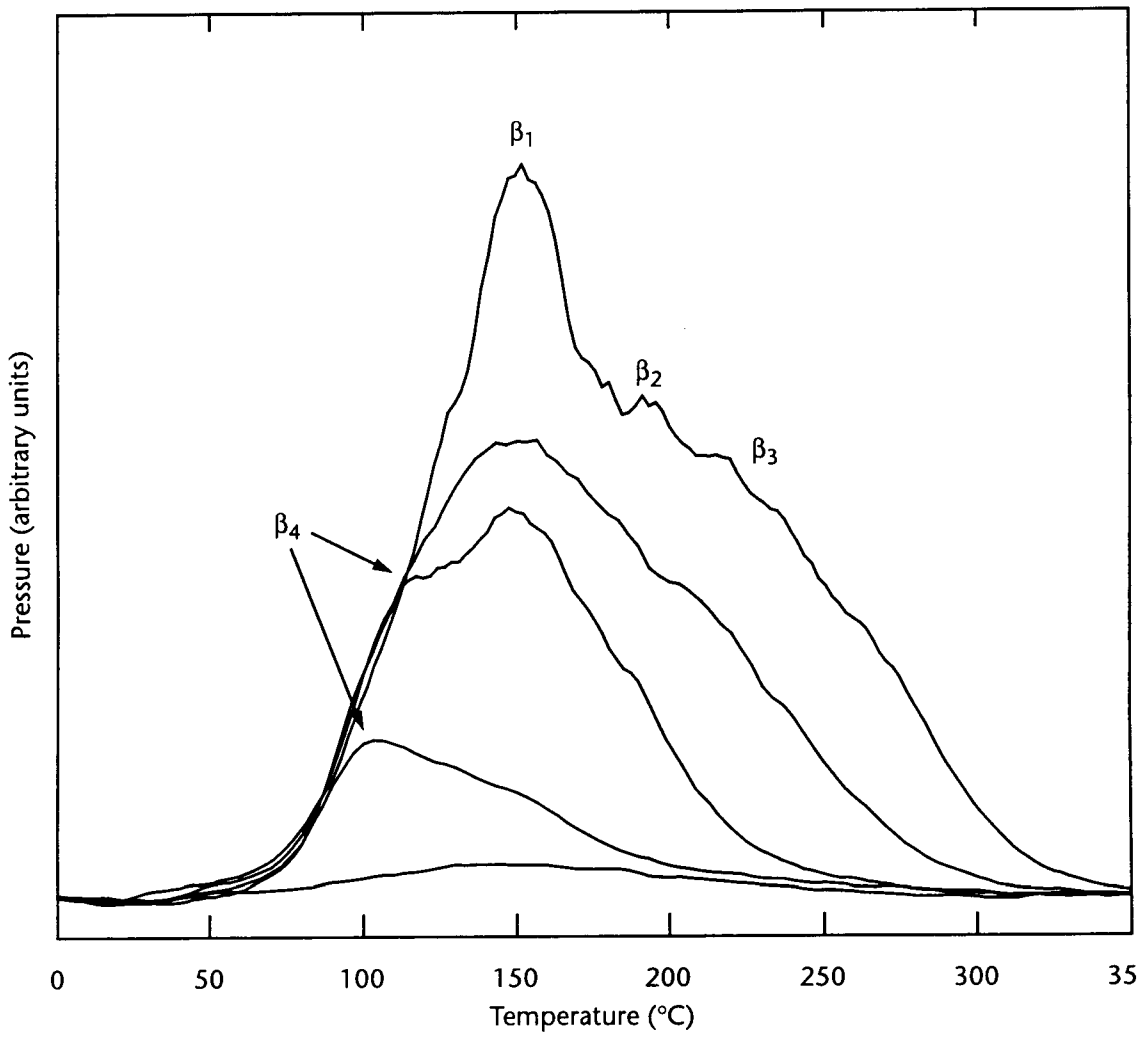

Figure 3-31. TPRS m/e=4 peaks for saturation doses (10 Langmuirs) of deuterium on clean and sulfided (0–0.4 monolayers) Mo(110)

The data in Figure 3-33 are fit using the following equation for second order kinetics,

$$A_t = A_0\left(1 - \frac{1}{(1 - Kpt)}\right) \qquad \text{Equation 3-8}$$

where A_t is the peak area at time t and A_0 is the maximum peak area. The factor K is described in the equation below:

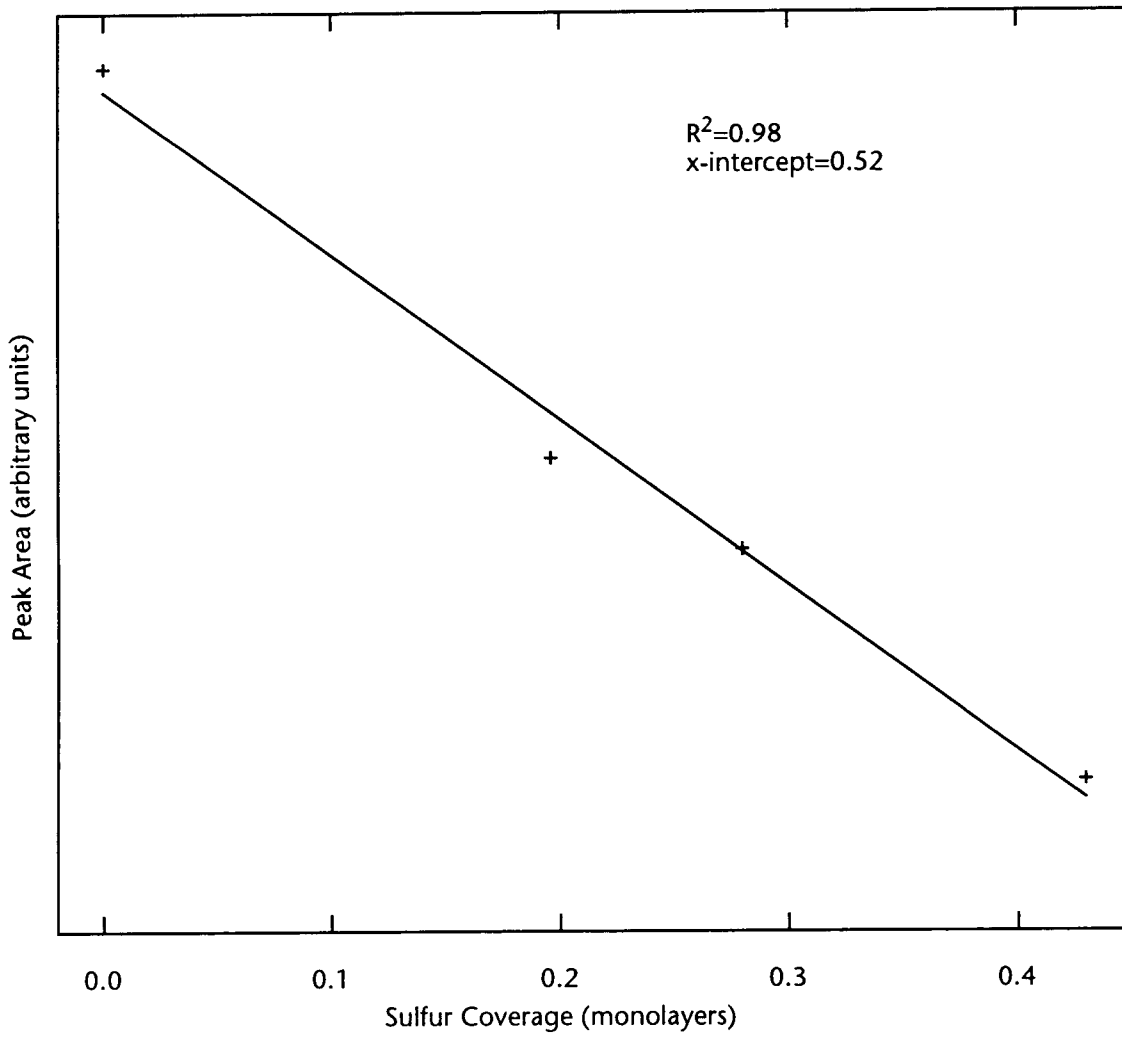

Figure 3-32. TPRS m/e=4 peak areas for saturation doses (10 Langmuirs) of deuterium on clean and sulfided Mo(110)

$$K = \frac{2}{(2\pi mkT)^{1/2}}\frac{s}{N} \qquad \text{Equation 3-9}$$

where m is the mass of a D_2 molecule, k is Boltzmann's constant, T is the temperature, s is the sticking coefficient, and N is the surface density of deuterium atom sites. The 2 in the numerator of Equation accounts for the fact that there are two D atoms per D_2 molecule. For all S coverages, the

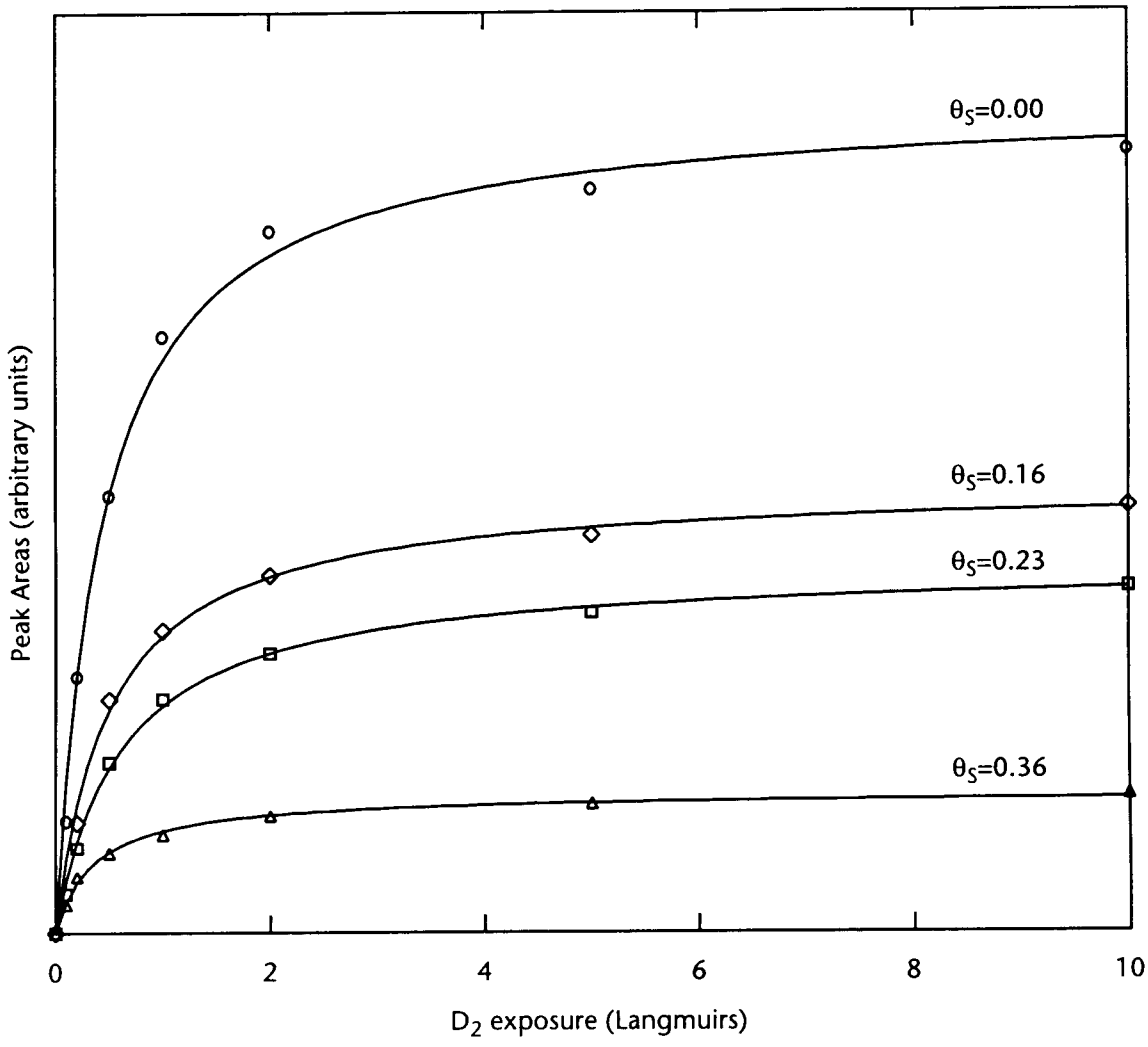

Figure 3-33. TPRS m/e=4 peak areas for varying doses (0.02–10 Langmuirs) of deuterium on clean and sulfided Mo(110).

goodness of fit is R^2=0.99 or better, reflecting the (largely) second order nature of D_2 adsorption on Mo(110).

3.3.2.3 *D_2/C/Mo(110)*

Because the decomposition of furan deposits C on the Mo(110) surface, an analogous set of experiments to those discussed above (on sulfided Mo(110)

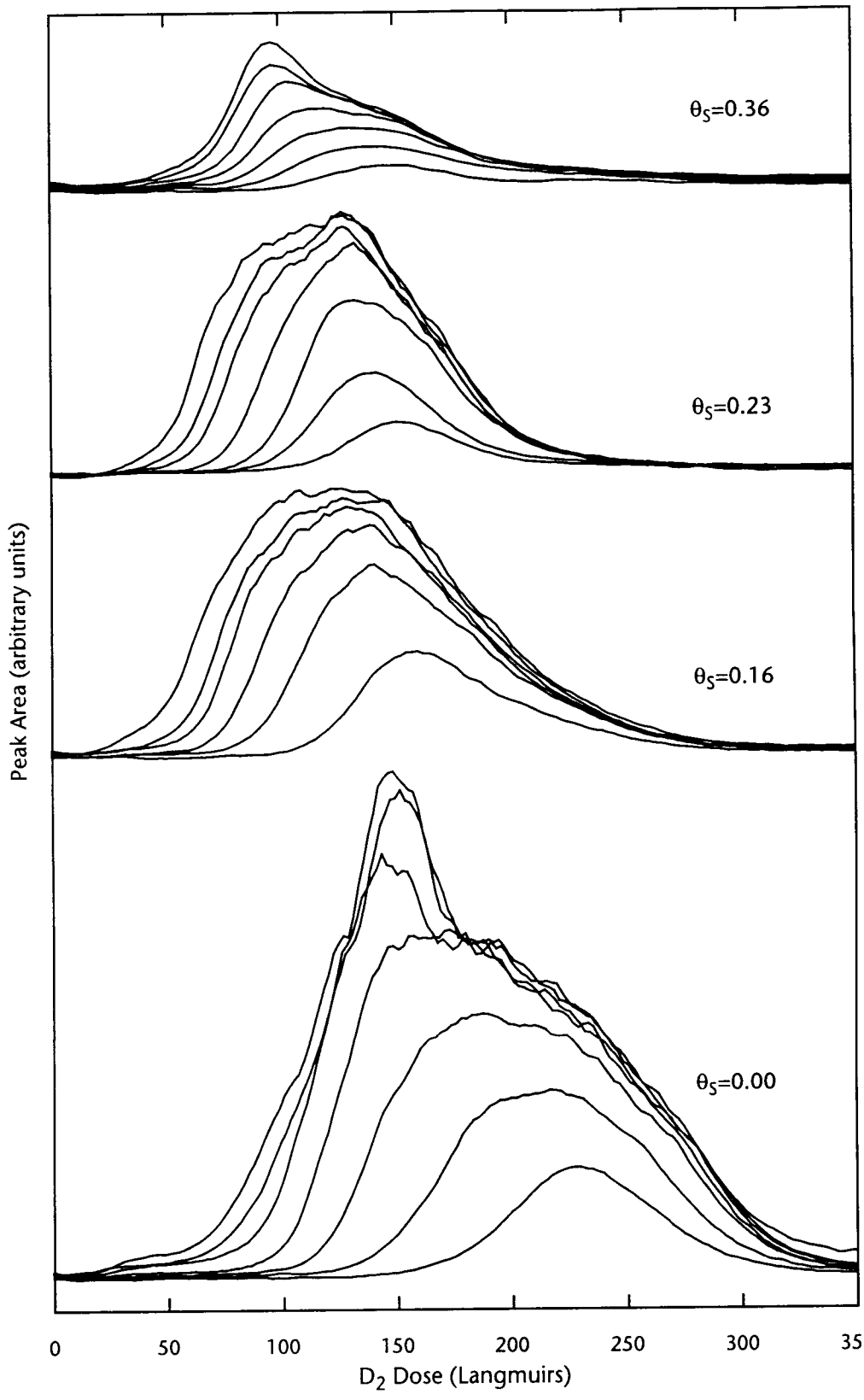

Figure 3-34. TPRS m/e=4 peaks for varying doses (0.01–10 Langmuirs) of deuterium on clean and sulfided Mo(110)

was carried out using pre-adsorbed carbon instead. Carbon overlayers were deposited by adsorbing ethylene on the clean Mo(110) surface at 600°C, which is above the H_2 desorption and ethylene decomposition temperatures. AES revealed that the resulting carbon layer had the characteristic carbidic lineshape, indicating strong C–Mo surface bonds.

Unlike the effect of sulfur, pre-adsorbed carbon does not change the location or the general shape of the deuterium TPRS peaks as is shown in Figure 3-35.

The peak areas are plotted against carbon coverage in Figure 3-36.

The x-intercept of 0.52 for D_2/C/Mo(110) joins the previous values of 0.56 for furan/S/Mo(110) and 0.51 for D_2/S/Mo(110) indicating that half a monolayer of either S or C seems to be effective at blocking adsorption.

As in the D_2/S/Mo(110) study above, a series of experiments was done on each of four different Mo(110) surfaces. A peak area summary of that data is given in Figure 3-37 below while the TPRS curves are shown in Figure 3-38.

Second order desorption kinetics seems to be the rule for D_2/C/Mo(110) as well; the curve fits (using the equation described above) yielded a good fit (R^2=0.98 or better). The TPRS peaks in Figure 3-38 show that there is not much chemical effect with respect to D_2 desorption on the Mo(110) surface due to C coverage.The size of the spectra are reduced but peak locations stay roughly the same, no matter the C coverage.

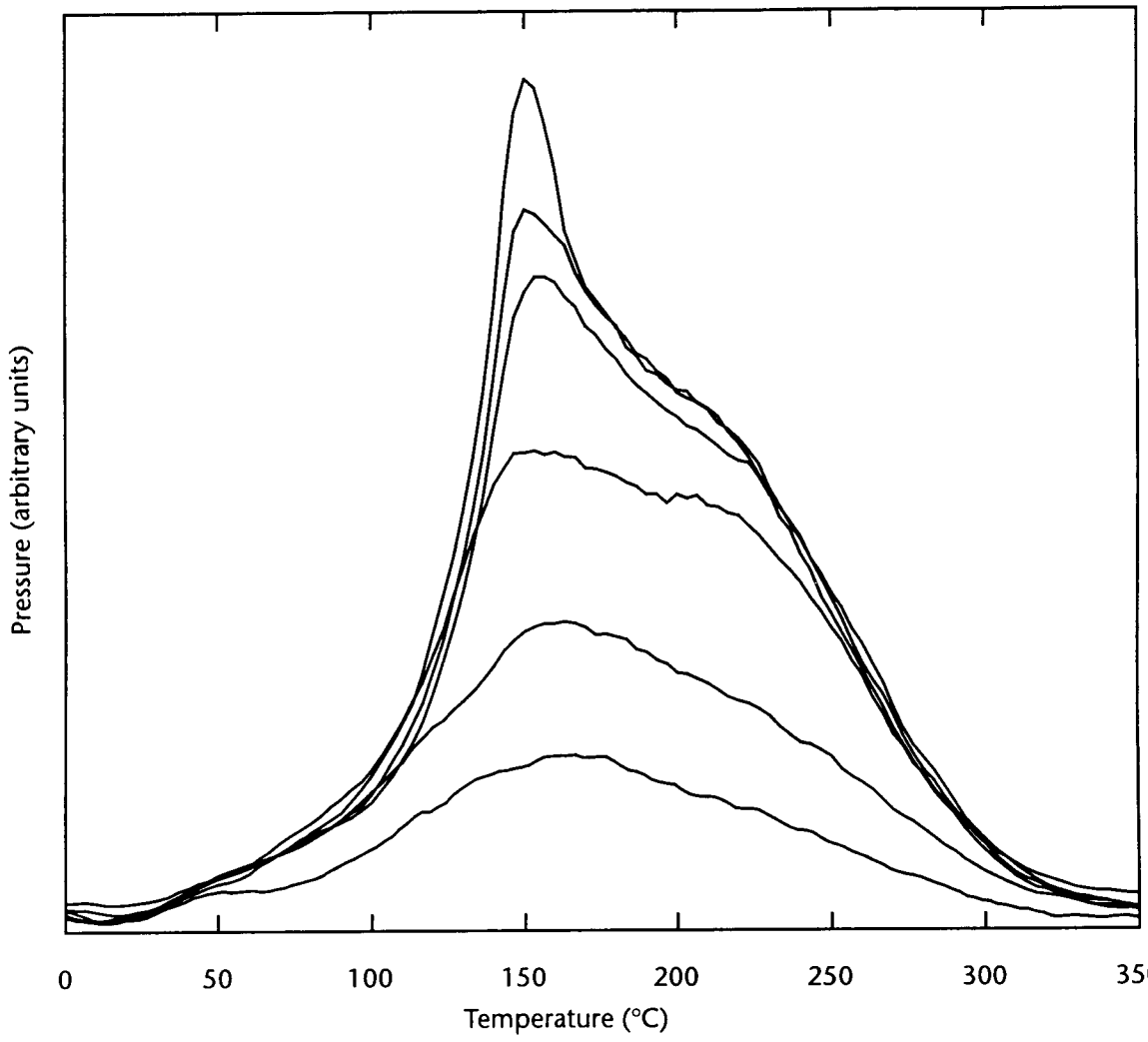

Figure 3-35. TPRS m/e=4 peak areas for saturation doses (10 Langmuirs) of deuterium on clean and carbon-covered Mo(110).

Carbon seems to block H_2 adsorption mainly through a physical blocking of adsorption sites. Since H_2 requires two adjacent sites to adsorb, C coverage of approximately 0.5 monolayers effectively passivates the Mo(110) surface.

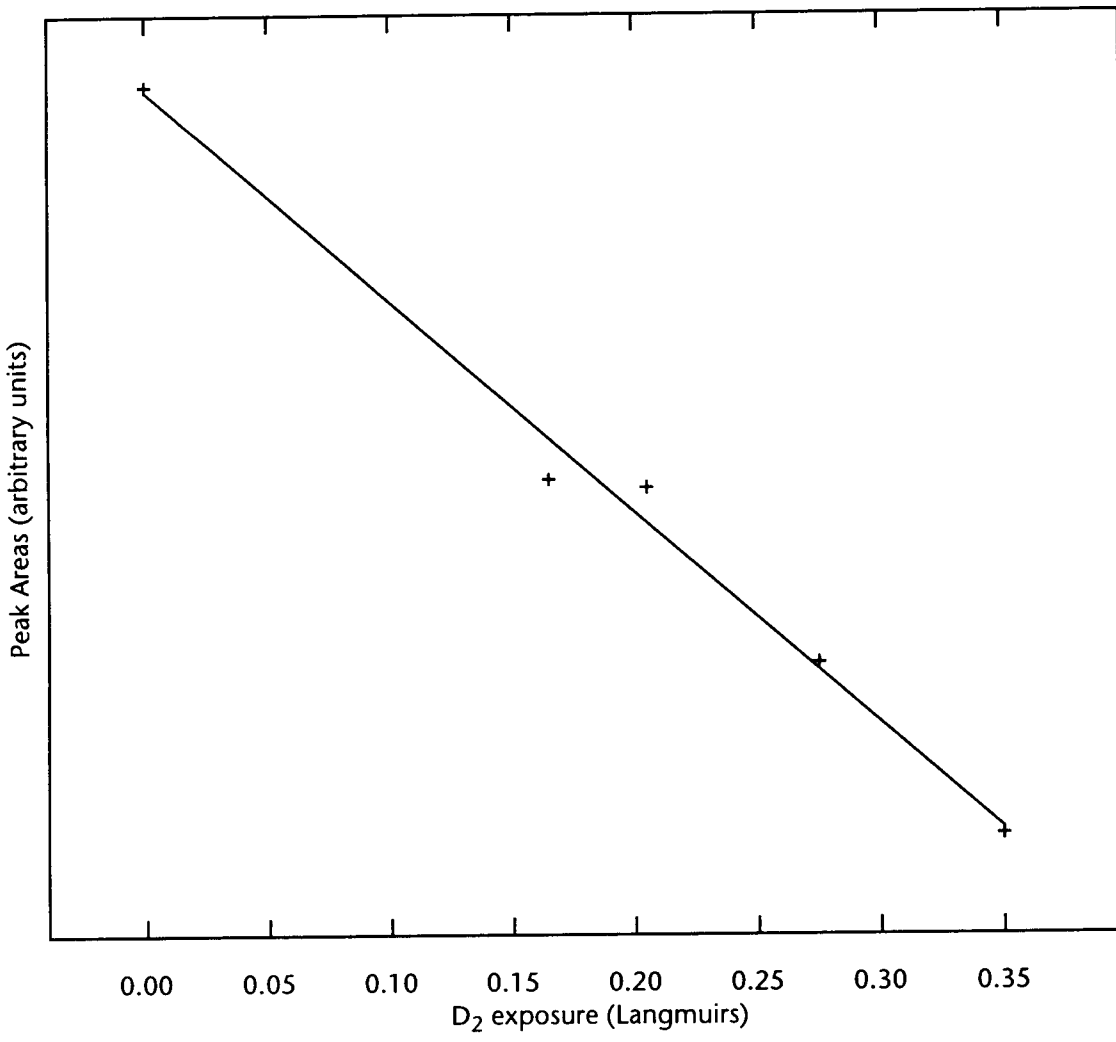

Figure 3-36. TPRS m/e=4 peak areas for saturation doses (10 Langmuirs) of deuterium on clean and carbon-covered Mo(110).

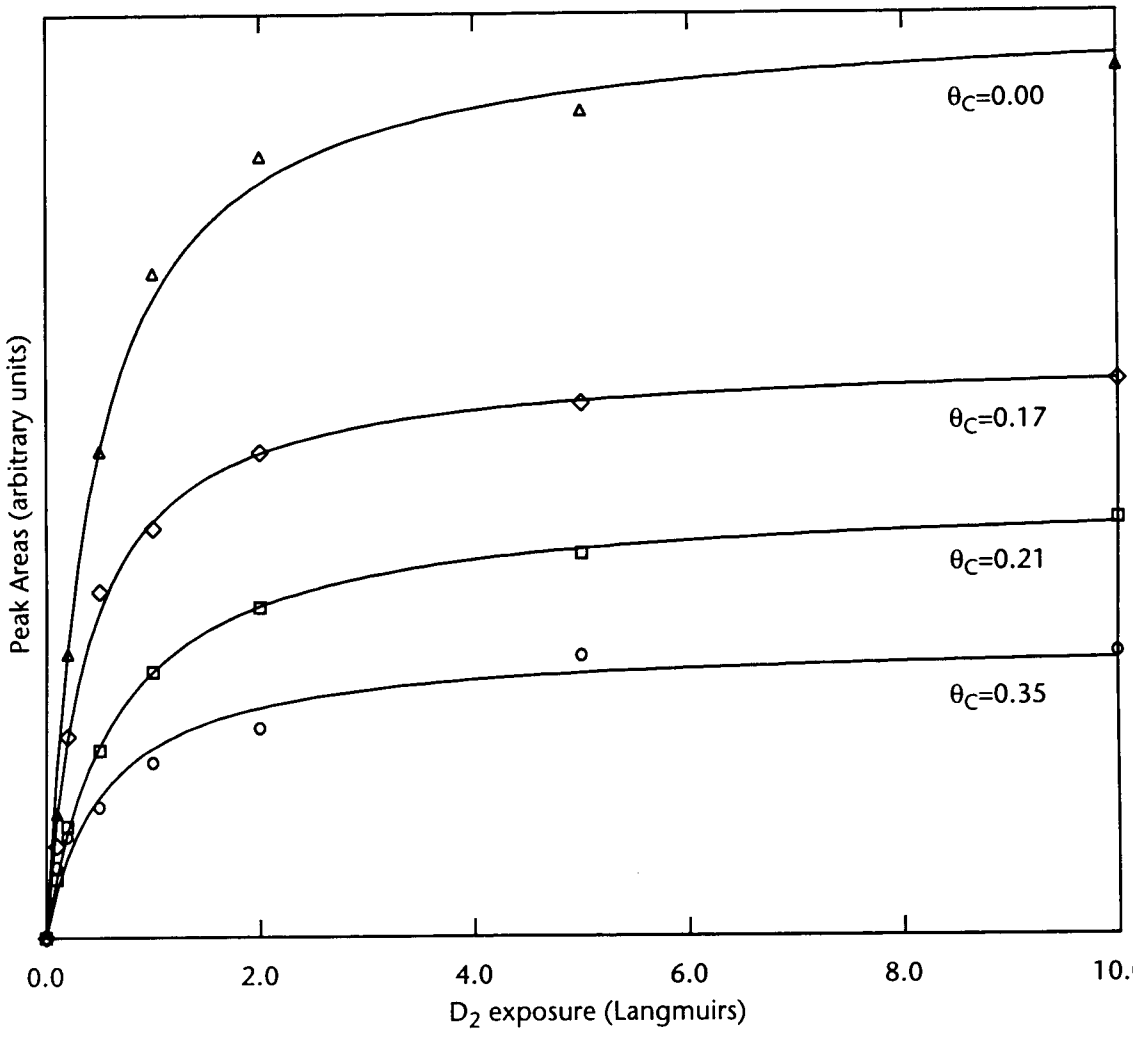

Figure 3-37. TPRS m/e=4 peak areas for varying doses (0.02–10 Langmuirs) of deuterium on clean and carbon-covered Mo(110).

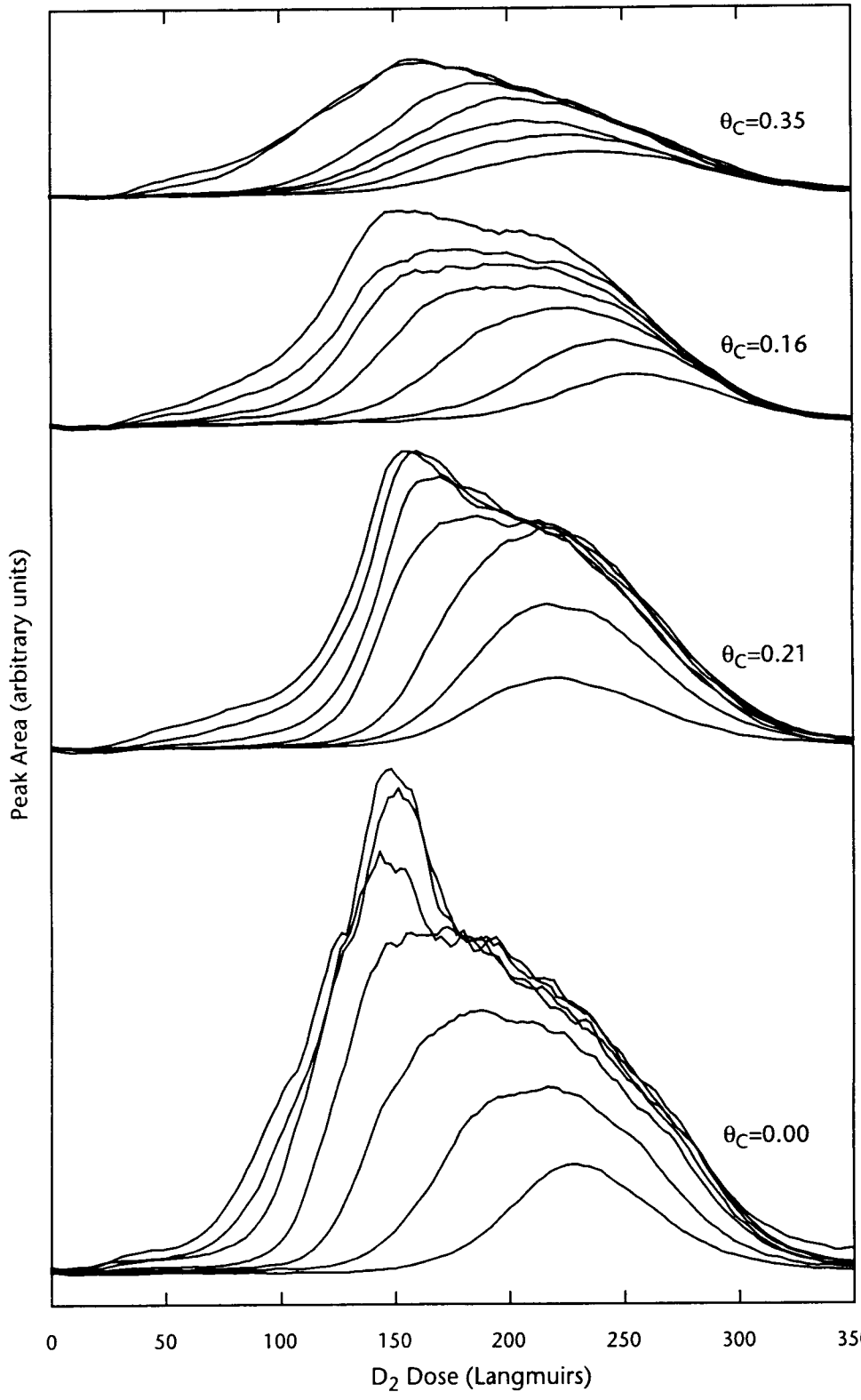

Figure 3-38. TPRS m/e=4 peaks for varying doses (0.01–10 Langmuirs) of deuterium on clean and sulfided Mo(110)

3.3.3 Carbon Monoxide on Clean And Sulfur-Modified Mo(110)

Like hydrogen, carbon monoxide is a frequent guest in surface science labs, mainly due to its well-defined and documented behavior and its ability to act as a reliable probe of surface chemistry. Whether or not CO dissociates on a given transition metal surface is largely determined by how well the metal d-bands overlap the CO $2\pi^*$-orbital[65]. In general, metals on the left side of the transition metal series have better mixing between their d-bands and the CO antibonding orbital, thus weakening the CO bond. Conversely, the d-band of metals on the right side of the series does not overlap with the CO $2\pi^*$-orbital, and little electron donation occurs.

Some adsorbates (e.g. potassium on Pt(111)[66]) can alter a surface's electronic properties by accepting or donating electrons from/to the metal. This alters the metal's d-band and its overlap with the orbitals of co-adsorbates (such as CO) over an area much larger than the physical size of the adsorbate molecule. CO is a good probe of this sort of effect since it is sensitive to the d-bands of the metal.

3.3.3.1 *CO/Mo(110)*

CO on molybdenum single crystal surfaces has been studied extensively[67,68,69]. Below 0°C, CO adsorbs molecularly, first in four-fold hollows (up to θ_C=0.5),

---

65. K. Christmann, O. Schober, G. Ertl, and M. Neumann, J. Chem. Phys., **60**, 4528, (1974)

66. K. Christmann, O. Schober, G. Ertl, and T. Pignet, Surf. Sci., **54**, 365, (1976)

then in "on-top" sites. During TPRS, the CO adsorbed in on-top sites desorbs molecularly between 0 and 200°C and the remaining CO dissociates and then recombines to desorb in a composite peak between 600 and 1000°C.

On Mo(110), the composite high temperature desorption peak is thought (by some researchers) to be composed of at least two peaks that correspond to sequentially populated surface states[70]. The desorption energies for these states have been determined to be 99 and 50 $\frac{\text{kcal}}{\text{mol}}$. There is some debate on whether there are actually two separate binding sites or whether lateral adsorbate-adsorbate interactions are responsible. High resolution electron energy loss spectroscopy (HREELS) on the Mo(100) surface has shown that only one adsorption site is responsible for the high temperature peaks[71].

Figure 3-39 shows the results of a TPRS run for a saturation dose of CO on clean Mo(110). The high temperature peak appears "cut off" because the temperature ramp ended at 800°C. The general shape and position of the peaks is in good agreement with the literature. As the initial coverage of CO decreases, the only effect is a decrease in the size of the desorption peaks.

---

67. J. McCarty and R.J. Madix, J. Catalysis, **38**, 402, (1975)

68. J.B. Benziger, E.I. Ko, and R.J. Madix, J. Catalysis, **64**, 132, (1984)

69. K.A. Pearlstine and C.M. Friend, J. Am. Chem. Soc., **107**, 5898, 91985

70. E. Gillet, J.C. Chiarena, and M. Gillet, Surf. Sci., **66**, 596, (1977)

71. H. Ibach and D.L. Mills, *Electron Energy Loss Spectroscopy and Surface Vibrations*, Academic Press, New York, p. 284 (1982)

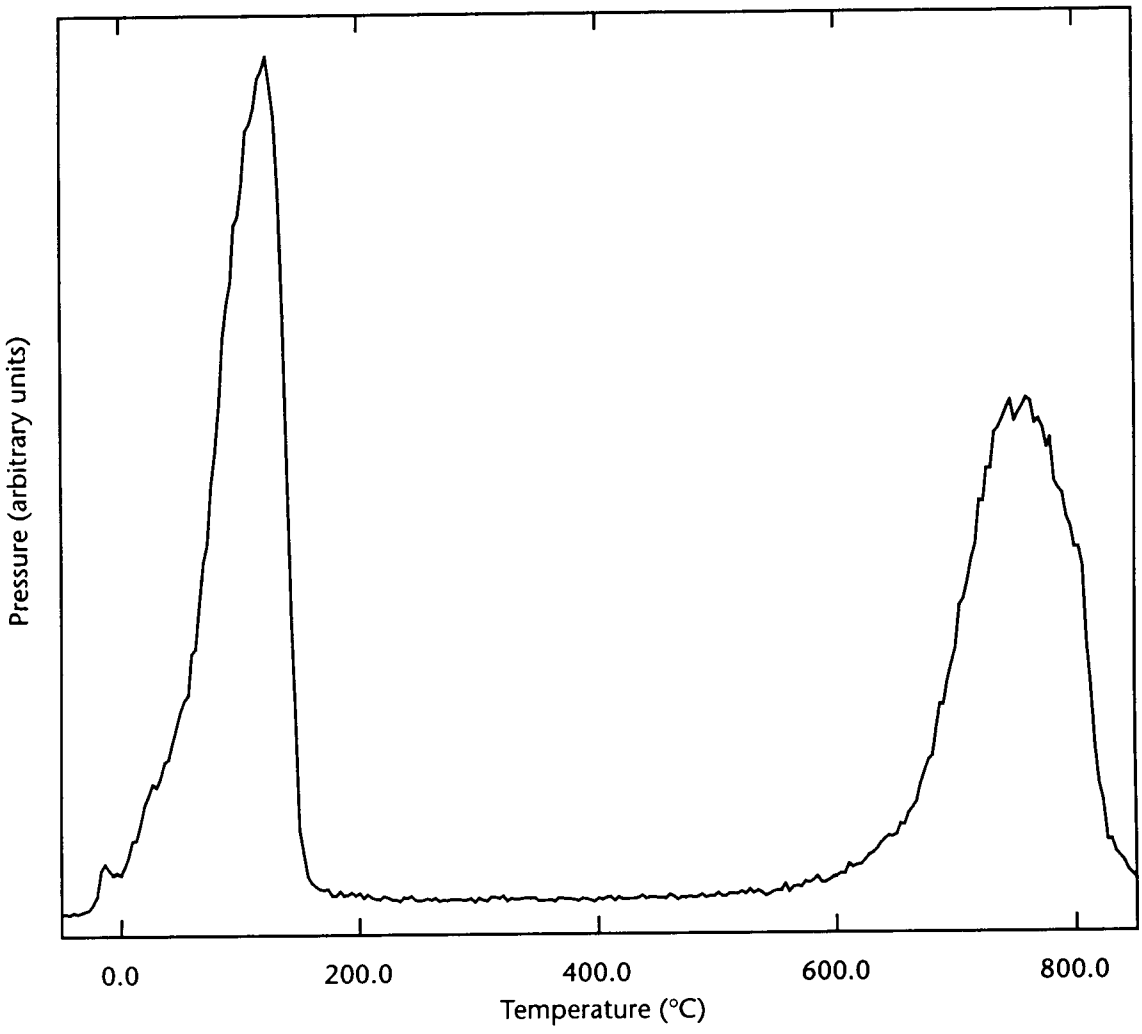

Figure 3-39. TPRS m/e=28 peak for saturation dose (10 Langmuirs) of CO on clean Mo(110)

To explore the adsorption capacity of the Mo(110) surface for CO, an uptake experiment was done, with incremental doses of CO being applied to the clean Mo(110) surface at room temperature. The AES C and Mo peak heights are plotted in Figure 3-40. The data was fit using the equation for second order (dissociative) adsorption described in the section titled: "D_2/S/Mo(110)" on page 99.

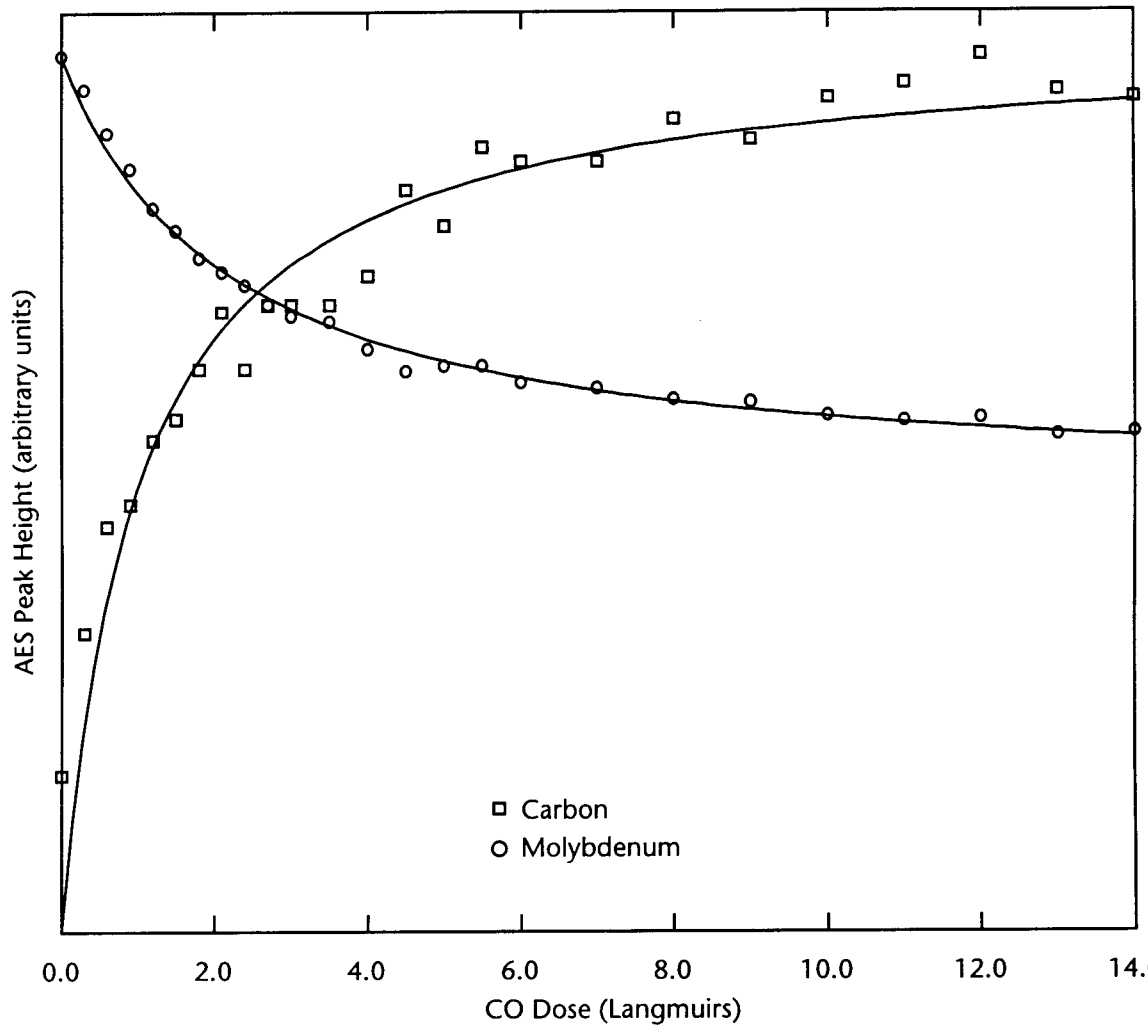

Figure 3-40. AES C and Mo peak heights as a function of CO dose on clean Mo(110).

A normalized representation (using C/Mo AES peak ratios) of the same data is plotted in Figure 3-41.

To probe the change in the surface CO as a function of temperature, the room temperature CO saturated surface was treated with a series of 1 minute anneals at increasing temperatures. After each anneal period the C and Mo AES peaks

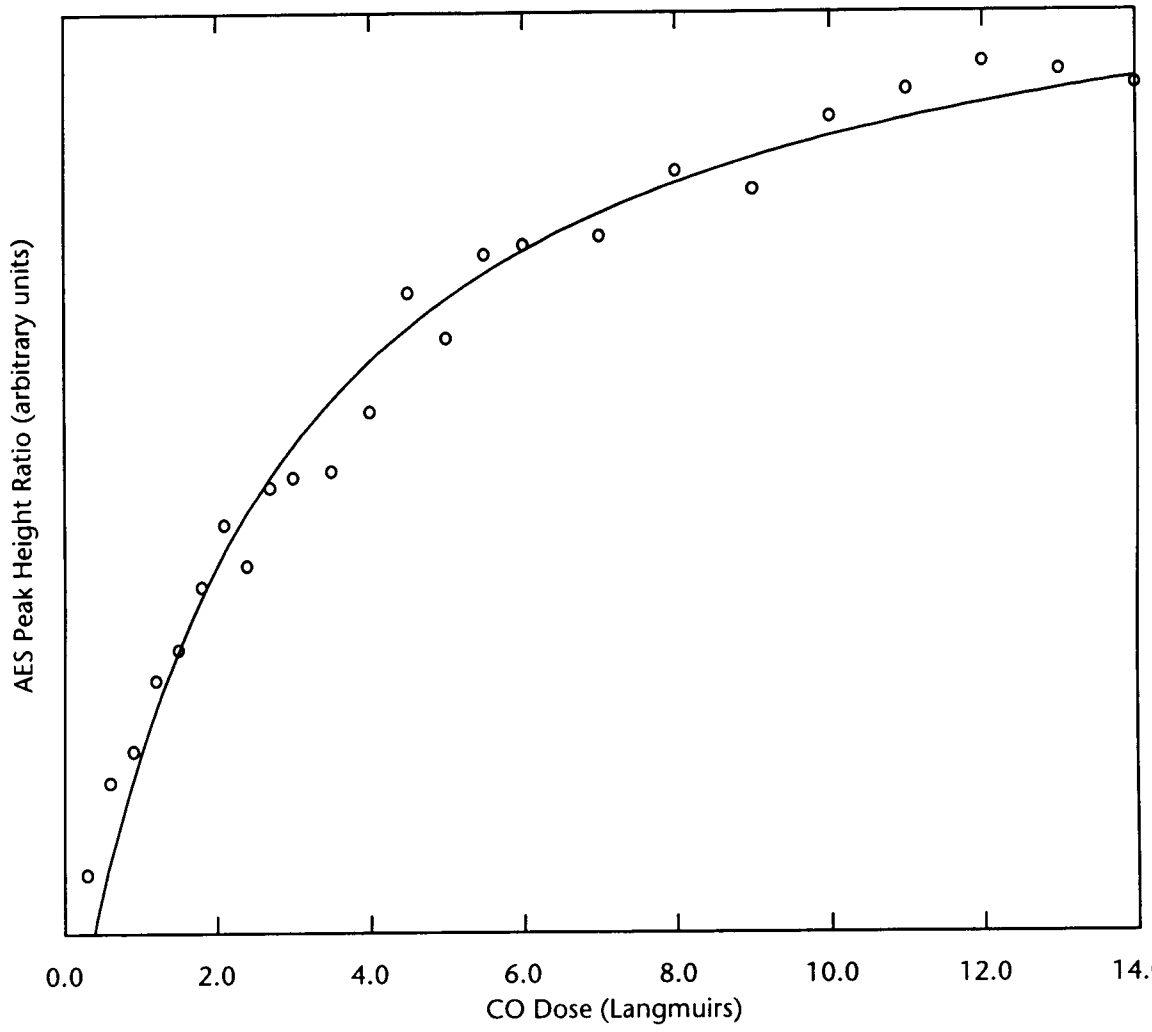

Figure 3-41. AES C/Mo peak height ratio as a function of CO dose on clean Mo(110).

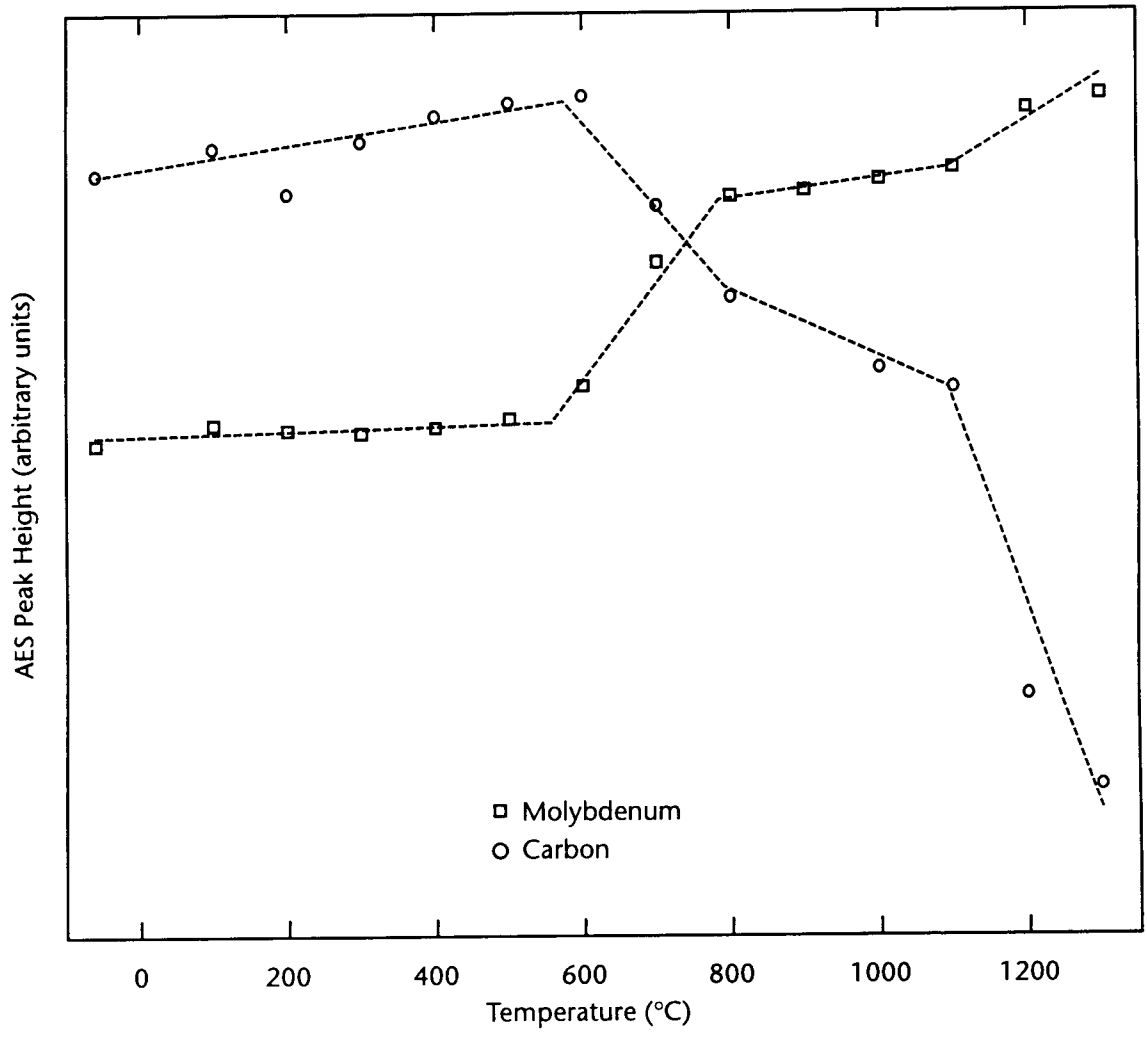

Figure 3-42. C and Mo AES peak heights as a function of anneal temperature for a saturation dose of CO on clean Mo(110)

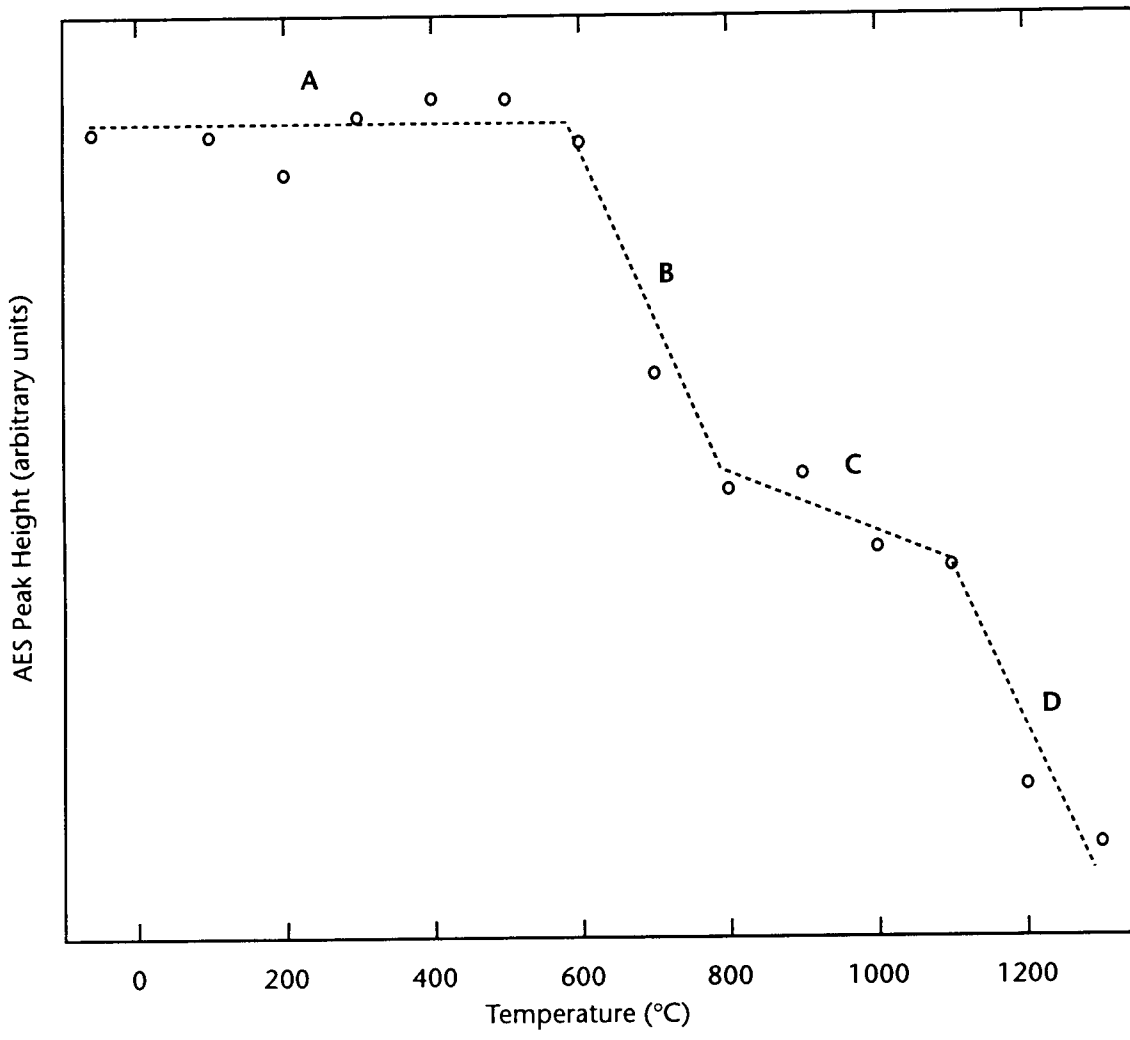

Figure 3-43. C/Mo AES peak height ratios as a function of anneal temperature for a saturation dose of CO on clean Mo(110)

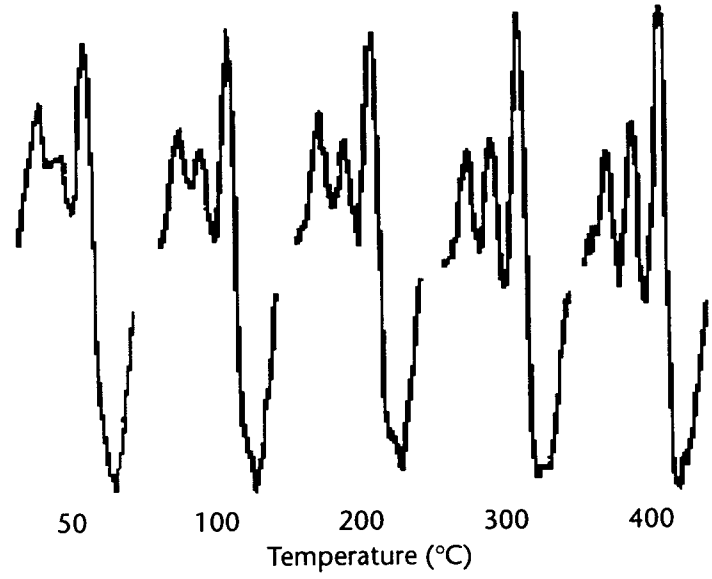

Figure 3-44. C AES peak shape as a function of anneal temperature for a saturation dose of furan on clean Mo(110)

were recorded; the results of which are plotted in Figure 3-42. Figure 3-43 shows the same data in C/Mo AES peak height ratio form.

It is clear that there are four distinct regions in the two plots above; they are labeled A-D in Figure 3-43. The four regions are explained below:

A. Part of the molecularly bound CO desorbs and the rest decomposes. The AES C peak shape changes from that associated with molecular CO to that characteristic of a carbide layer (see Figure 3-44). The increase in the size of the carbidic C peak is attenuated by the loss of CO in the low temperature TPRS peak.

B. Part of the surface C and O recombines and desorbs as CO. This accounts for the relatively rapid decrease in the C/Mo signal and agrees with the TPRS data.

C. Completion of the desorption of recombinant CO and the beginning of C indiffusion, a transitional stage.

D. Rapid indiffusion of surface C.

3.3.3.2 *CO/S/Mo(110)*

Pre-adsorbed sulfur inhibits the adsorption of CO on the Mo(110) surface and causes the high temperature m/e=28 TPRS peak to migrate to lower temperatures (i.e. it lowers the desorption energy). Figure 3-45 is a plot of the m/e=28 TPRS spectrum for saturation doses of CO on four sulfided Mo(110) surfaces. There is no effect on the low temperature peak other than a direct physical blocking of adsorption as S coverage increases.

These results parallel those found for CO/S/Mo(100), namely that S has little chemical effect on the TPRS peaks other than shifting the desorption peak maxima. The main S-induced change is the Van der Waal's radius physical blocking of CO adsorption sites.

3.3.3.3 *CO/D_2/S/Mo(110) and D_2/CO/S/Mo(110)*

Because the TPRS of furan in the presence of 5 x 10^{-7} torr of flowing D_2 from the sulfided Mo(110) surface gave rise to an unexpectedly high m/e=30 peak, a similar experiment was carried using CO instead of furan. For comparison purposes, Figure 3-46 shows the TPRS m/e=28, 29, and 30 peaks (assigned to CO, $C^{13}O$, and CO^{18} respectively) for this experiment in the absence of D_2.

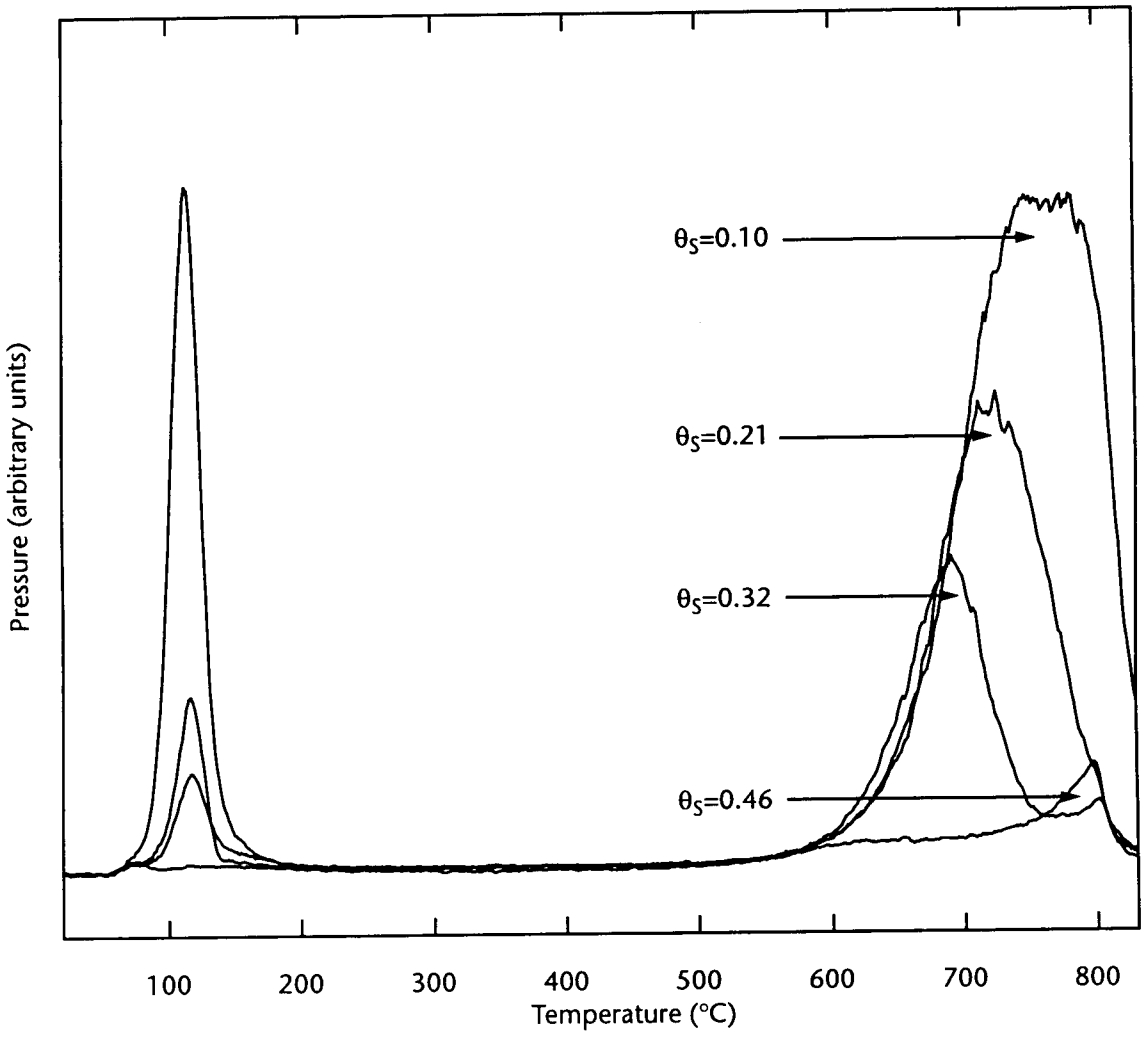

Figure 3-45. TPRS m/e=28 peak areas for saturation doses (10 Langmuirs) of carbon monoxide on clean and sulfided Mo(110)

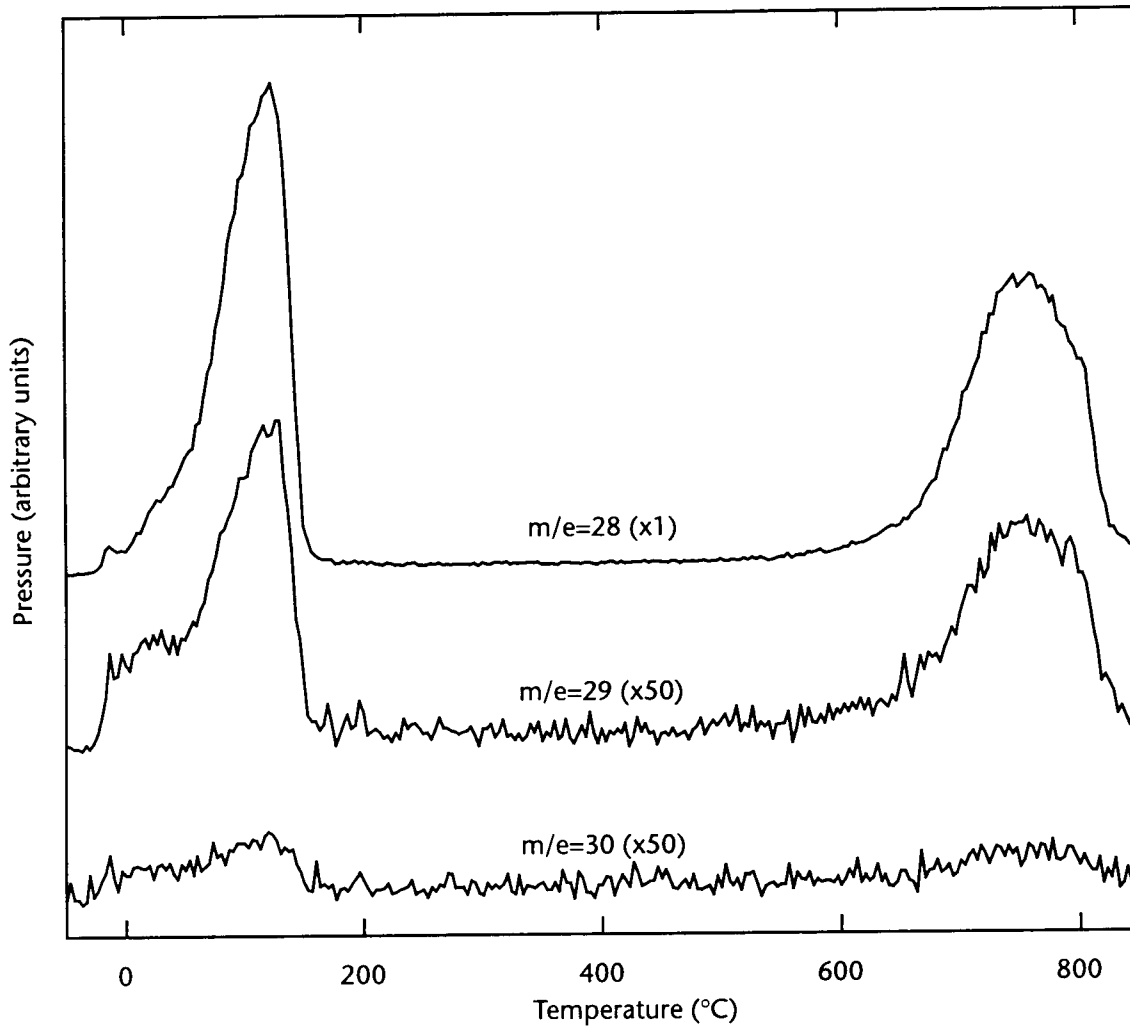

Figure 3-46. TPRS m/e=28, 29, and 30 peaks for a saturation dose of CO on Mo(110)

When the same experiment is carried with a D_2 background pressure, the TPRS peaks in Figure 3-47 are the result.

The m/e=30 peak is roughly 10 times bigger than in the absence of flowing D_2. This agrees well with the furan results, additional evidence that the m/e=28 peak resulting from the TPRS of furan on sulfided Mo(110) is due to CO desorption.

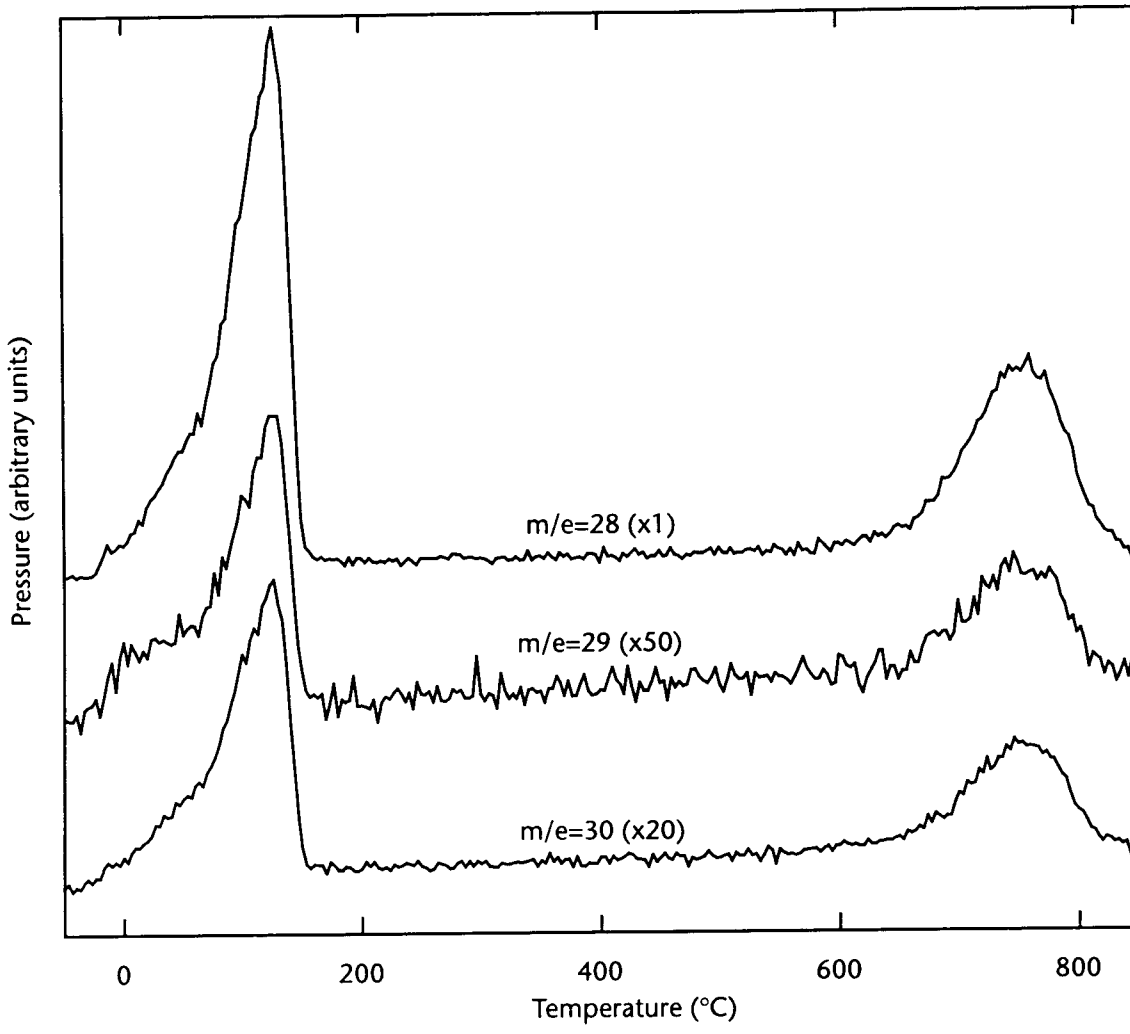

Figure 3-47. TPRS m/e=28, 29, and 30 peaks for an experiment carried out with 5 x 10^{-7} torr of flowing deuterium and a saturation dose of CO on sulfided (0.14 monolayer) Mo(110)

3.3.4 Ethylene and Propylene on Clean And Sulfur-Modified Mo(110)

Like hydrogen and carbon monoxide, the study of small hydrocarbons on transition metals is a well-traveled path in surface chemistry. On most transition metals, hydrocarbons undergo sequential dehydrogenation during thermal desorption until all hydrogen has desorbed and the carbon backbone remains on the surface[72,73,74].

Unsaturated hydrocarbons typically bond parallel to the surface through the π-bond system; one well known example is ethylene on Pt(111)[75]. In many cases, the π-bond rehybridizes to a double, or in some cases, a single bond indicating significant interaction with the surface[76]. Sometimes stable surface species form during dehydrogenation, stopping dehydrogenation until the stable species decomposes releasing hydrogen in a reaction-limited desorption peak. If the temperature of this reaction-limited desorption peak is sufficiently far from the desorption-limited peak the TPRS spectrum appears as two or more peaks. In most cases, the thermal desorption spectrum is dependent on the initial coverage of the hydrocarbon; peak maxima change temperature as the coverage changes.

The effect of pre-adsorbed sulfur on ethylene or propene adsorption is usually similar to that in the case of CO on transition metals – chemisorption and subsequent decomposition is blocked.

3.3.4.1 *C_2H_4/Mo(110) and C_3H_6/Mo(110)*

The adsorption of ethylene on clean Mo(110) exhibits the same general behavior as others have reported for this and other transition metal

---

72. N.V. Richardson and J.C. Campuzano, Vacuum, **31**, 449, (1981)

73. B.A. Sexton, Surf. Sci., **163**, 99, (1985)

74. M. Salmeron and G.A. Somorjai, J. Phys. Chem., **85**, 3835, (1982)

75. H. Steininger, H. Ibach, and S. Lehwald, Surf. Sci., **117**, 685, (1982)

76. J.E. Parmeter, M.M. Hills, and W.H. Weinberg, J. Am. Chem. Soc., **108**, 3563, (1986)

surfaces[77,78,79,80]. Ethylene irreversibly decomposes on clean Mo(110) with gaseous hydrogen the only desorbing species. As Figure 3-48 shows, the TPRS spectra are dependent on the initial ethylene coverage. The high temperature peak is well-defined and in the same temperature range as the TPRS peak resulting from hydrogen desorbing from Mo(110). There is a slight increase in the desorption peak maximum as the ethylene dose increases.

At saturation ethylene coverage, a new desorption peak appears (at ~60°C) at a temperature much lower than for D_2 chemisorption. This indicates that the new peak is the result of a dehydrogenation-limited process, i.e. the hydrogen that desorbs is probably desorbing directly from a hydrocarbon fragment, instead of from the Mo(110) surface.

The C/Mo AES peak height ratios resulting from the TPRS runs above are plotted in Figure 3-49

Saturation was achieved at approximately 2 Langmuirs, and the uptake curve was fit using a second-order desorption kinetics equation (see the section titled: "D_2/S/Mo(110)" on page 99 for a detailed description of this equation).

Once saturation coverage was achieved, the state of the semi-decomposed ethylene on the Mo surface was probed by monitoring the AES C/Mo peak height ratio and peak shape as a function of anneal temperature.

---

77. S.H. Overbury, Surf. Sci., **184**, 319, (1987)

78. M.B. Young and A.J. Slavin, Surf. Sci., **245**, 56, (1991)

79. J.G. Serafin and C.M Friend, J. Am. Chem. Soc., **111**, 6019, (1989)

80. J.T. Roberts and C.M. Friend, Surf. Sci., **202**, 405, (1988)

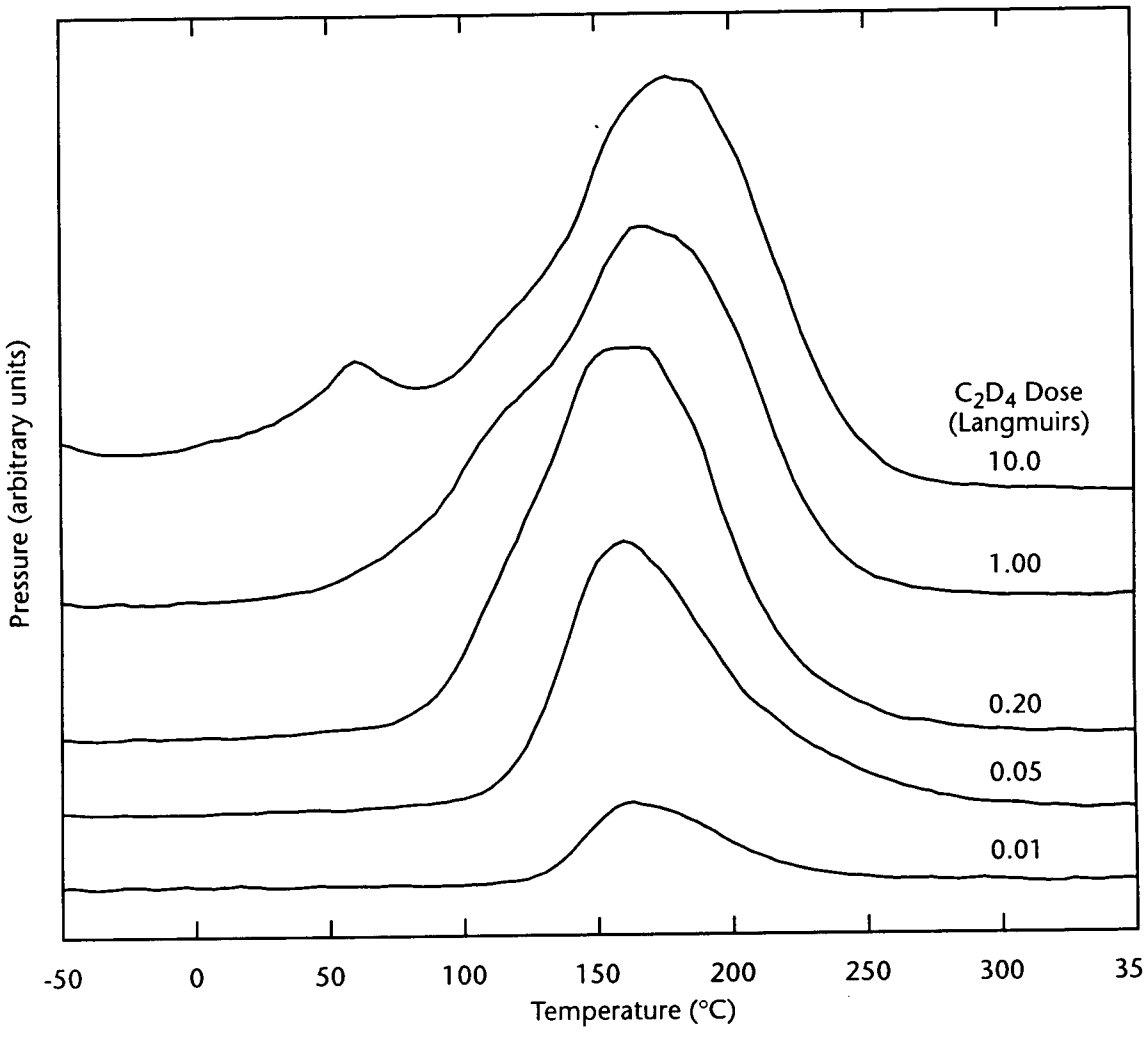

Figure 3-48. TPRS m/e=4 peaks for varying doses (0.01-10 Langmuirs) of C_2D_4 on clean Mo(110)

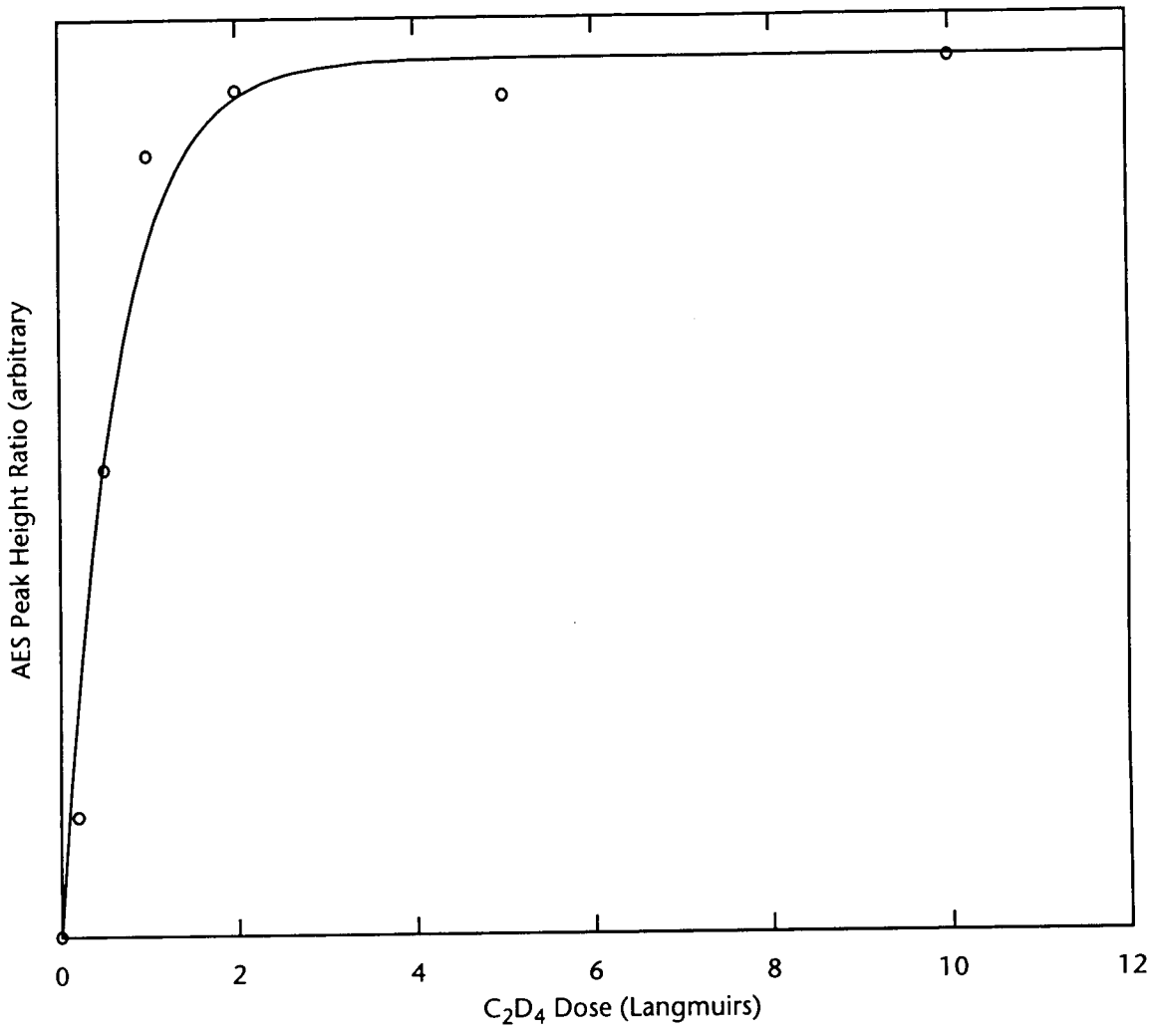

Figure 3-49. AES C/Mo peak height ratio (after 400°C heating) as a function of C_2D_4 dose on clean Mo(110)

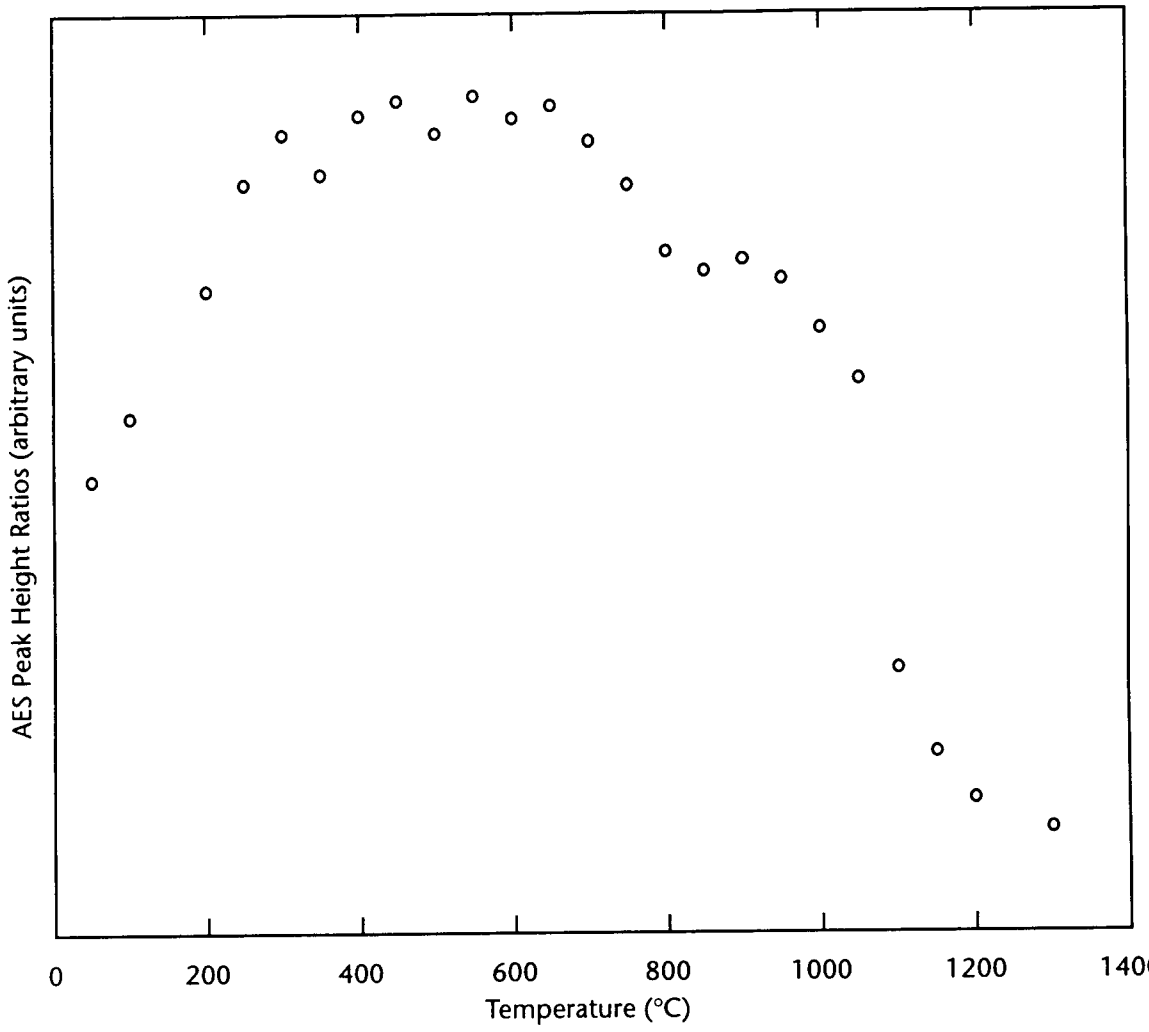

Figure 3-50. AES C/Mo peak height ratio as a function of anneal temperature for a saturation dose of C_2D_4 on clean Mo(110)

The C AES peak initially indicates that no strong C–Mo bonds are formed, instead, the carbon is "amorphous" i.e. neither graphitic nor carbidic. In this case the carbon is probably present as C_2H_x fragments π-bonded to the surface. Between 50 and 350°C, the C AES peak changes to a carbidic line shape, over roughly the same temperature range in which all the H_2 desorbs from the surface. The carbidic AES peak shape appearing indicates that strong C–Mo bonds are formed as the hydrogen leaves.

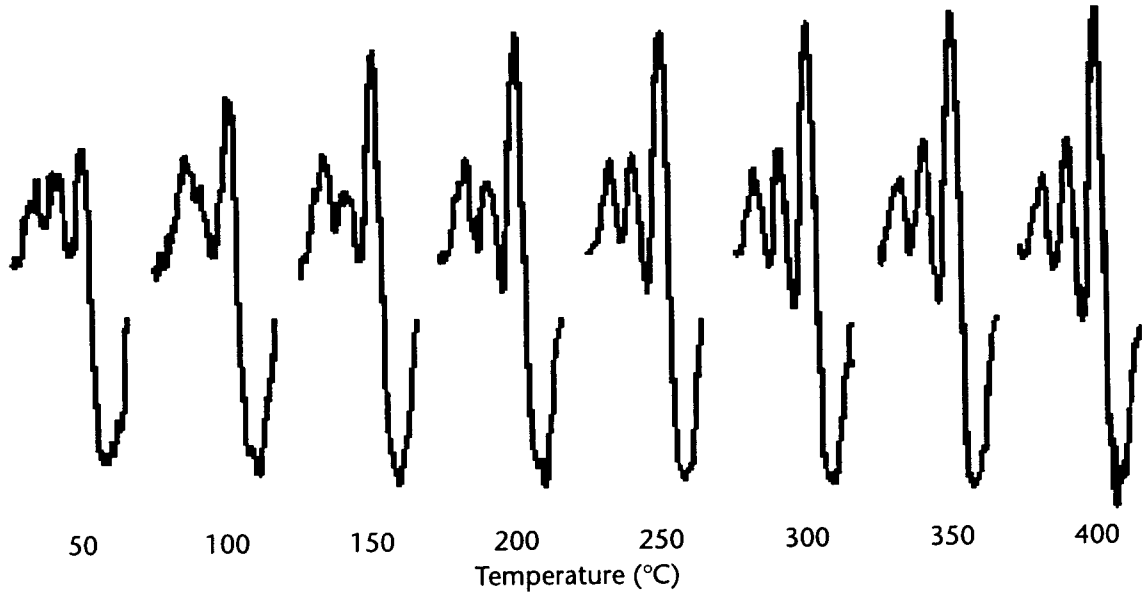

Figure 3-51. C AES peak shape as a function of anneal temperature for a saturation dose of ethylene on clean Mo(110)

The C/Mo ratio stays stable in the range 350-650°C; this could reflect the decomposition of the carbon skeleton left after H_2 desorption or could be due to the stability of the C–Mo bonds in this temperature range. The 650–1050°C range sees the loss of roughly 40% of the surface carbon; the remaining carbon disappears rapidly above 1050°C. Where that carbon goes is not clear, although indiffusion into the bulk Mo is likely.

Propene adsorbed on clean Mo(110) in varying amounts behaves slightly different than ethylene. The TPRS spectra for varying doses of propene on clean Mo(110) are plotted in Figure 3-52.

Two immediate differences are apparent from the ethylene TPRS spectra: the desorption peaks don't migrate to higher temperatures as the propene dose increases, and no low temperature peak appears at saturation propene coverage.

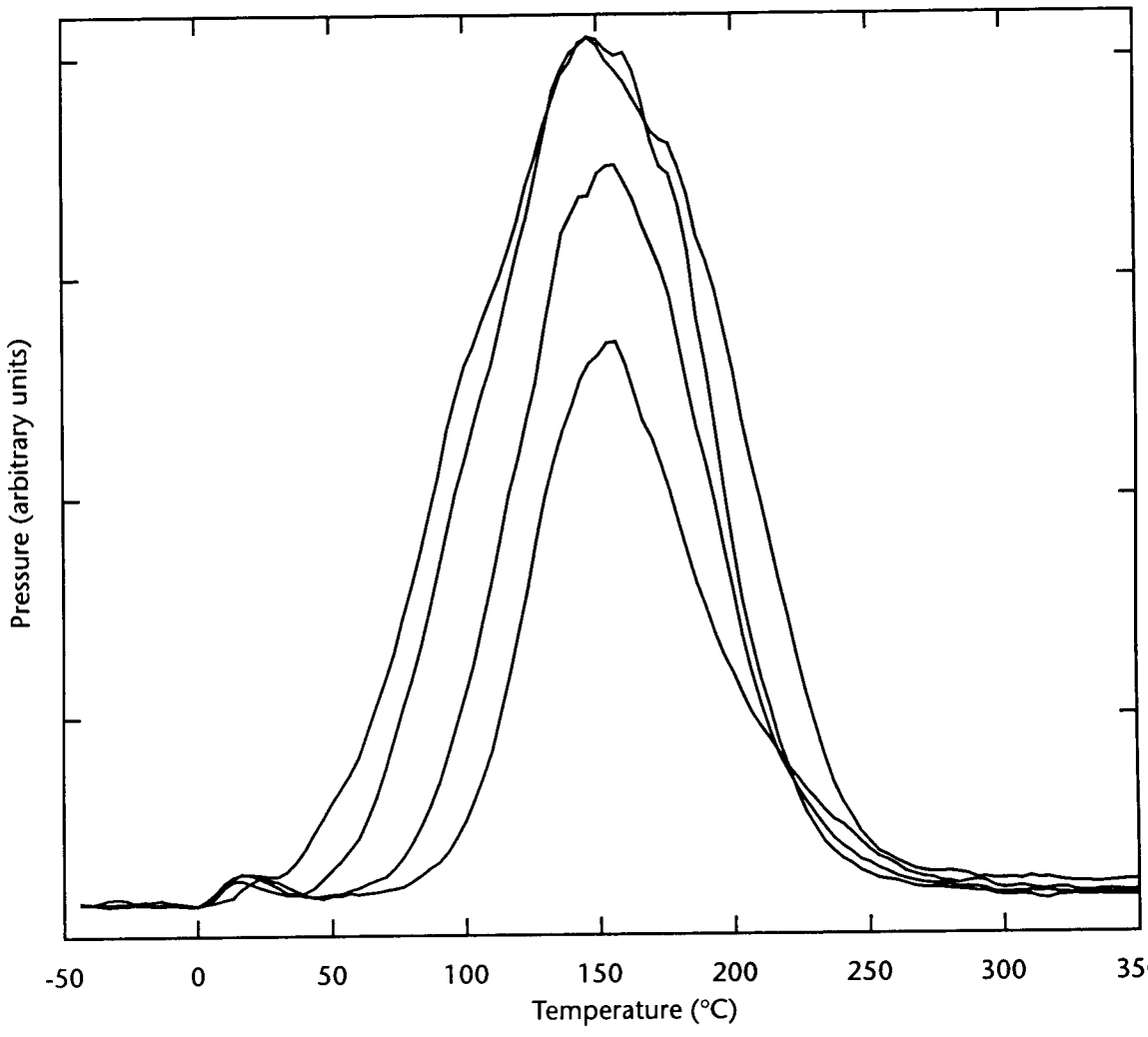

Figure 3-52. TPRS m/e=2 peaks for varying doses (0.01-10 Langmuirs) of C_3H_6 on clean Mo(110)

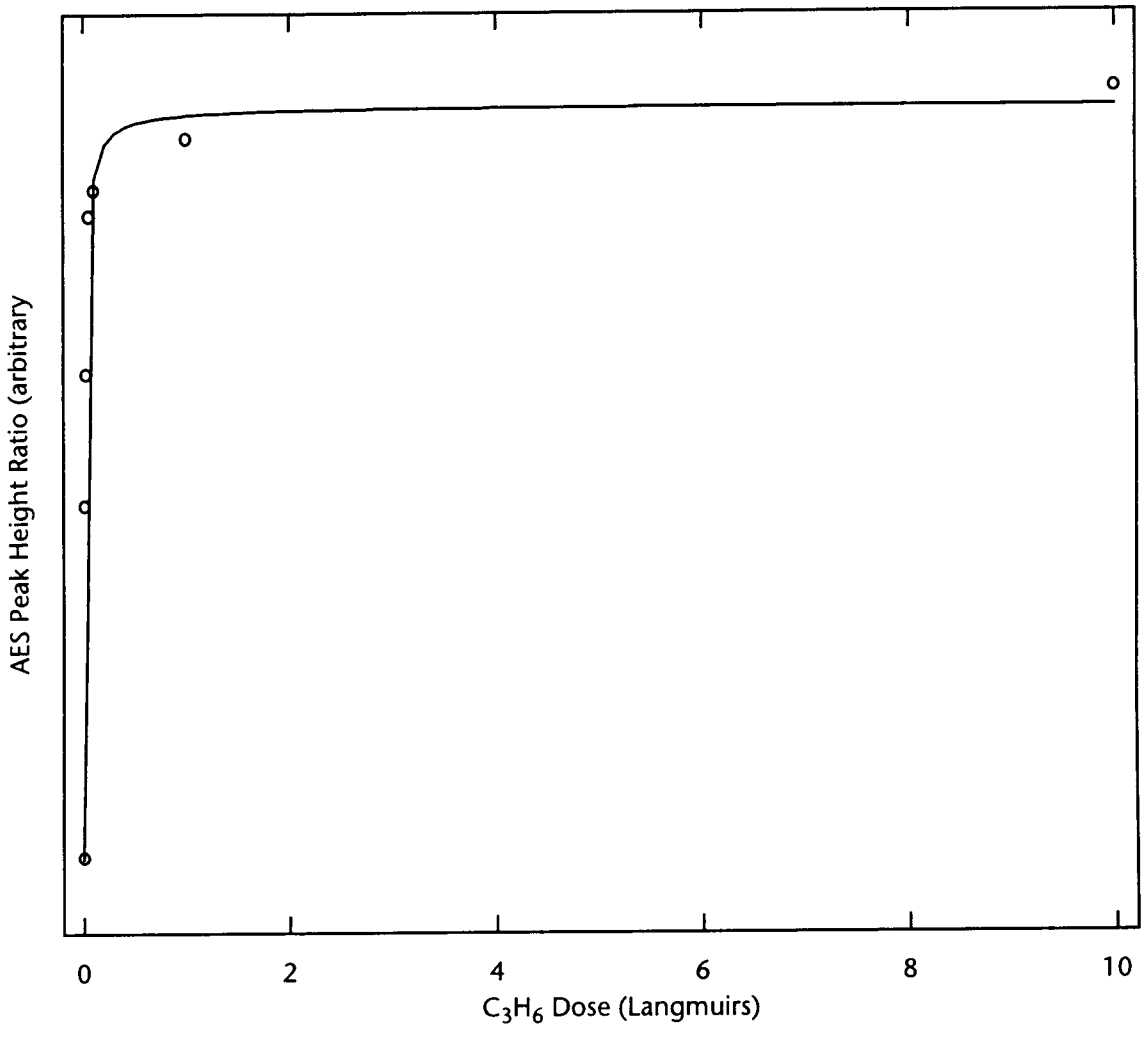

Figure 3-53. AES C/Mo peak height ratio (after 400°C heating) as a function of C_3D_6 dose on clean Mo(110)

The C.Mo AES peak height ratio uptake plot is shown in Figure 3-53.

The second-order kinetics curve fit is not nearly as close as for ethylene; this is probably due to the added methyl group modifying the decomposition and desorption process.

The state of the surface carbon resulting from a saturation dose of propene is similar to ethylene.

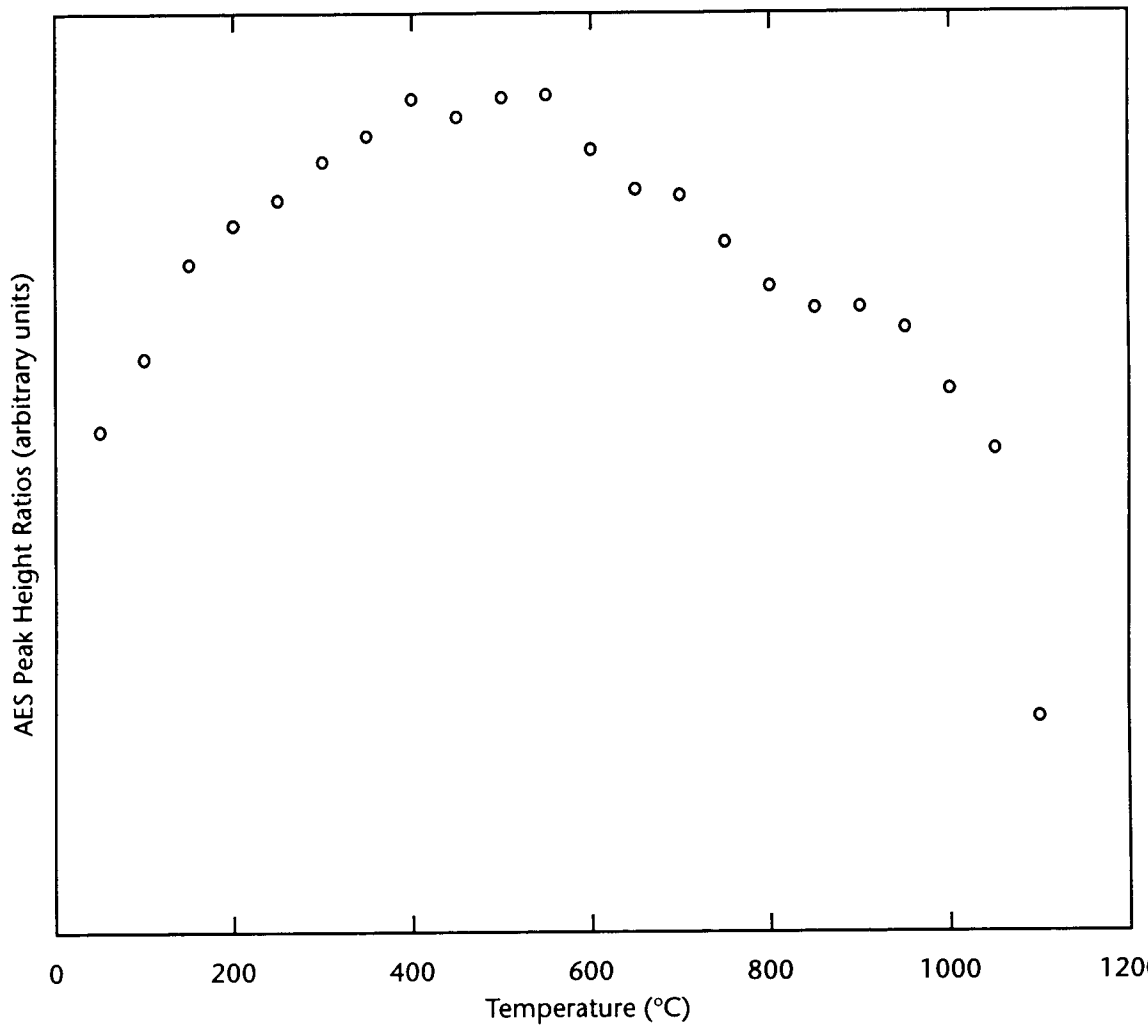

Figure 3-54. AES C/Mo peak height ratio as a function of anneal temperature for a saturation dose of C_2D_4 on clean Mo(110)

Although the TPRS spectra demonstrate that dehydrogenation is complete by 250°C, the C AES peak growth continues until 400°C. This seems to support the idea that dehydrogenation is followed by C–C bond breaking, and the subsequent formation of strong carbidic C–Mo bonds.

An experiment was performed using propene to probe the upper limit for surface carbon uptake. The surface was held at 600°C while it was exposed to

propene. 600 °C is above the desorption temperature for H_2 and the decomposition temperature for surface carbon chains, thus ensuring that the carbon deposited on the surface is carbidic.

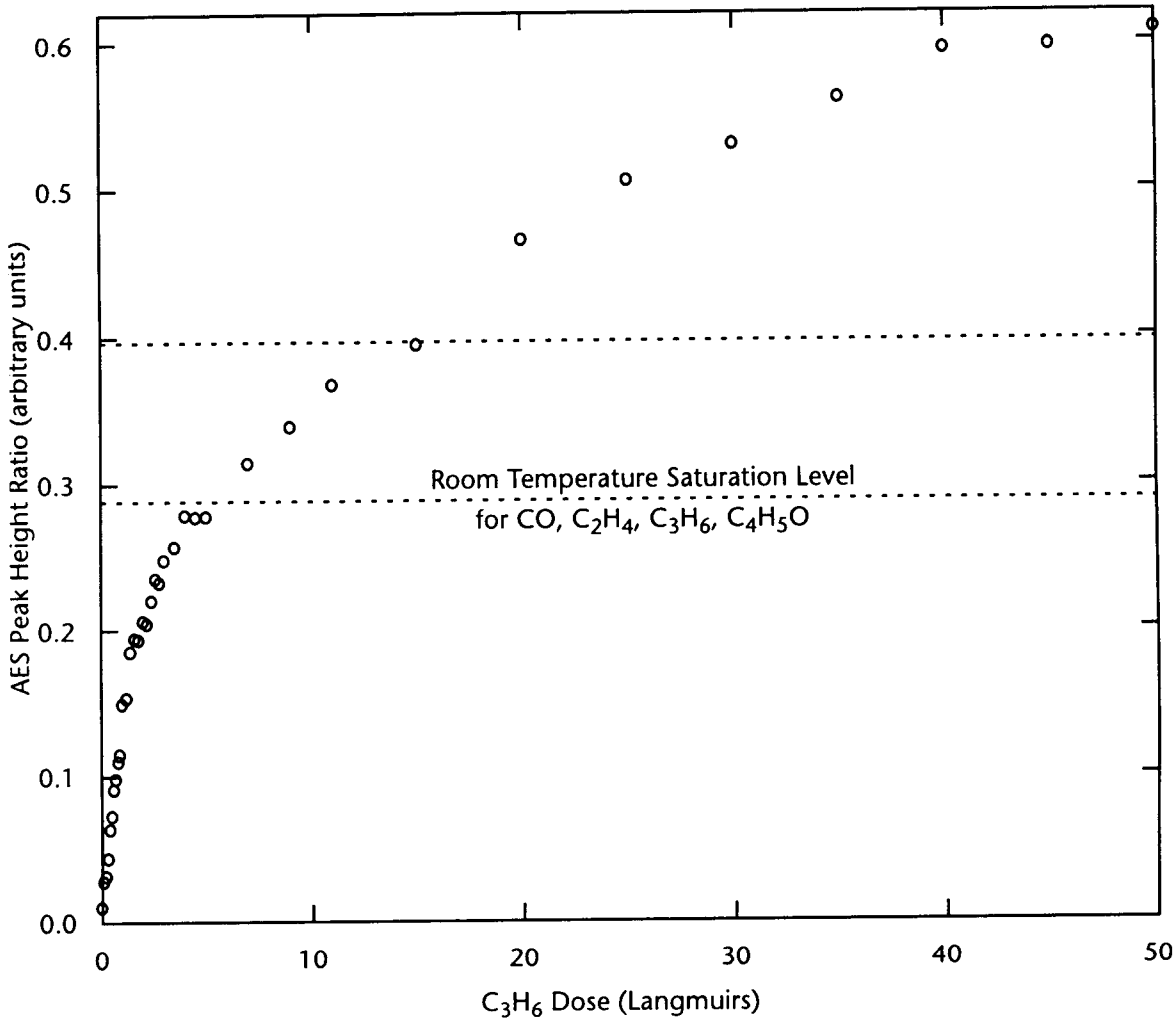

Figure 3-55. AES C/Mo peak height ratio as a function of C_3D_6 dose at 600°C on clean Mo(110)

At room temperature, the saturation C/Mo AES ratio peak height ratio was about 0.28 for all of the carbon containing species examined in this work (CO, C_2H_4, C_3H_6, and C_4H_5O). However, at 600°C the saturation C/Mo AES ratio peak

height ratio was double that, a little over 0.60. This agrees with other research on C_2H_4/Mo(110) that found a C/Mo AES peak ratio of 0.2 corresponded to a C:Mo atom ratio of 0.37[81]. Based on this interpretation, the maximum C:Mo atom ratio is approximately unity and the room temperature saturation C/Mo peak ratio is equivalent to about 0.5 monolayers of carbon.

Although the data in Figure 3-55 do not match either first or second order kinetic equations, a second interpretation of the data takes advantage of the fact that the low coverage part of the curve shows a good fit for first order chemisorption.

The data in Figure 3-56 are fit (R^2=0.992) using the following equation for first order kinetics,

$$H_t = H_0(1 - \exp(-Kpt)) \qquad \text{Equation 3-10}$$

where p is the partial pressure of C_3H_6, H_t is the C/Mo AES peak height ratio at time t, and H_0 is the maximum peak height ratio. The factor K is described in the equation below:

$$K = \frac{3}{(2\pi mkT)^{1/2}} \frac{s}{N_C} \qquad \text{Equation 3-11}$$

where m is the mass of a C_3H_6 molecule, k is Boltzmann's constant, T is the temperature, s is the sticking coefficient, and N_C is the surface density of carbon

81. M.B. Young and A.J. Slavin, Surf. Sci., **245**, 56, (1991)

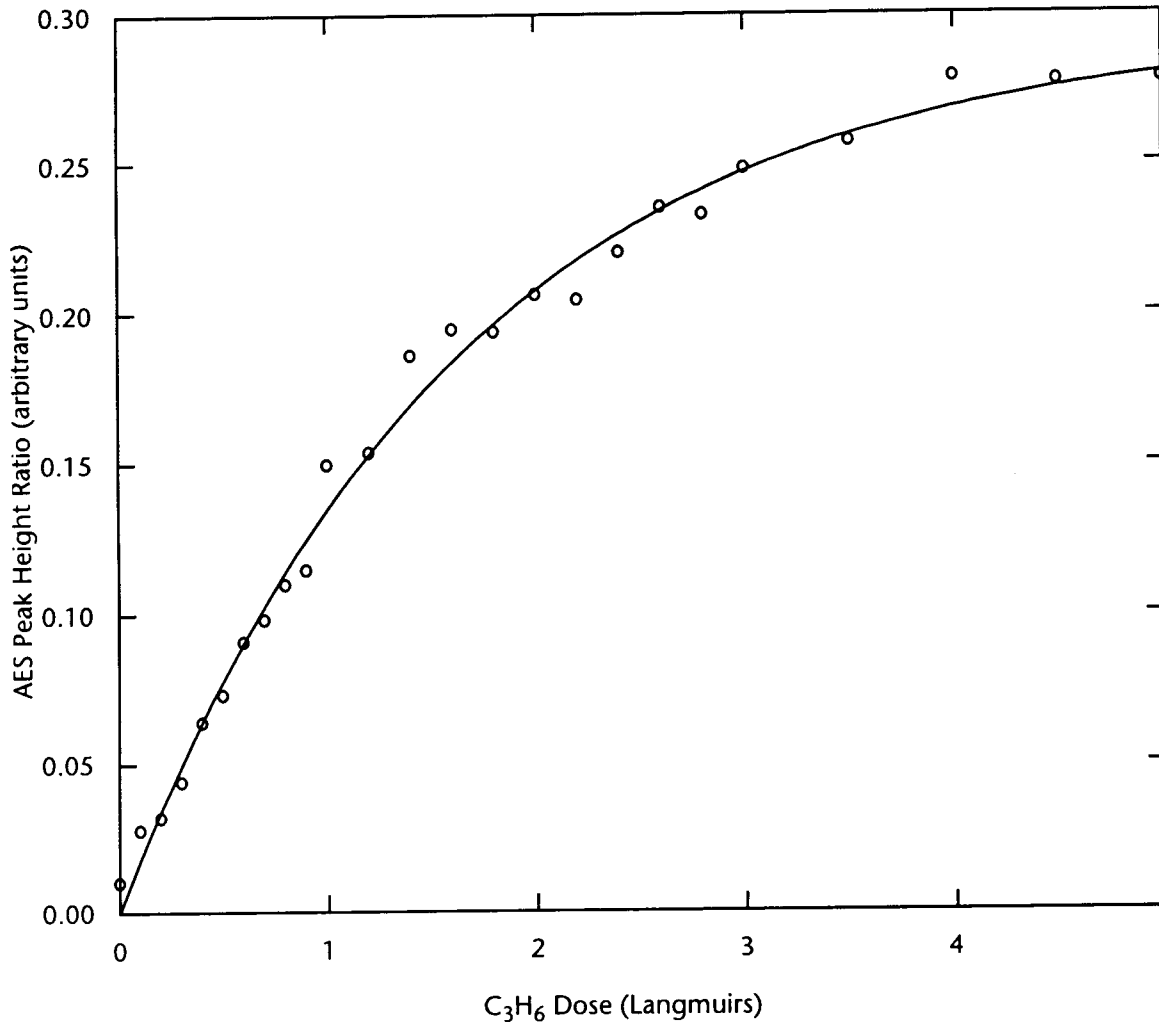

Figure 3-56. AES C/Mo peak height ratio as a function of C_3H_6 dose at 600°C on clean Mo(110) for low C_3H_6 coverage

atom sites. The 3 in the numerator accounts for the fact that there are three C atoms per C_3H_6 molecule.

Based on this curve fit (assuming a sticking coefficient of unity as found on W(110) and Ta(110)[82,83]) H_0=0.294±.006 and N_C=1.08±.05x$10^{19}m^{-2}$. H_0 agrees

82. F.A. Londry, A.J. Slavin, and P.R. Underhill, Surf. Sci., **140**, 521, (1984)

83. J.G. MacMillan, A.J. Slavin, and K.J. Sunderland, Surf. Sci., **173**, 138, (1986)

well with the C/Mo AES peak ratio for room temperature hydrocarbon saturation noted in Figure 3-55 (C/Mo=0.28). The site density of $1.08x10^{19}$ m^{-2} is about 75% of the Mo atom surface density ($N_{Mo}=1.43x10^{19}m^{-2}$). Extrapolating from N_C to N_{Mo} yields a C/Mo peak height of 0.389 for a C to Mo ratio of unity, which in Figure 3-55 corresponds with a "break" in the data at approximately 15 Langmuirs of C_3H_6. Thus in this scenario, a monolayer of C occurs at a C/Mo peak height ratio of 0.4 and the C/Mo ratio increase from 0.4 and 0.6 is due to multi-layer adsorption.

3.3.4.2 *C_2H_4/S/Mo(110) and C_3H_6/S/Mo(110)*

Pre-adsorbed sulfur on Mo(110) was observed to decrease the chemisorption and subsequent decomposition of both ethylene and propene as measured by the integrated areas of TPRS hydrogen m/e=2 peaks. This result is similar to the effect pre-adsorbed sulfur had on hydrogen, carbon monoxide, and furan adsorption. The TPRS results for C_2H_4/S/Mo(110) are presented in .

There are numerous changes in the TPRS m/e=2 spectra in addition to a simple decrease in size. The two largest peaks in the case of the clean surface are β_1 and β_3; the β_2 and β_4 peaks are present as shoulders on the large β_3 peak. As S coverage increases the β_3 peak decreases rapidly until at θ_S=0.30, it is gone, leaving well-resolved β_2 and β_4 peaks and a poorly resolved third peak between the two that is probably a composite of β_2 and any remaining intensity due to β_3. This matches well with previous work involving saturation doses of ethylene on sulfided Mo(110)[84].

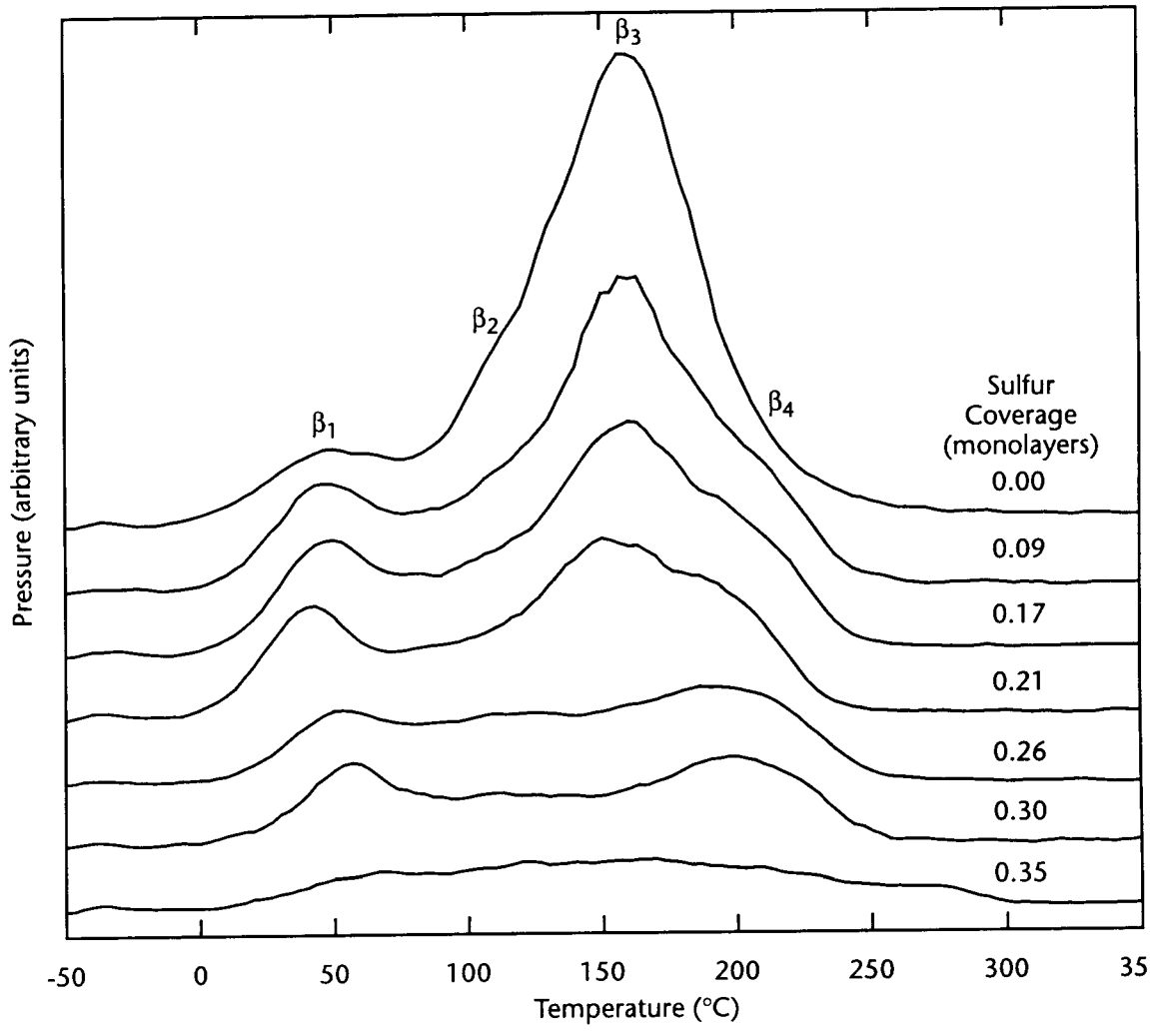

Figure 3-57. TPRS m/e=2 peaks for saturation doses (10 Langmuirs) of C_2H_4 on sulfided Mo(110)

Similar TPRS results for C_3H_6/S/Mo(110) are presented in Figure 3-58, although the sharp TPRS peak definition that occurred in the ethylene runs is not present.

At θ_S=0.0 there is only one large desorption peak that is obviously a composite of at least three, and possibly all four, peaks observed in the ethylene spectra.The peak intensity centered at 150°C decreases with increasing

84. J.T. Roberts and C.M. Friend, Surf. Sci., **202**, 405, (1988)

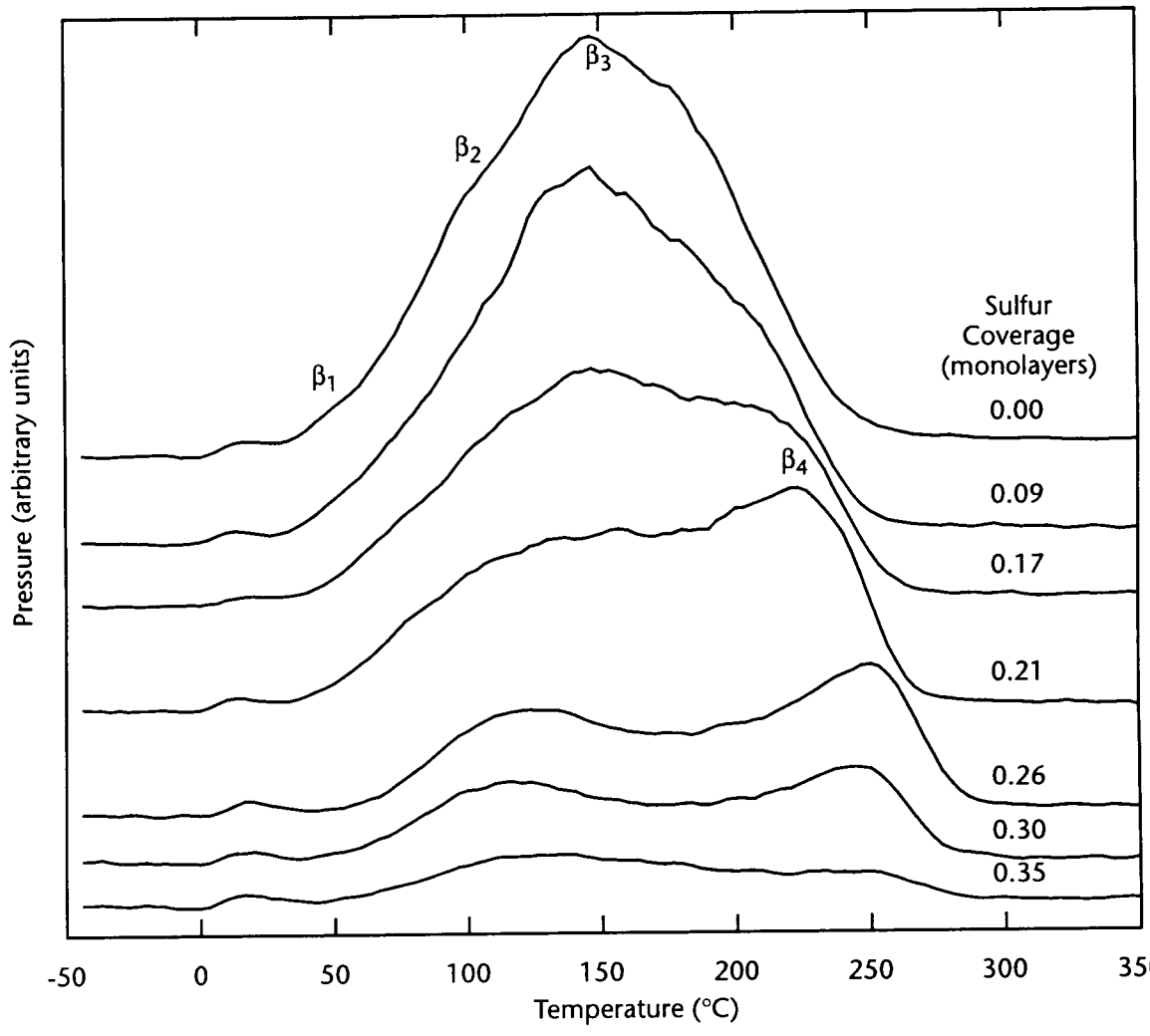

Figure 3-58. TPRS m/e=2 peaks saturation doses (10 Langmuirs) of C_3H_6 on sulfided Mo(110)

S coverage revealing a peak centered at 225°C by θ_S=0.21. As the S coverage increases to

0.26 monolayers, the very small β_1 intensity disappears and the β_2 peak is more clearly visible, in contrast to C_2H_4/S/Mo(110). In addition, the β_4 peak migrates to 250°C before disappearing.

The C/Mo AES peak height ratios were measured after each C_3H_6 TPRS run and are plotted as function of S coverage in Figure 3-59.

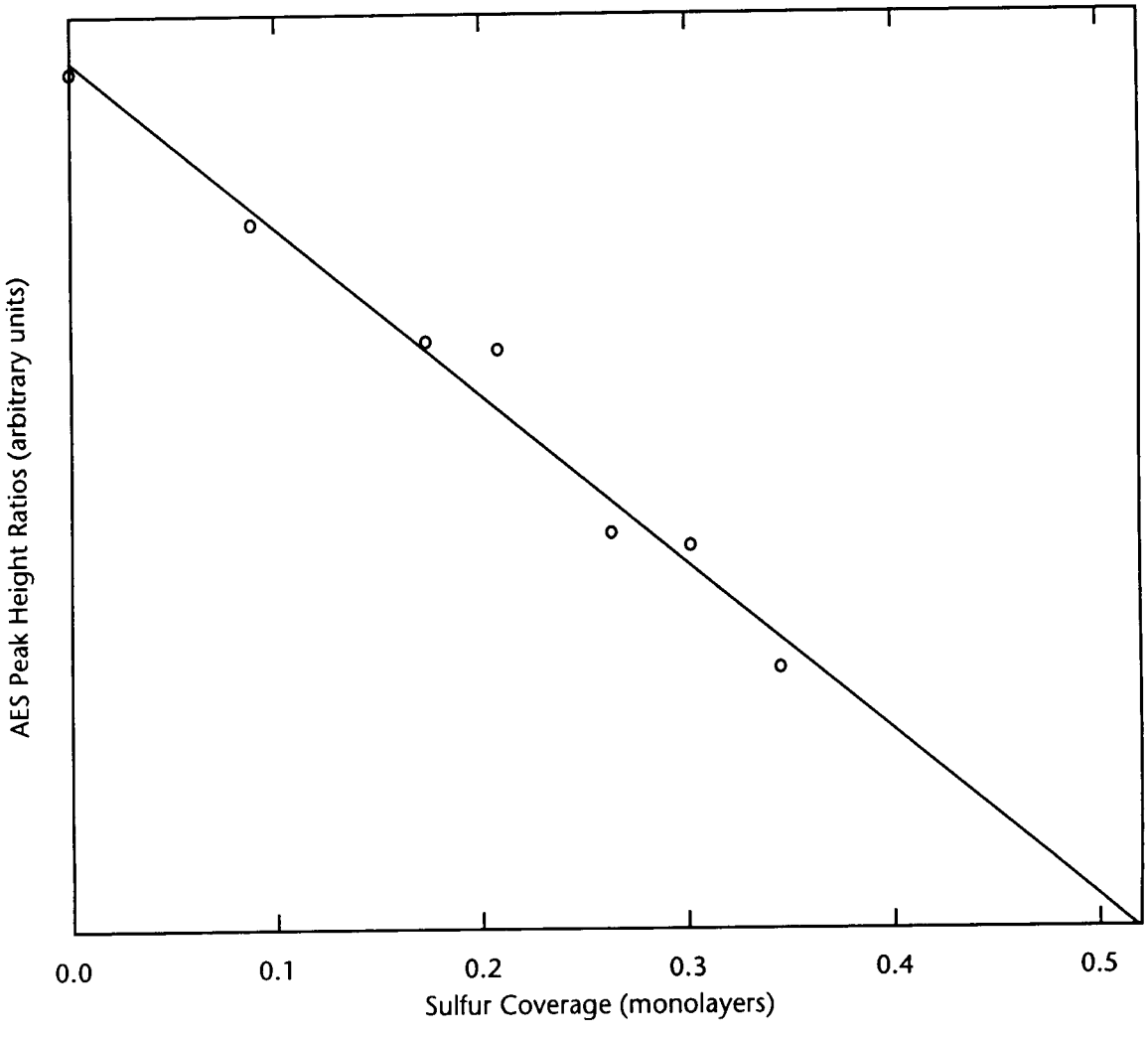

Figure 3-59. AES C/Mo peak height ratio as a function of sulfur coverage for a saturation dose of C_3H_6 on clean Mo(110)

These results indicate that increasing surface sulfur monotonically blocks the adsorption and subsequent reaction of propene on Mo(110). The x-intercept of 0.52 is in agreement with results discussed above that indicate that $\theta_S \geq 0.5$ completely passivates the Mo(110) surface to hydrocarbon adsorption.

CHAPTER 4: CONCLUSIONS

4.1 DISCUSSION

The overarching goal of this research was to investigate the interactions of a model synfuel reactant with a model HDO catalyst in UHV. Furan was chosen as a model reactant because of its ubiquity in synfuels derived from plant materials, and its well-defined chemistry. Clean and sulfided molybdenum single crystal surfaces were the choice for a model catalyst; sulfided Mo surfaces are common substrates in UHV studies of HDS and HDO. Similar investigations of the HDS of thiophene (the S-containing analog of furan) on sulfided Mo(100) and (110) served as a guide and provided an indication that achieving HDO in UHV might prove difficult if not impossible.

4.1.1 Furan on Clean and Sulfur-Modified Mo(110)

The major result of this study is not very different from what others have found true for thiophene on clean and sulfided Mo, although there is just enough of a surprise twist to make it interesting or, at the very least, worthy of note. Furan decomposes on clean and sulfided Mo(110) surfaces yielding gaseous hydrogen, surface carbon, and, in a departure from thiophene chemistry, gaseous CO. While the presence of CO is surprising based on thiophene results, the fact that CO is a stable gas-phase species and CS is not makes it less surprising. The production of CO and propene reported in the very low pressure pyrolysis of furan is additional evidence that CO production is

reasonable. CO produced in this process desorbs in two peaks, a low temperature peak composed of molecularly adsorbed CO, and a high temperature peak resulting from recombinant surface C and O.

The hydrogen TPRS spectrum typically had two well-defined peaks; the low temperature peak was desorption limited, composed of hydrogen produced below the normal desorption temperature for hydrogen. The high temperature peak is dependent on a reaction-limited process, the reaction being the dehydrogenation of a surface hydrocarbon fragment produced by the abstraction of CO from molecularly adsorbed furan. At low furan doses, the desorbing hydrogen produced only one peak.

A similar result was observed for thiophene on Mo(110)[1]. The explanation for this behavior is that at low temperatures, furan probably bonds parallel to the surface through its π-bond system. This type of bonding is common for small unsaturated hydrocarbons due to the overlap of the metal substrate's d-band with the adsorbates π-bond system. This arrangement makes all four hydrogens available for abstraction by the substrate at low temperatures. At higher furan doses, there isn't room for only this type of bonding; additional furan probably is bound to the surface via a σ-bond to an oxygen lone pair or via one of the α-carbons after dehydrogenation. Either arrangement would make the α-hydrogens available for desorption at low temperatures (the desorption limited TPRS peak). The β-hydrogens would only become available for desorption after dehydrogenation of the surface hydrocarbon fragment remaining after the

---

1. J.T. Roberts and C.M. Friend, Surf. Sci., **186**, 201, (1987)

abstraction of CO and the α-hydrogens. Results from the study of benzene on clean Mo(110)[2] support the notion that at low coverages furan π-bonds parallel to the surface and at higher coverages, a mixture of π and σ bonded furan is present.

Pre-adsorbed sulfur gradually passivates the surface to furan adsorption, until at $\theta_S \geq 0.5$ furan adsorption is completely blocked. Sulfur pre-adsorption prior to furan dosing and TPRS never produced any gaseous products besides molecular furan, H_2, and CO.

An attempt was made to encourage HDO of furan by carrying out furan TPRS runs in the presence of pre-dosed, co-dosed, and background D_2. No combination of furan and D_2 brought about the production of any product besides gaseous hydrogen and CO, except for DCO at m/e=30. The existing TPRS peak at m/e=30 is due to isotopically substituted CO^{18}, however in the presence of flowing D_2, the m/e=30 peak area increased by a factor of ten. DCO production probably occurs via an Ely-Rideal mechanism in which a gas-phase deuterium molecule interacts with surface-bound CO to form gaseous DCO.

4.1.2 D_2, CO, C_2H_4, and C_3H_6 on Clean and Sulfur-Modified Mo(110)

In order to fully understand the furan/Mo(110) system, it was necessary to investigate the interactions of other molecules suspected of taking part in the process, namely D_2 and CO. Because C_2H_4 and C_3H_6 are similar or identical to

---

2. A.C. Liu and C.M. Friend, J. Chem. Phys. **89**, 4396, (1988)

potential surface hydrocarbon fragments, their reactions with clean and sulfided Mo(110) were examined as well.

D_2 desorbs from the clean Mo(110) surface from three sequentially populated desorption sites. The two high temperature sites are second-order while the high-coverage low-temperature site seems to be first-order. Pre-adsorbed sulfur blocks the adsorption of deuterium and changes the appearance of the TPRS peaks. A new low temperature peak (at ~100°C) is populated for $\theta_S \geq 0.25$ with hydrogen production above 200°C completely shut down. Pre-adsorbed carbon serves only to limit hydrogen adsorption with little change to the desorption peak shape or location. No matter the pre-treatment of the Mo(110) surface, the adsorption of pure hydrogen was never able to reproduce the furan m/e=2 TPRS spectrum.

CO on clean and sulfided Mo(110) behaved as CO does on other transition metal surfaces. A low temperature TPRS desorption peak is attributed to molecularly adsorbed CO, while a high temperature peak is populated by recombinant C and O resulting from CO decomposition. Above 1100°C, the AES C signal decreases rapidly, probably due to surface C dissolving into the bulk substrate. TPRS of CO on Mo(110) in flowing D_2 results in the same increase in the TPRS m/e=30 signal as when furan is the adsorbate.

C_2H_4 and C_3H_6 are probable candidates for the hydrocarbon fragments remaining on the Mo(110) surface after the initial stages of the TPRS of furan. Both unsaturated hydrocarbons decomposed on clean and sulfided Mo(110) producing only gaseous H_2 and surface C during TPRS. The m/e=2 spectra were

more complicated than those obtained from the TPRS of H_2 with features similar to those observed for the TPRS of furan. This supports the hypothesis that surface hydrocarbon decomposition is responsible for the reaction-limited hydrogen TPRS peaks.

AES C peak shapes also support this hypothesis. At low temperatures, the AES C peak shape indicates that the carbon on the surface resulting from the adsorption of ethylene or propene is amorphous, i.e. not strongly bonded to the substrate. As the temperature increases, the AES C peak changes from a shape characteristic of amorphous carbon to one more indicative of carbidic carbon (carbidic carbon is strongly bound to the substrate). This is the logical result of dehydrogenation and subsequent decomposition of hydrocarbon surface fragments. A similar AES C peak transition is observed for both furan and CO adsorption. Usually the peak shape changes are complete at the same temperature that hydrogen desorption is finished.

4.2 CONCLUSIONS

This research explored the reactions of furan on clean and sulfided Mo(110) with and without the presence of background hydrogen. The reactions of hydrogen, carbon monoxide, ethylene, and propene on clean and sulfided Mo(110) were also examined. All adsorbates exposed to clean or sulfided Mo(110) decomposed yielding gaseous H_2 and surface C. Furan TPRS yielded the unexpected but explicable production of gaseous CO. In the presence of background hydrogen the only change was the ten-fold increase in the m/e=30

peak due to the Ely-Rideal production of DCO. Both sulfur and carbon pre-adsorption resulted in a Van der Waal's radius blocking of adsorption sites. Sulfur pre-adsorption also caused the chemical shifting of H_2 TPRS peaks

Future studies exploring this topic should focus on higher background pressures of hydrogen than were possible in this study. Hydrogenation of furan HDO products is very dependent on the local concentration of hydrogen. In this research, surface hydrocarbon fragments decomposed as the temperature increased; if higher hydrogen pressures were possible, perhaps a different decomposition pathway would result.

BIBLIOGRAPHY

1. E. Furimsky, Catal. Rev.—Sci. Eng., 25, 421, (1983)

2. J.R. Longanbach and R.Bauer, ACS Symp. Ser., 32, 476, (1975)

3. J.N. Bowden and D.W. Brinkman, Department of Energy Report DOE/BETC/4162-10, (1980)

4. G.R. Hill, W.H. McClennen, G.S. Metcalf, Wang Hoah-Hsing, and H.L.C. Henzellaar, Proc. Int. Conf. Coal Sci., Duesseldorf, FRG, Paper C-25, 477, (1981)

5. J.M.J.G. Lipsch and G.C.A. Schuit, J. Catal., 15, 179, (1980)

6. O. Weisser and S. Landa, *Sulfide Catalysts: Their Properties and Applications*, Pergamon Press, New York, (1973)

7. E. Furimsky, Catal. Rev.—Sci. Eng., 25, 421, (1983)

8. S. Krishnamurthy, S. Panvelker, and Y.T. Shah, AIChe Journal, 27, 994, (1981)

9. J. B-son Bredenberg, M. Huuska, J. Raty, and M. Karpio, J. Catal., 77, 242, (1982)

10. C. Lee and D.F. Ollis, J. Catal., 87, 325, (1984)

11. E. Furimsky, Appl. Catal., 6, 159, (1983)

12. E. Furimsky, Catal. Rev.—Sci. Eng., 25, 421, (1983)

13. S. Krishnamurthy, S. Panvelker, and Y.T. Shah, AIChe Journal, 27, 994, (1981)

14. E. Furimsky, Catal. Rev.—Sci. Eng., 25, 429, (1983)

15. S. Krishnamurthy, S. Panvelker, and Y.T. Shah, AIChe Journal, 27, 994, (1981)

16. R.K.M.R. Kallury, W.M. Restivo, T.T. Tidswell,. D.G.B. Boocock, A. Crimi, and J. Douglas, J. Catal., 96, 535, (1985)

17. C. Lee and D.F. Ollis, J. Catal., 87, 325, (1985)

18. E. Furimsky, Catal. Rev.—Sci. Eng., 25, 431, (1983)

19. E. Furimsky, Catal. Rev.—Sci. Eng., 25, 430, (1983)

BIBLIOGRAPHY, CONTINUED

20. R.P.H. Gasser, An Introduction to Chemisorption and Catalysis by Metals, p. 54, Oxford University Press, New York, (1985)

21. F. Zaera, E.B. Kollin, and J.L. Gland, Surface Sci., 184, 75, (1987)

22. A.J. Gellman, M.H. Farias, M. Salmeron, and G.A. Somorjai, Surface Sci., 136, 217, (1984)

23. D.G. Kelly, M. Salmeron, and G.A. Somorjai, Surface Sci., 175, 465, (1986)

24. J.T. Roberts and C.M. Friend, Surface Sci., 186, 201, (1987)

25. Metals Handbook, American Society for Metals, Cleveland, OH, pp. 159-162, (1948)

26. M.E. Jones, Dept. of Chem., Univ. of CO Boulder, Personal communication, 1990

27. W. Heegemann, K.H. Meister, E. Bechtold, and K. Hayek, Surf. Sci., 49, 161, (1975)

28. P. Auger, J. Phys. Radium, 6, 205, (1925)

29. R.E Weber and W.T. Peria, J. Appl. Phys., 38, 4355, (1967)

30. G. Panzner and W. Diekmann, Surf. Sci., 160, 253, (1985)

31. R. Ducros, G. Piquard, B. Weber, and A. Cassuto, Surf. Sci., 54, 513, (1976)

32. K. Ishikawa and Y. Tomida, J. Vac. Sci. Technol. 15, 1123, (1978)

33. J.E. Lennard-Jones, Trans. Farad. Soc., 28, 333, (1933)

34. R.P.H. Gasser, An Introduction to Chemisorption and Catalysis by Metals, p. 15, Oxford University Press, New York, (1985)

35. P.A. Redhead, Trans. Faraday Soc., 57, 641, (1961)

36. H.R. Han and L.D. Schmidt, J. Phys. Chem, 75, 221, (1971)

37. F. Zaera, E.B. Kollin, and J.L. Gland, Surf. Sci., 166, L149, (1986)

38. G. Binnig and H. Rohrer, Surf. Sci., 126, 236, (1983)

39. J.A. Prybyla, P.J. Estrup, S.C. Ying, Y.J. Chabal, and S.B. Christman, Phys. Rev. Letters, 58, 1877, (1987)

BIBLIOGRAPHY, CONTINUED

40. L.J. Clarke, Surf. Sci., 91, 131, (1980)

41. T.J. Haas and A.G. Jackson, J. Chem. Phys., 44, 2921, (1966)

42. L. Morales de la Garza and L.J. Clarke, J. Phys. Chem., C14, 5391, (1981)

43. K.W. Frese, Surf. Sci., 182, 85, (1987)

44. T.W. Haas and J.T. Grant, Appl. Phys. Lett., 16, 172, (1970)

45. M.A. Chesters, B.J. Hopkins, A.R. Jones, and R. Nathan, Surf. Sci., 45, 740, (1974)

46. J. Oudar, Catal. Rev. Sci. Eng., 22, 171, (1980)

47. H. Wise and J. McCarty, Surf. Sci., 133, 311, (1983)

48. J. Oudar, Catal. Rev. Sci. Eng., 22, 171, (1980)

49. L. Peralta, Y. Berthier, and J. Oudar, Surf. Sci., 55, 199, (1976)

50. H. Ohtani, C.T. Kao, M.A. Van Hove, and G.A. Somorjai, Prog. Surf. Sci., 23, 155, (1986)

51. W. Heegemann, K.H. Meister, E. Bechtold, and K. Hayek, Surf. Sci., 49, 161, (1975)

52. C. Kittel, Introduction to Solid State Physics, John Wiley and Sons, New York, 100, (1976)

53. K.A.R. Mitchell, Surf. Sci., 149, 93, (1985)

54. T.W. Capehart, C.W. Seabury, G.W. Graham, and T.N. Rhodin, Surf. Sci., 120, L441, (1982)

55. J. Toofan, G.R. Tinseth, and P.R. Watson, J. Vac. Sci. Technol. A, 12, 2246, (1994)

56. CRC Handbook of Chemistry and Physics, 58th ed., R.C. Weast, Ed, CRC Press, Cleveland, (1975)

57. F. Zaera, E.B. Kollin, and J.L. Gland, Surf. Sci., 166, L149, (1986)

58. M.H. Farias, A.J. Gellman, G.A. Somorjai, R.R. Chianelli, and K.S. Liang, Surf. Sci., 140, 181, (1984)

BIBLIOGRAPHY, CONTINUED

59. L. Peralta, Y. Berthier, and J. Oudar, Surf. Sci., 55, 199, (1976)

60. A. Sánchez, J.J. de Miguel, E. Martinez, and R. Miranda, Surf. Sci., 171, 157, (1986)

61. W. Witt and E. Bauer, Ber. Bunsenges. Phys. Chem., 90, 248, (1986)

62. J.J. de Miguel, A. Sánchez, E. Martinez, and R. Miranda, Vacuum, 37, 455, (1987)

63. J.M Wilson, Surf. Sci., 59, 315, (1976)

64. A. Sánchez, J.J. de Miguel, E. Martinez, and R. Miranda, Surf. Sci., 171, 157, (1986)

65. M.H. Farias, A.J. Gellman, G.A. Somorjai, R.R. Chianelli, and K.S. Liang, Surf. Sci., 140, 181, (1984)

66. F. Zaera, E.B. Kollin, and J.L. Gland, Surf. Sci., 166, L149, (1986)

67. N.R. Avery and N. Sheppard, Proc. Roy. Soc. (London), A405, 1, (1986)

68. B.E. Limpricht, Ber., 3, 90, (1870)

69. A. Jaquemain, Bull. Assoc. Chim., 54, 529, (1937)

70. B. Johnston and H. Frey, J. Am. Chem. Soc., 60, 1623, (1938)

71. L. Fierz-David, Chem. and Ind., 44, 942, (1925)

72. E. Furimsky, J.A. MacPhee, L. Vancea, L.A. Ciavaglia, and B.N. Nandi, Fuel, 62, 395, (1983)

73. H. Christiansson, Iva, 18, 89, (1947)

74. C.D. Hurd and A.R. Goldsby, J. Am. Chem. Soc., 54, 2530, (1932)

75. J.T. Roberts and C.M. Friend, Surf. Sci., 186, 201, (1987)

76. J.G. Serafin and C.M. Friend, J. Am. Chem. Soc., 111, 6019, (1989)

77. M.A. Grela, V.T. Amorebieta, and A.J. Colussi, J. Phys. Chem., 89, 38, (1985)

78. A. Lifshitz, M. Bidani, and S. Bidani, J. Phys. Chem., 90, 5373, (1986)

BIBLIOGRAPHY, CONTINUED

79. T.E. Caldwell, I.M. Abdelrehim, and D.P. Land, J. Am. Chem. Soc., 118, 907, (1996)

80. J. Stohr, J.L. Gland, E.B. Kollin, R.J. Koestner, A.L. Johnson, E.L. Muetterties, and F. Sette, Phys. Rev. Letters, 53, 2161, (1984)

81. G.R. Schoofs, R.E. Preston, and J.B. Benziger, Langmuir, 1, 313, (1985)

82. J. Stohr, E.B. Kollin, D.A. Fischer, J.B. Hastings, F. Zaera, and F. Sette, Phys. Rev. Letters, 55, 1468, (1985)

83. F. Zaera, E.B. Kollin, and J.L. Gland, Surf. Sci., 184, 75, (1987)

84. E. Gillet, J.C. Chiarena, and M. Gillet, Surf. Sci., 66, 596, (1977)

85. J.T. Roberts and C.M. Friend, Surf. Sci., 186, 201, (1987)

86. J.T. Roberts and C.M. Friend, Surf. Sci., 186, 201, (1987)

87. M.B Young and A.J. Slavin, Surf. Sci., 245, 56, (1991)

88. G. Panzner and W. Diekmann, Surf. Sci., 160, 153, (1985)

89. J.T. Roberts and C.M. Friend, Surf. Sci., 186, 201, (1987)

90. D.G. Kelly, Doctoral Dissertation, U.C. Berkeley, 171 (1990)

91. G. Ertl, Ber. Bunsenges. Phys. Chem., 86, 425, (1982)

92. C.M. Mate, B.E. Bent, and G.A. Somorjai in: Hydrogen in Catalysis — Theoretical and Practical Aspects, Z. Paul Ed., Marcell Dekker, Inc., New York, (1990)

93. K. Christmann, O. Schober, G. Ertl, and M. Neumann, J. Chem. Phys., 60, 4528, (1974)

94. J.T. Yates and J.D. Carette, Phys. Rev. Letters, 39, 209, (1977)

95. K. Christmann, O. Schober, G. Ertl, and M. Neumann, J. Chem. Phys., 60, 4528, (1974)

96. K. Christmann, O. Schober, G. Ertl, and T. Pignet, Surf. Sci., 54, 365, (1976)

97. M. Kiskinova and D.W. Goodman, Surf. Sci., 108, 64, (1981)

98. J. Benziger and R.J. Madix, Surf. Sci., 94, 119, (1980)

BIBLIOGRAPHY, CONTINUED

99. M. Kiskinova and D.W. Goodman, Surf. Sci., 108, 64, (1981)

100. M. Mahnig and L.D. Schmidt, Z. Phys. Chem. Neue Folge, 80, 71, (1972)

101. D.G. Kelly, Doctoral Dissertation, U.C. Berkeley, 163 (1990)

102. K. Christmann, O. Schober, G. Ertl, and M. Neumann, J. Chem. Phys., 60, 4528, (1974)

103. K. Christmann, O. Schober, G. Ertl, and T. Pignet, Surf. Sci., 54, 365, (1976)

104. J. McCarty and R.J. Madix, J. Catalysis, 38, 402, (1975)

105. J.B. Benziger, E.I. Ko, and R.J. Madix, J. Catalysis, 64, 132, (1984)

106. K.A. Pearlstine and C.M. Friend, J. Am. Chem. Soc., 107, 5898, 91985

107. E. Gillet, J.C. Chiarena, and M. Gillet, Surf. Sci., 66, 596, (1977)

108. H. Ibach and D.L. Mills, Electron Energy Loss Spectroscopy and Surface Vibrations, Academic Press, New York, p. 284 (1982)

109. N.V. Richardson and J.C. Campuzano, Vacuum, 31, 449, (1981)

110. B.A. Sexton, Surf. Sci., 163, 99, (1985)

111. M. Salmeron and G.A. Somorjai, J. Phys. Chem., 85, 3835, (1982)

112. H. Steininger, H. Ibach, and S. Lehwald, Surf. Sci., 117, 685, (1982)

113. J.E. Parmeter, M.M. Hills, and W.H. Weinberg, J. Am. Chem. Soc., 108, 3563, (1986)

114. S.H. Overbury, Surf. Sci., 184, 319, (1987)

115. M.B. Young and A.J. Slavin, Surf. Sci., 245, 56, (1991)

116. J.G. Serafin and C.M Friend, J. Am. Chem. Soc., 111, 6019, (1989)

117. J.T. Roberts and C.M. Friend, Surf. Sci., 202, 405, (1988)

118. M.B. Young and A.J. Slavin, Surf. Sci., 245, 56, (1991)

119. F.A. Londry, A.J. Slavin, and P.R. Underhill, Surf. Sci., 140, 521, (1984)

120. J.G. MacMillan, A.J. Slavin, and K.J. Sunderland, Surf. Sci., 173, 138, (1986)

BIBLIOGRAPHY, CONTINUED

121. J.T. Roberts and C.M. Friend, Surf. Sci., 202, 405, (1988)

122. J.T. Roberts and C.M. Friend, Surf. Sci., 186, 201, (1987)

123. A.C. Liu and C.M. Friend, J. Chem. Phys. 89, 4396, (1988)